Forschungszentrum Jülich
in der Helmholtz-Gemeinschaft

Institut für Chemie und Dynamik der Geosphäre
ICG-IV: Agrosphäre

Analysis of the adsorption kinetics of pyrene to soil using laser-induced fluorescence spectroscopy [LIF]

Guido Mennicken

Jül-4178

Analysis of the adsorption kinetics of pyrene to soil using laser-induced fluorescence spectroscopy [LIF]

Guido Mennicken

Berichte des Forschungszentrums Jülich ; 4178
ISSN 0944-2952
Institut für Chemie und Dynamik der Geosphäre
ICG-IV: Agrosphäre Jül-4178
D 82 (Diss., Aachen, RWTH, 2005)

Zu beziehen durch: Forschungszentrum Jülich GmbH · Zentralbibliothek
D-52425 Jülich · Bundesrepublik Deutschland
☎ 02461 61-5220 · Telefax: 02461 61-6103 · e-mail: zb-publikation@fz-juelich.de

1. Introduction

2. Evaluation of current measurement techniques

3. Materials and methods

4. Results

Glossary

a	hydrodynamic radius [L]
A_{em}	Absorption at the emission wavelength, non-dimensional
A_{ex}	Absorption at the excitation wavelength, non-dimensional
Ap	Pore cross-sectional area [L^2]
c	Dissolved mass [$M\ L^{-3}$]
C_0	Initial pyrene concentration [$M\ L^{-3}$]
C_{eq}	Equilibrium concentration [$M\ L^{-3}$]
CME	Coefficient of model efficiency, non-dimensional
C_t	Concentration at time t [$M\ L^{-3}$]
cv_{Bottom}	Solute flux at the soil column outlet [$ML^{-2}\ t^{-1}$]
cv_{Top}	Solute flux across the soil surface [$ML^{-2}\ t^{-1}$]
d	Layer thickness [L]
D	Effective dispersion coefficient [L^2t^{-1}]
D_{eff}	Effective diffusion coefficient [L^2t^{-1}]
D_{water}	Diffusion coefficient in water [L^2t^{-1}].
D^w	Dispersion coefficient [L^2t^{-1}]
Disp.	Dispersivity [L]
ε	Extinction coefficient depending on frequency [$L^3\ M^{-1}\ L^{-1}$]
F_0	Frictional factor, non-dimensional
F_1	Steric hindrance factor, non-dimensional
f	Fraction of the exchange sites assumed to be in equilibrium with the solution phase, non-dimensional
$f_{Lakowicz}$	Lakowicz correction factor, non-dimensional
F_{Renkin}	Renkin factor, non-dimensional
f_{OC}	Carbon fraction [%]
Hu	Humic substances

I_0	Excitation intensity [*absorbed photons*, $L^{-2}t^{-1}$]
I_F	Fluorescence intensity [*emitted photons*, $L^{-2}t^{-1}$]
I_F^0	Initial fluorescence intensity of the fluorophore [*emitted photons*, $L^{-2}t^{-1}$]
$I_{F\ eq.}^{I}$	Fluorescence intensity at instantaneous equilibrium [$photons \bullet L^{-2}t^{-1}$]
$I_{F\ eq.}^{I+II}$	Fluorescence intensity at true equilibrium [$photons \bullet L^{-2}t^{-1}$].
$I_{F\ blank}$	Fluorescence intensity in the absence of the fluorophore [$photons \bullet L^{-2}t^{-1}$]
θ	Volumetric water content [L^3L^{-3}]
J_w	Darcy´s flux [Lt^{-1}]
k_{ads}	Adsorption rate constant [t^{-1}]
k_{bin}	Binding rate constant [$L^3t^{-1}M^{-1}$]
k_{des}	Desorption rate constant [t^{-1}]
K_d	Distribution coefficient [L^3M^{-1}]
K_b	Binding constant [L^3M^{-1}]
$k = 1/\tau eff$	Rate constant of permeation [t^{-1}]
k_f	Freundlich constant [L^3M^{-1}]
K_{OC}	Carbon matter Partition coefficient [L^3M^{-1}]
L_{mb}	Membrane thickness [L]
Mw	Molecular weight [M mol^{-1}]
MWCO	molecular weight cut-off
n	Freundlich exponent
N_A	Avogadro´s number, non-dimensional
Φ_F	Quantum yield [*emitted photons*/*absorbed photons*]
pn	pore number, non-dimensional
ρ	Soil bulk density [ML^{-3}]
q	Volumetric flux density [Lt^{-1}]

R	Ratio of the fluorescence intensity in the absence and in the presence of the fluorophore, non-dimensional
r_p	Pore radius [L]
s	Adsorbed substance [M M^{-1}]
S_k^e	Adsorbed Pyrene following an instantaneous sorption equilibrium [M M^{-1}]
S_k^k	Adsorbed Pyrene following a rate-limited sorption equilibrium [M M^{-1}]
TOC	Total organic carbon content [M L^{-3}]
τ_{eff}	Effective diffusion time [t]
v	Pore water velocity [Lt^{-1}]
ω	First order rate constant [t^{-1}]
x_o	Observed value at time t [user defined dimension]
x_s	Simulation result at time t [same dimension as x_o]
$x_{o\ mean}$	Arithmetic mean of the observed values

1. Introduction

The main objective of this work was to contribute to the development of an in-situ analytical method for polycyclic aromatic hydrocarbons (PAH´s) in soils. Beside natural sources like forest fires, PAH´s result from any incomplete combustion of organic material. Man-made sources come from heating systems, industrial power generators, diesel engines or gaswork sites (Dabestani and Ivanov 1999). For that reason, the US Environmental Protection Agency (EPA) indicates 16 PAH´s as priority pollutants (see appendix 1). The background level for PAH´s in soils of Europe and North-America varies between 50 µg/kg and 500 µg/kg soil (Maxin and Kögel-Knabner 1995). Because pyrene is widely prevalent as a soil contaminant and only little information is available about its sorption kinetics to soils (Hwang et al. 2003), pyrene was chosen as a model compound for PAH´s in this work.

The classic way to analyse the adsorption characteristics of compounds to soil are batch experiments. They are easy to handle and useful for sorption equilibrium studies. One aim of this work was to follow the adsorption kinetics of pyrene to soil components. In this case batch studies are not the ideal instrument. Maxin and Kögel-Knabner (1995) reported, that the adsorption of PAH´s to water soluble soil components is completed within 15 min and therefore it is difficult to analyse it by batch experiments due to the time-consuming phase separation. Additionally many authors emphasise the advantages of procedures without a separation step for the adsorption analysis (Belardi, Pawliszyn 1989, Ohlenbusch et al. 2000). Aiken and Leenheer (1993) point out, that centrifugation and filtration processes lead to a concentration of the sample and therefore the quantity and quality of the interactions between the components and the sample might be changed.

In this context, we intended to show the potentials and limitations of the laser-induced fluorescence spectroscopy (LIF) as an in-situ, real-time method for the analysis of adsorption kinetics in soil. Until now, laser applications in the pedosphere and in aquifer systems are scarce. Recent investigations of petroleum products in soils have shown that a quantitative determination of oil contaminations on soil surfaces is possible with LIF spectroscopy (Schade and Bublitz 1996, Löhmannsröben and Roch 1997). These measurements were carried out on the soil surface or through the glass wall of soil columns. In combination with measurements in a flow-through cell at the column outlet, the breakthrough of free pyrene can be observed (Baumann et al. 2000).

The advantages of the LIF are its high sensitivity, the short measurement times and the high spatial resolution (Niessner et al. 1991). Baumann et al. (2000) reported a limit of detection of 300 ng/l for pyrene in natural ground water. Thus, LIF sensor systems can be used to examine the heterogeneity of soils: With several sensors a fine spatial resolution can be obtained, and such the heterogeneity of the medium can be assessed. A replacement of conventional fluorescence analytical techniques is also possible if the sensor is placed at the end of the column. The intense monochromatic laser excitation source allows a very selective excitation of the compound of interest. The reduced level of scattered light also improves the signal to noise ratio of the fluorescence signal (Donard et al. 1989).

In the presence of humic substances, the excitation of pyrene by the laser source is limited only to truly dissolved pyrene molecules. Based on this observation, Gauthier et al. (1986) established the fluorescence quenching method. The fluorescence of polycyclic aromatic hydrocarbons associated with humic acids is quenched, which means the excitation energy is emitted radiationless as heat. This allows the distinction between dissolved PAH´s and PAH´s, sorbed to organic carbon, without separating the equilibrated phases (Backhus and Gschwend 1990).

One of the experimental challenges of the LIF is to avoid a significant photolysis effect. The high intensity of the excitation light can lead to the photochemical decomposition of pyrene. Previous studies indicated that the direct photolysis is an important process for most PAH´s (Zepp and Schlotzhauer 1979; Larson and Weber 1994). Only a few authors (e.g. Chen et al. 1996) quantified the photolysis effect for the applied laser system. Our particular interest was to determine in-situ the extent of photolysis on mineral surfaces.

The adsorption kinetics of pyrene were investigated in batch- and column experiments. For the understanding of the sorption processes, transport models for column experiments are an important tool. The breakthrough curves of pyrene in two annealed soils were modelled by Hydrus-1D, Version 2.0 (J. Šimůnek, M. Šejna and Th. van Genuchten). One of the models integrated in Hydrus-1D is the Two-site sorption concept (Selim et al. 1987; van Genuchten and Wagenet 1989) This model assumes that the sorption sites can be divided into two fractions. Sorption on one fraction of the sites is assumed to be instantaneous, while sorption on the remaining sites is considered to be rate-limited and therefore time dependent.

Based on these literature data, the main objectives of our work were defined.

The most important aim was the development of an optical probe head for the in-situ laser-induced fluorescence spectroscopy in soils. The main requirements for the probe head were a high efficiency for the light transition, a low eigen-signal, low distortion of the fluorescence spectra, no aging effect and good cleaning properties. One important criteria for the development of the probe head was the relevance of the measured data for the average component concentration in the soil. Naturally, the probe head data show the chemical heterogeneity of the soil. This is one of the advantages of fluorescence analysis. But the measurement volume should exceed a critical volume, to make it insensitive against single crystals or artefacts caused by the installation of the probe head.

The second focus of our work was to measure in-situ adsorption kinetics to soil compounds. The data measured in-situ by LIF spectroscopy may help to achieve new insights under semi-natural conditions. Most existing methods are conducted under unnatural water to soil ratios or show other disadvantages that may lead to artificial adsorption data. An optical method, like the laser-induced fluorescence spectroscopy can offer the opportunity, just to observe the processes involved without disturbance.

The third main focus of our work is derived from this aim. The LIF is an observation method, but due to the relative high pulse intensity of the laser source, it may also change the compounds of interest. Therefore, the characterisation of the photobleaching effect in solution, but also in-situ on sand surfaces, was another important aspect of this work.

Furthermore, it was our interest, to proof the applicability and the potential of the LIF probe head for batch and soil column experiments. The LIF spectroscopy makes it possible to conduct batch experiments at natural water to soil ratios. The comparison between these experiments and soil column transport experiments can lead to valuable insights of the adsorption kinetics of compounds in stagnant and streaming soil solutions. The unique opportunity of the LIF, to measure in-situ 3D fluorescence spectra with a high temporal resolution, is one of the striking properties of this analytical method. These spectra were compared with fluorescence spectra of the soil column effluent, to validate the in-situ fluorescence data.

1.1 Polycyclic aromatic hydrocarbons (PAH) in soil

1.1.1 Characteristics of hydrophobic organic compounds

Hydrophobic organic compounds (HOC) differ fundamentally from polar and ionic water soluble chemicals. Their high affinity to surfaces leads for instance to an uneven phase equilibrium and therefore to different transport behaviour in soils. Hydrophobicity also hinders the chemical and biological degradation and increases bioaccumulation within the food web (Johnson, Amy 1995, Haitzer et al. 2000 and Amellal et al. 2001).

Regarding their strong environmental impact, chlorinated dioxins, polychlorinated biphenyls (PCB´s) and polycyclic aromatic hydrocarbons (PAH´s) are among the most important organic pollutants. All PAH´s have two or more condensed benzene rings, and may in addition also contain cyclopentadiene or cyclohexane. The higher the molecular weight of a compound, the lower its water solubility. For example phenanthrene (Mw =178.2) has a water solubility of 1080 µg/l at 25 °C whereas the water solubility of chrysene (Mw =228.3) is 1.02 µg/l at the same temperature (Billington et al. 1988). Because pyrene is ubiquitous in the environment (Marschner 1999) it was chosen as a model compound for PAH´s in this work.

PAH´s result from any incomplete combustion of organic material, so they can be found in all ecosystems. Beside natural sources like forest fires, volcanoes etc., there are a lot of anthropogenic sources like for example diesel engines, power plants or heating systems (Marschner 1999). For that reason, the US Environmental Protection Agency (EPA) indicates 16 PAH´s as priority pollutants (see Appendix. 1).

Outstanding problems are caused by abandoned gaswork sites where illuminating gas was produced. To produce this illuminating gas, mineral coal is carbonised at temperatures above 700 °C with limited oxygen supply. Products of this process are different fractions of tar. One of these fractions is mineral coal pitch which contains up to 10 g/kg benz(a)pyrene.

The total number of contaminated gaswork sites in Europe and the USA is estimated to be more than 4000 (Baumann et al. 2000). Soil at the gaswork sites can contain several grams PAH per kg. A gaswork site previously studied in Germany had an average level of 6.87 g/kg soil (Mennicken 2000).

1.1.2 Adsorption of PAH´s to soils

A better understanding of desorption, decomposition and transport processes is needed for the risk assessment of contaminated sites. Due to their low water solubility PAH´s adsorb fast to the surface of soil components and especially to amphiphilic dissolved or particulate organic matter. The higher the hydrophobicity of the analysed PAH´s, the higher their affinity to the organic matter. Numerous authors were able to prove the coherence of the K_{OW}-values (octanol/water partition coefficient) of several substances, as a measure of their hydrophobicity, and their partition coefficients (K_{OC}-values) towards humic substances (Mc Carthy and Jimenez 1985, Chiou and Kile 1994, Curtis et al. 1986).

The driving thermodynamic force for adsorption of HOC to soil are hydrophobic interactions, which result in an increase of entropy. It is known that in water hydrophobic organic molecules like PAH´s are surrounded by layers of ordered water molecules. Attaching to soil surfaces, these layers are destroyed within the contact zone. The molecules which were in an ordered state, are now in a free state, resulting in a higher entropy (Schlautmann and Morgan 1993).

Experimental results of the adsorption of HOC´s to organic and mineral surfaces can be described by the Freundlich equation. This equation describes the amount of adsorbed substance s [M/M] as a function of the dissolved mass c [M/L^3] under equilibrium conditions.

$$s = k_f \cdot c^n \quad \Leftrightarrow \quad k_f = \frac{s}{c^n} = s\, c^{-n} \qquad (1)$$

For a given surface, at a given temperature in a defined system, the Freundlich constant k_f [L^3/M] is specific for the compound. The Freundlich exponent is a measure for the non-linearity of the adsorption. The correlation is linear, if the exponent is one. An exponent less than one means that the adsorption capacity decreases at higher concentrations. The physical explanation is that adsorbed molecules are gradually blocking the access to other binding sites, so that less sites are available (anticooperative binding).
In a situation where adsorbed molecules encourage the adsorption of further molecules, the Freundlich exponent will be above one (cooperative binding). Experiments at very low concentrations can be described often by a linear correlation, because the influence of absorbed molecules is negligible with regard to the number of binding sites (Schulze 1998).

Due to experimental limitations, most sorption isotherms in literature are measured either at very low concentrations or with a certain amount of organic solvents. Consider pyrene as an example, the maximum water solubility at room temperature is around 132 µg/l (Reza et al. 2002: 133.1 µg/l at 25.55 °C; Dabestani and Ivanov 1999: 132 µg/l at 25 °C).

To avoid microcrystals and other artefacts (de Maagd et al. 1998), it is reasonable to use maximum concentrations of 100 µg/l for experiments. Consequently all further concentrations for measuring sorption isotherms will be even lower. Considering realistic water to soil ratios, natural soils will adsorb nearly all pyrene and the free pyrene concentration in the aqueous phase will fall below the detection limit. But even in soils where all organic material has been removed, free pyrene will only be measurable at highest concentrations. Generating sorption isotherms and making decisions about their shape on the basic of limited data points is quite problematic. To escape this problem and to gain stable solutions, many researchers solve pyrene in methanol and add up to 1 % methanol to the stock solution (Raber et al. 1998, Whitcomb and Campiglia 2002). Most authors expect, that this amount of methanol will not influence the shape of the sorption isotherm (Chefetz et al. 2000). Obviously, an experimental verification of this point of view is impossible.

In soils, hydrophobic organic compounds adsorb mainly to humic substances and only to a minor degree to mineral surfaces (Chiou and Kile 1994, Marschner 1999, Xing 2001). For this reason, the ratio of the sorbed mass s [M M^{-1}] to the dissolved mass c [M L^{-3}] is often normalised to the organic carbon fraction f_{OC} of the soils. The resulting K_{OC}-values [L^3 M^{-1}] make it possible to compare the sorption capacity of soils with different carbon contents.

$$K_{OC} = \frac{s}{c \cdot f_{OC}} \qquad (2)$$

It should be noticed that not only the transport of PAH´s is affected by humic substances, but also their bioavailability and their biodegradation (Shelton and Doherty 1997, Zimmermann et al. 1999, Haitzer et al. 1998, 2000).

Sorption coefficients for pyrene to diverse humic substances were determined by solid phase extraction (Georgi 1997), fluorescence quenching (Danielsen et al. 1995), C_{18} analysis (Maxin and Kögel-Knabner 1995), the solubility enhancement method (Danielsen et al. 1995) and the complexation-flocculation method (Laor and Rebhun 1997).

Many authors focus on the relevance of chemical structure, molecular weight, functional groups and hydrophobicity of the humic compounds. Gauthier et al. (1987) determined partition coefficients for pyrene and 14 different humic and fulvic acids. They were able to show, that humic compounds with a higher aromaticity bind more pyrene.

Perminova et al. (1999) measured partition coefficients for pyrene, fluoranthene and anthracene in 26 samples of humic substances. With different analytical methods they where able to proof the positive correlation between the grade of aromaticity of the humic compounds and the K_{OC}-values.

According to Xing (2001), the degree of aromaticity influences the adsorption mechanism of PAH´s. The author analysed the sorption of naphthalene and phenanthrene to humic acids from different depths of the same soil profile. With increasing depth, the aromaticity of the humic compounds increased, whereas the Freundlich exponents decreased. The author attributes this to a bimodal mechanism of sorption, which can be traced back to expanded and condensed sorption sites.

Beside the influence of aromaticity, Chiou et al. (1998) examined the influence of different compositions of humic substances due to diverse morphogenesis. The authors investigated the adsorption of naphthalene, phenanthrene and pyrene to five soils and seven sediments. The tests showed that K_{OC} values where twice as high for the sediments compared to the soils, although the aromaticity was equal in both groups. There has been recent evidence that aliphatic structures are also important for the binding of PAH´s (Chefetz et al. 2000).

1.2 Humic Substances

The characterisation of humic substances, which are defined operationally, still requires fundamental research to be carried out. It is beyond dispute, that the major part of humic substances consists of decomposition products originating from microbes, animals and plants (Simpson et al. 2002). Traditionally they are divided into three fractions based on their solubility at different pH values. At pH 1 the soluble fraction of humic substances is defined as fulvic acids. Humic acids are insoluble at pH 1, but can be dissolved in a cold sodium hydroxide solution. The third fraction, defined as humins is insoluble in aqueous solutions for any pH value (Rice and Lin 1993, Chien and Bleam 1998).

The heterogeneous morphogenesis of humic substances leads to varying properties of the resulting compounds (Hopkins et al. 1993, Martin et al. 1998). The process of humification contains the degradation of high polymer substances from organisms, as well as the linkage of smaller molecules by polymerisation and condensation reactions. Because the reactants can be combined in many ways, the resulting macromolecules will differ in detail, even if their basic plan of construction is the same (Tombacz 1999). Therefore, two humic molecules with a high molecular weight are unlikely to have exactly the same composition (Hayes and Swift, 1990)

Due to the ability of the reactants for cross linking, humic substances were always considered as polydisperse macromolecules. Schulten und Schnitzer (1993) verified this by mass spectroscopy, electron microscopy, degradation studies and NMR measurements. The authors see humic substances as a macromolecular network, wherein aliphatic and aromatic domains alternate. The main reactants in this model are alkylbenzenes. The most important functional groups in the resulting macromolecules are carboxyl and hydroxyl groups, phenols, alcohols, carboxyl ester and ether, and nitrogen within nitriles and heterocyclic structures. The idea that humic substances are polymers of high molecular weight is corroborated by findings of Leenheer (1991), Lobartini et al. (1997) and Martin et al. (1998).

In 1986, Wershaw presented the first model, that describes humic compounds as substances with comparatively low molecular weights. They are amphiphile, that means they have separated hydrophilic and hydrophobic domains. Within soil, these molecules build

membrane or micelle like structures. The origin of these compounds are enzyme catalysed depolymerisation and oxidation reactions of herbal biopolymers.

Based on this model, Piccolo et al. (1996a) define humic substances as randomly self-associating aggregates of small subunits, weakly held together by hydrophobic forces and hydrogen bonding. These aggregates show apparent macromolecular properties.
This characterisation of humic compounds is mainly based on results of size-exclusion chromatography (SEC) and high performance size exclusion chromatography (HPSEC). Using these technics, the addition of organic acids (mono, di, tri carboxylic acids and oxy acids) causes a shift to higher elution volumes. A similar shift is not observed after addition of mineral acids, phenols or alcohols. The authors interpret this as an unambiguous indication, that the aliphatic part of the organic acids enters the interior of the micelle-like aggregates and alter the stereochemical hydrophobic arrangement of the humic material. At the same time, the hydrophilic carboxyl groups of the organic acid are positioned at the interfaces between the micelles and water and diminish the hydrophobicity of the humic compounds. As a result the micelles resolve into smaller aggregates. These aggregates are small enough to infiltrate into the pores of the gel and, as a consequence, need more time to pass the SEC column (Piccolo et al. 1996a, 1996b, 1999, 2002).

Objection against these conclusions was raised by Perminova (1999) and Varga et al. (2000). Both lead back the results of Piccolo et al. (1999) to other effects than size exclusion mechanisms. Especially the high gradient of the electrolyte concentration between the chromatographic zone and the borate buffer, which was used for elution, may be responsible for the observed effects. Furthermore Perminova (1999) points out that the aliphatic part of surface active substances has to comprise at least eight carbon atoms to be able to enter micelle-like structures, which is not the case for the applied organic acids.

1.3 PAH mobility in soils

It is proved that humic substances can act as surfactants between PAH and aqueous media, and thus the concentration of the organic compound can be enhanced significantly (Frimmel 2000). Considering the enhancement of the PAH solubility in the presence of humic substances, carrier-facilitated transport models for PAH has been developed.

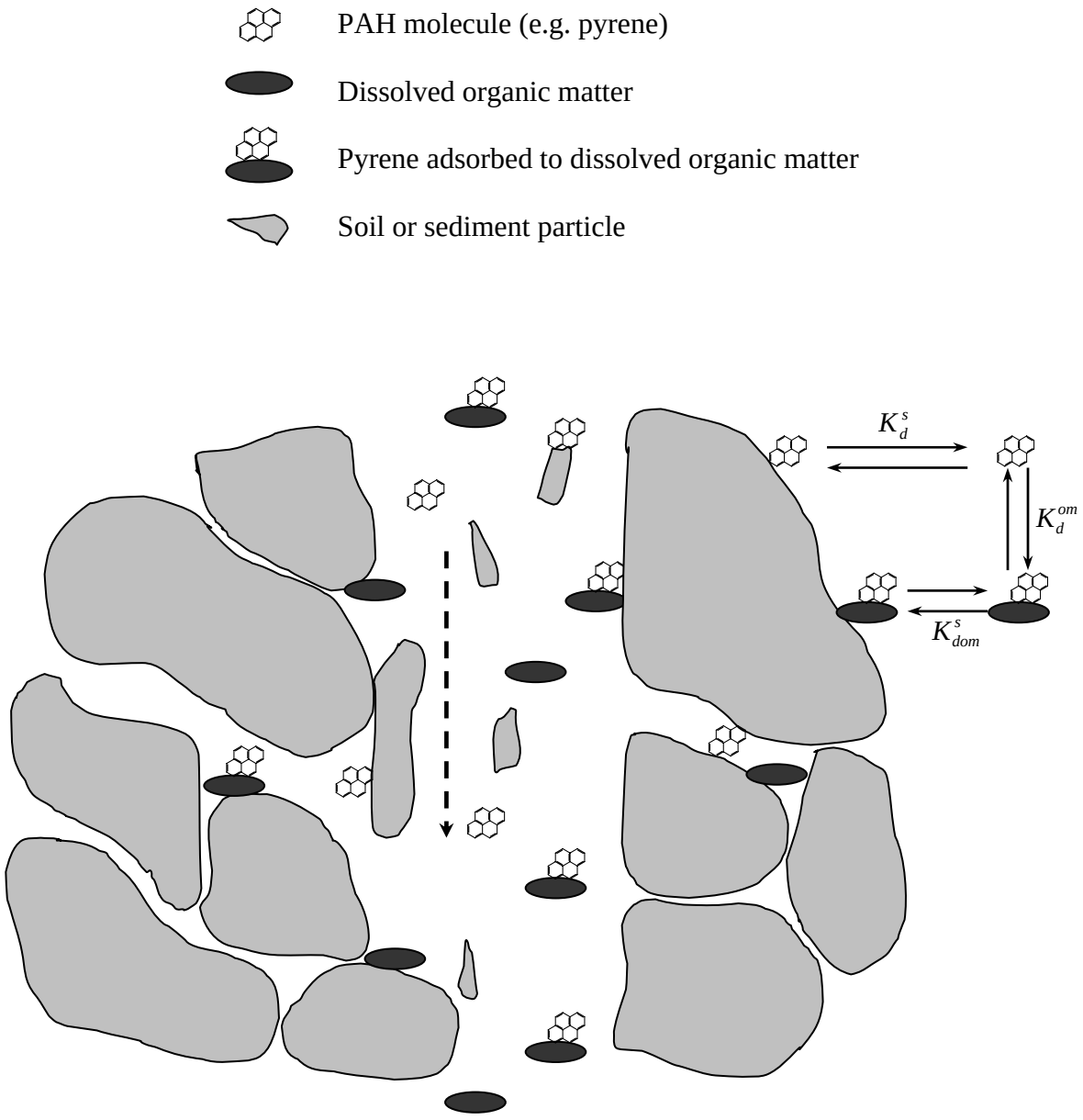

Fig. 1: Interactions between polycyclic aromatic hydrocarbons (e.g. pyrene), dissolved organic matter and soil particles. The arrow shows the flow direction of the pore water (according to Magee et al. 1991 and Vereecken et al. 2001, modified).

Starting from such three phase transport models, many authors studied the influence of dissolved organic matter (DOM) (Magee et al. 1991, Dunnivant et al. 1992, Johnson 2000). By definition DOM is the fraction of dissolved material, that can pass through 0.45 µm pores. Because DOM is thus defined operationally, there are numerous conformities, regarding morphogenesis and composition, with soluble humic substances like humic and fulvic acids (Guggenberger et al. 1998, Six et al. 2001). Furthermore the so-defined DOM contains “truly” dissolved OM but also OM associated with mineral colloids smaller than 0.45 µm. The solubility of DOM and its capacity to adsorb non-polar organic molecules is depending on ionic strength, pH-value and temperature of the soil solution (Jardine et al. 1989, Lüers and ten Hulscher 1996).

For the transport of hydrophobic compounds, adsorbed to DOM, not only the interaction of the compound and DOM becomes important, but also the interaction between the mineral soil compounds and the DOM. The combination of the sorption processes to dissolved and solid soil compounds gives a complex picture of molecule interactions. Fig. 1 gives a schematic overview of the processes involved.

1.4 Pyrene dialysis kinetics

The dialysis technique is based on the idea of dividing a reaction vessel into two compartments without influencing the sorption characteristics of the compounds involved. Therefore, two conditions should be fulfilled: The dialysis membrane should be incoherent for all compounds of interest. Furthermore one of the reacting substances should not be able to pass the membrane, while the other compound can pass it without any hindrance.

The escape of pyrene from the dialysis bag with the volume V_{int} [L^3] through the microporous membrane to the surrounding glass cylinder solution V_{ext} [L^3] can be formulated by an exponential law of the type:

$$C_t = C_{eq}\left(1 - e^{-kt}\right) \quad \text{or} \quad \frac{C_t}{C_{eq}} = 1 - e^{-kt} \quad \Leftrightarrow \quad \ln\left(1 - \frac{C_t}{C_{eq}}\right) = -kt \qquad (3)$$

where C_t [$M\ L^{-3}$] is the pyrene concentration outside the dialysis bag at time t , C_{eq} [$M\ L^{-3}$] is the concentration at equilibrium and $k = 1/\tau_{eff}$ [t^{-1}] is the rate constant of permeation. τ_{eff} [t] is the effective diffusion time through the membrane (Guillot et al. 1985).

According to the mass law of conservation

$$C_{eq} = C_0 \frac{V_{int}}{V_{ext} + V_{int}} \qquad (4)$$

where C_0 [$M\ L^{-3}$] is the initial pyrene concentration in the dialysis bag. For a microporous membrane, k is related to the following experimental parameters:

$$k = \frac{1}{\tau_{eff}} = \frac{D_{eff}\, pn A_p}{L_{mb}}\left(\frac{1}{V_{ext}} + \frac{1}{V_{int}}\right) \qquad (5)$$

D_{eff} [L^2t^{-1}] is the effective pyrene diffusion coefficient, pn the pore number, A_p [L^2] the pore cross-sectional area and L_{mb} [L] the membrane thickness (Cannell and Rondelez 1980). If the pore radius r_p [L] is much greater than the hydrodynamic radius a [L] of the pyrene molecule, D_{eff} can be put equal to the pyrene diffusion coefficient in water D_{water}.[L^2t^{-1}]. If the molecular

weight cut-off (MWCO) of the membrane is low, D_{eff} will have a strong dependency on r_p. If the hydrodynamic radius of the molecule and the pore radius are of the same order of magnitude, the Renkin equation can be used for non-ionic substances (Renkin 1954). This equation takes into consideration steric hindrance and frictional effects at the entrance and within the pores.

The Renkin equation is given by the product of the frictional factor F_0 and the steric hindrance factor F_1.

$$F_{Renkin} = F_0 * F_1 \qquad (6)$$

These factors are defined as:

$$F_0 = 1 - 2.1\left(\frac{a}{r_p}\right) + 2.1\left(\frac{a}{r_p}\right)^3 - 0.95\left(\frac{a}{r_p}\right)^5 \qquad (7)$$

$$F_1 = \left(1 - \frac{a}{r_p}\right)^2 \qquad (8)$$

It follows that $D_{eff} = D_{water}\, F_{Renkin}$ (9)

1.5 Fluorescence measurements

1.5.1 Background Physics of Fluorescence

Fluorescing molecules are able to absorb a photon at a defined band of wavelength. The absorbed energy leads to the excitation of one electron from the ground state S_0 to the first excited state S_1. The change of the electronic state takes 10^{-15} s and, according to the Franck-Condon principle, electronic spin and the distance between the atomic nuclei remain constant over this period. The process does not lead to the lowest vibrational level of the S_1-niveau but to a higher level within the S_1 cascade. In a vibrational relaxation (radiationless decay), the electron transfers energy to adjacent molecules and reaches the lowest vibrational state of S_1. If the energy difference between S_1 and S_0 is adequate, the electron remains long enough (~ 10^{-9} s) in the excited state to emit spontaneously the energy as fluorescence (Tausch and Paterkiewicz 1988, Stohrer 1991, Institute of Organic Chemistry 2002).

The relation between the absorbed energy and the fluorescence intensity is described by Perrin´s Law. I_F is the observed fluorescence, Φ_F is the quantum yield, c is the fluorophore concentration and d is the path length.

$$I_F = \Phi_F I_0 (1 - e^{-\varepsilon(\bar{\nu})cd}) \qquad (10)$$

$$\cong \Phi_F I_0 \varepsilon(\bar{\nu}) cd \qquad (11)$$

I_F = fluorescence intensity [$emitted\ photons \bullet L^{-2}t^{-1}$]
Φ_F = quantum yield [$emitted\ photons / absorbed\ photons$]
I_0 = excitation intensity [$absorbed\ photons \bullet L^{-2}t^{-1}$]
ε = extinction coefficient depending on frequency [$L^3\ M^{-1}\ L^{-1}$]
c = concentration [$M\ L^{-3}$]
d = layer thickness [L]

According to the Franck-Condon principle, the fluorescence light is always emitted at a longer wavelength, thus with a lower energy, than the absorbed light. The gap between both wavelength is called Stokes shift. For pyrene the absorption maxima are 238 nm, 273 nm and 335.5 nm while the emission maxima in water are at 372.5 nm, 383 nm and 392.5 nm.

The Jablonski diagram shows the energy levels of the excited electron, the fluorescence and the competing processes like internal conversion, intersystem crossing or phosphorescence.

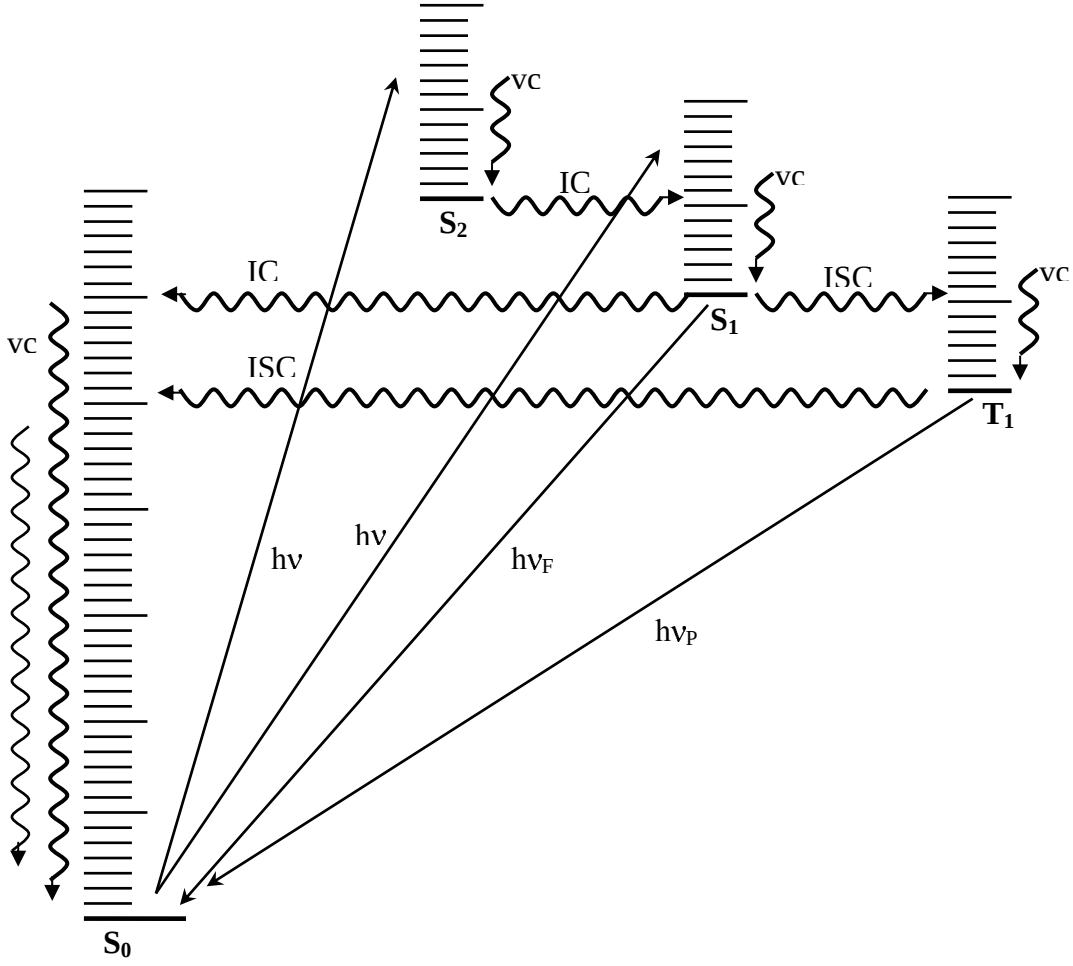

Fig. 2: Jablonski diagram

vc = vibrational cascade: In collisions with adjacent solvent molecules the excited molecule loses energy as heat. The v.c. leads to the lowest energy level in the same vibrational state.

IC = internal conversation: isoenergetic transition, with perpetuation of spin, to a high excited level of a lower vibrational state.

ISC = intersystem crossing: isoenergetic transition, with reversal of spin, to a high excited level of a lower vibrational state.

$h\nu$ = excitation light, $h\nu_F$ = fluorescence, $h\nu_P$ = phosphorescence

1.5.2 Principles of Fluorescence Quenching

Gauthier et al. (1986) introduced the fluorescence quenching method for the determination of equilibrium constants for the binding of PAH´s to dissolved humic materials. The method is based upon the observation that the intensity of fluorescence is proportionally decreased upon the addition of humic or fulvic acids. The process, which reduces the fluorescence intensity is called quenching.

In general, there are two different types of quenching processes that can occur: static and dynamic quenching. In static quenching, a nonfluorescent complex is formed between the ground state fluorophore and the quencher. In dynamic quenching, the quencher reacts with the excited state of the fluorophore. Therefore, both molecules must collide during the lifetime of the excited state and release the energy radiationless to the surrounding medium. The quenching of pyrene by humic acids is dominated by a static quenching process which can be adequately described by the derivation of the Stern-Volmer Equation (Gauthier et al. 1986, Kumke and Löhmannsröben 1994, Zimmermann et al. 1999):

$$PAH + Hu \leftrightarrow PAH - Hu \qquad (12)$$

$$K_b = \frac{[PAH - Hu]}{([PAH][Hu])} = \frac{k_{bind}}{k_{des}} \qquad (13)$$

Where Hu is the abbreviation for humic substances, PAH-Hu for humic-associated PAH and K_b [$L^3 \cdot M^{-1}$] is the binding constant. The binding and desorption rate constants are symbolised as k_{bin} [$L^3 t^{-1} M^{-1}$] and k_{des} [t^{-1}]. The mass balance is described by the following equation, where C_{PAH} is the total concentration of polycyclic aromatic hydrocarbons. The [] brackets symbolise the free concentration [$M \cdot L^{-3}$] of the given substance.

$$C_{PAH} = [PAH] + [PAH - Hu] \qquad (14)$$

Combining equation 13 and 14 yields the following one:

$$\frac{C_{PAH}}{[PAH]} = 1 + K_b[Hu] \qquad (15)$$

Assuming that the fluorescence intensity I_F [$photons \bullet L^{-2}t^{-1}$] is proportional to free PAH concentration in solution, the Stern-Volmer equation is commonly used to describe the relationship between the fluorescence quenching and the quencher concentration. I_{F0} [$photons \bullet L^{-2}t^{-1}$] is the initial fluorescence intensity of the fluorophore.

$$\frac{I_F^0}{I_F} = 1 + K_b[Hu] \qquad (16)$$

1.5.3 Inner filter effect

One problem of fluorescence measurements in solution is the absorption of excitation and fluorescence light on the way through the sample which is referred as the inner filter effect. This problem is of particular interest in turbid or coloured solutions, like solutions of humic acids. To correct the measured results for the inner filter effect, Lakowicz (1983) suggested the following terms:

$$f_{Lakowicz} = 10^{\frac{Aex + Aem}{2}} \qquad (17)$$

Where A_{ex} (non-dimensional) is the absorption by the solution at the excitation wavelength. A_{em} (non-dimensional) is the absorbance at the emission wavelength. Taking into account the Lakowicz correction factor ($f_{Lakowicz}$), the measured fluorescence can be corrected:

$$I_F^{corr\,La} = \left(I_F - I_{F\,blank}\right) * f_{Lakowicz} \qquad (18)$$

Where I_F [$photons \bullet L^{-2}t^{-1}$] is the fluorescence intensity of the sample with fluorophore and $I_{F\,blank}$ [$photons \bullet L^{-2}t^{-1}$] is the fluorescence intensity in the absence of the fluorophore.

The fluorescence quenching of fluorophore along the humic substances concentration is given by R which is the ratio of the fluorescence intensity of the fluorophore in the absence of humic substances $I^0_{F\ corr\ La}$ [$photons \bullet L^{-2}t^{-1}$] to the fluorescence intensity in the presence of humic substances $I_{F\ corr\ La}$ [$photons \bullet L^{-2}t^{-1}$].

$$R = \frac{I^{0}_{F\,corr\,La}}{I_{F\,corr\,La}} \qquad (19)$$

Applying the Lakowicz factor to equation 16 and normalising the data for the organic carbon content [OC], one obtains:

$$K_{OC} = \frac{R-1}{[OC]} \quad \left[L^{3} M^{-1} = \frac{1}{M L^{-3}} \right] \qquad (20)$$

The presented equation is based on the assumption, that the fluorescence is detected in the middle of the cuvette. Although the correction term of Lakowicz is relatively simple, it leads to results which are close to the correction terms of Parker (1968), Gauthier et al. (1986) and Kubista et al. (1994). The method of MacDonald et al. (1997) leads to lower binding coefficients between humic acid and pyrene. While for the computation of the correction factor according to Lakowicz, only the absorption coefficients of the excitation and the emission wavelength as well as the cuvette dimensions have to be known, in all other cases additional geometrical parameters have to be determined (Zimmermann et al. 1999).

1.6 Models for pyrene sorption kinetics

1.6.1 The Two-Domain or Bicontinuum model

Natural soils display heterogeneities in the microscale of an individual particle or aggregate. For modelling batch systems, a two domain or bicontinuum model is generally admitted with two-site adsorption kinetics (Piatt et al. 1996).

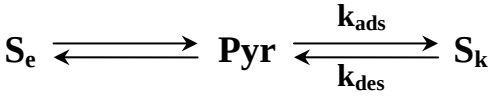

S_e: Adsorbed Pyrene [M M^{-1}] following an instantaneous sorption equilibrium
S_k: Adsorbed Pyrene [M M^{-1}] following a rate-limited sorption equilibrium
k_{ads}: Adsorption rate constant [t^{-1}]
k_{des}: Desorption rate constant [t^{-1}]

The basic assumption of the model is the existence of two classes of sorption sites. Sorption is instantaneous for one class and is rate-limited for the other one. Sorption on the rate-limited sites can be described by first order rate equations while an equilibrium isotherm equation describes the instantaneous sorption equilibrium.

For the application of the model, the adsorption process is divided into two steps. A reversible spontaneous adsorption, which is fixed by definition at time t = 0, and an adsorption kinetic step at $t \geq 0$, which is modelled by a reversible adsorption/desorption reaction.

1.6.2 Spontaneous adsorption of pyrene

The spontaneous adsorption at a fraction f of the total soil surface can be generally modelled by the Stern-Volmer equation (15). The instantaneous sorbed mass of pyrene S_1 can be determined with fluorescence measurements by taking the ratio of two fluorescence intensities. The pyrene fluorescence intensity is measured before I_F^0 [$photons \bullet L^{-2}t^{-1}$] and

immediately after $I_{F\,eq}^{I}$ [$photons \bullet L^{-2}t^{-1}$] the contact of the pyrene solution to the soil matrix. The difference of both values is proportional to the amount of pyrene sorbed instantaneously.

1.6.3 Rate-limited sorption of pyrene

For the rate-limited adsorption kinetics, the variation of the free pyrene concentration in time is given by the following general relation (Steinfeld et al. 1989):

$$Pyr_{free}(t) = \frac{Pyr^{I}_{free\,eq.}}{(k'_{ads} + k_{des})}\left[k_{des} + k'_{ads}\, e^{-(k'_{ads}+k_{des})t}\right] \qquad (21)$$

In the same way the fluorescence intensity I_F [$photons \bullet L^{-2}t^{-1}$] measures the adsorption kinetics along time:

$$I_F(t) = \frac{I^{I}_{F\,eq.}}{(k'_{ads} + k_{des})}\left[k_{des} + k'_{ads}\, e^{-(k'_{ads}+k_{des})t}\right] \qquad (22)$$

or

$$I_F(t) = \frac{I^{I}_{F\,eq.}}{k'_{ads}/k'_{des} + 1} + \frac{(k'_{ads}/k_{des})I^{I}_{F\,eq.}}{k'_{ads}/k_{des} + 1}\, e^{-(k'_{ads}+k_{des})t} \qquad (23)$$

A nonlinear curve-fitting of the results gives the rate constants k'_{ads} / k_{des}, $k'_{ads} + k_{des}$ [t^{-1}] and $I_F{}^{I}_{eq.}$ [$photons \bullet L^{-2}t^{-1}$].

In the case of known $I_F{}^{I}_{eq.}$:

$$\frac{I_F(t)}{I^{I}_{F\,eq.}} = \frac{1 + (k'_{ads}/k_{des})e^{-(k'_{ads}+k_{des})t}}{k'_{ads}/k_{des} + 1} \qquad (24)$$

From (13) and (20) follows:

$$K_b = \frac{k'_{ads}}{k_{des} \cdot [sorbent]} \qquad (25)$$

A nonlinear curve-fitting of the results according to equation 23 is given by the Model YldFert1 from Origin, version 6.0 .

$$y = a + be^{-kx} \tag{26}$$

With $a = \frac{I^{I}_{F\,eq.}}{k'_{ads}/k_{des}+1}$, $b = \frac{(k'_{ads}/k_{des})I^{I}_{F\,eq.}}{k'_{ads}/k_{des}+1}$, $k = (k'_{ads} + k_{des})$ and $x = t$

It follows that $$\frac{b}{a} = \frac{k'_{ads}}{k_{des}} \tag{27}$$

According to the two-site adsorption kinetic model, it is thus possible to calculate k_{des} [t^{-1}] and $I_F{}^{I}{}_{eq.}$ [$photons \bullet L^{-2}t^{-1}$]. In true equilibrium during long measurement times, the free pyrene concentration is defined as $I_F{}^{I+II}{}_{eq.}$ [$photons \bullet L^{-2}t^{-1}$]. It is in equilibrium with the total absorbed mass of pyrene S_1+S_2 [M].

1.6.4 Calculation of f and K_d in the two domain model

For a complete description of the two domain or bicontinuum model, K_d [L^3 M^{-1}] and f values [non-dimensional] are necessary. These will be given by the measured fluorescence signals $I_F{}^{I+II}{}_{eq.}$ and $I_F{}^{initial}$ and the value calculated in equation 23 for $I_F{}^{I}{}_{eq.}$.

For the understanding of the following equations, the definitions of the mobile fraction and the retardation factor are necessary:

The mobile fraction of a substance (for example Pyrene) is defined by a mass ratio between its mobile mass and its total mass.

$$f_{mobile} = \frac{Pyr_{mobile}}{Pyr_{total}} = \frac{1}{R} \tag{28}$$

It must be remarked that the reciprocal of f_{mobile} is the retardation factor R. For soil column experiments (see 1.6.2), it represents the number of pore volumes that comply with a 50 % breakthrough of the solute. Now f and K_d can be defined as:

$$\frac{I_{F\,eq.}^{I}}{I_{F}^{initial}} = \frac{\left[Pyr_{free}\right]^{I}}{\left[Pyr_{initial}\right]} = \frac{1}{1 + K_d\, f\, \frac{m_S}{V_W}} \qquad (29)$$

$$\frac{I_{F\,eq.}^{I+II}}{I_{F}^{initial}} = \frac{\left[Pyr_{free}\right]^{I+II}}{\left[Pyr_{initial}\right]} = \frac{1}{1 + K_d\, \frac{m_S}{V_W}} = f_{mobile} \qquad (30)$$

The calculation of these parameter is based on the knowledge of the initial pyrene concentration. However, the initial fluorescence intensity of pyrene I_F^0, which corresponds to the initial concentration, can not be measured in-situ, because the adsorption to one type of sorption sites is instantaneous (22). Therefore the initial fluorescence intensity I_F^0 can only be measured ex-situ in the pyrene stock solution.

To solve this problem, a scaling factor for the fluorescence intensity between in-situ and ex-situ measurements must be determined. It can be calculated from the comparison of the in-situ and the ex-situ fluorescence signals of the pyrene solution under equilibrium conditions with the soil phase. Soil water samples for the ex-situ measurements are obtained after centrifugation. According to this procedure, $I_F^{initial}{}_{\text{in-situ}}$ can be derived from:

$$\frac{I_{F\,ex-situ}^{I+II}}{I_{F\,ex-situ}^{initial}} = \frac{I_{F\,in-situ}^{I+II}}{I_{F\,in-situ}^{initial}} \qquad (31)$$

Like the K_d value, the scaling factor is constant for one given test design and the adsorption of one compound by a given soil. Once it is determined, all in-situ measured adsorption kinetics can be interpreted without any further ex-situ measurements.

1.7 Pyrene transport in soil column experiments

For the modelling of the pyrene transport through the soil column, the following assumptions have been made: During the experiment, no significant chemical or biological degradation or production of pyrene can be observed. The solute exists only in the liquid or in the solid phase, there is no pass over into the gaseous phase. A homogeneous flow regime (physical equilibrium) is also assumed, but has to be surveyed by a conservative tracer like bromide.

Like for the batch-experiments, the two-site sorption model with one fraction of instantaneous sorption sites is considered. The effects of hydrodynamic dispersion, molecular diffusion and convective transport are calculated (Jury et al. 1991). The partial differential equation governing one-dimensional nonequilibrium chemical transport of solutes during transient water flow in a variable saturated rigid porous medium (Šimůnek and van Genuchten 1995) are taken as:

$$\frac{\partial \theta c}{\partial t} + \frac{\partial \rho s}{\partial t} = \frac{\partial}{\partial x}\left(\theta D^{w} \frac{\partial c}{\partial x} - \frac{\partial q c}{\partial x} \right) \qquad (32)$$

where c [ML^{-3}] is the solute concentration in the liquid phase, θ [L^3L^{-3}] the volumetric water content and s [MM^{-1}] the mass of the solute in the solid phase. q [Lt^{-1}] is the volumetric flux density, ρ [ML^{-3}] is the soil bulk density and D^w [L^2t^{-1}] is the dispersion coefficient. The dispersion coefficient represents the sum of the hydrodynamic dispersion and the molecular diffusion. The Freundlich adsorption isotherm relating s and c can be formulated as:

$$s = k_f c^n \qquad (33)$$

According to the two site-model, the sorption of pyrene is divided into the instantaneous sorption s_k^e [MM^{-1}] to one fraction of sites and the sorption to the remaining sites s_k^k [MM^{-1}], which is considered to be time dependent. At equilibrium we have for the type-1 (equilibrium) and type-2 (kinetic) sorption sites, respectively:

$$s^e = f s \qquad (34)$$

$$s^k = (1 - f)s \qquad (35)$$

where f [-] is the fraction of exchange sites assumed to be in equilibrium with the solution phase. Because type-1 sorption sites are always at equilibrium, differentiation of equation 34 gives immediately the sorption rate for the type-1 equilibrium sites:

$$\frac{\partial s^e}{\partial t} = f \frac{\partial s}{\partial t} \tag{36}$$

Sorption on the type-2 nonequilibrium sites is assumed to be a first order rate process (33). Following Toride et al. (1993), the mass balance equation for the type-2 sites is given by:

$$\frac{\partial s^k}{\partial t} = \varpi \left[(1-f) \frac{k_f \beta^n}{1+\eta \beta^n} - s^k \right] \tag{37}$$

where ω [t^{-1}] is the first order rate constant. Assuming a Freundlich Adsorption isotherm, η must be set to zero.

To facilitate a better overview of the model run, the initial and boundary conditions will be specified in “Discussion”.

To proof the suitability of the model applied, it is necessary, to define quality criteria for the fitted data. For this purpose Nash and Sutcliffe introduced in 1970 the frequently used coefficient of model efficiency. It is applied to all soil column breakthrough data in this work.

$$CME = \frac{\sum_{i=1}^{n} (x_o(t) - x_{omean})^2{}_i - \sum_{i=1}^{n} (x_o(t) - x_s(t))^2{}_i}{\sum_{i=1}^{n} (x_o(t) - x_{omean})^2{}_i} \tag{38}$$

where x_o is the observed value, x_s is the simulation result at time t and x_{omean} is the arithmetic mean of the observed values.

2. Evaluation of current measurement techniques

2.1 Sorption of PAH´s in batch experiments

For the quantitative description of the sorption and transport behaviour of a substance, it is necessary to measure all sorption parameters. The classic way to determine partition coefficients are batch experiments. Therefore a certain amount of soil or sediment is shaken in a constant volume of an aqueous solution of the compound. In different preparations, the concentration of the compound within the solution is varied. At the end of the experiment, liquid and solid phases are separated and the concentration of the compound is determined for both phases separately. Plotting the concentrations against each other for a constant temperature, the resulting Freundlich-isotherm follows equation 1. For the determination of the isotherm it is important, that both phases reached a sorption equilibrium, which means that the net rate of adsorption is zero.

The advantages of classic batch experiments with phase separation by centrifugation or ultra-filtration at the end of the test are relative high reproducibility, low laboratory effort and low time exposure. However phase separation is associated with some problems. Centrifugation and filtration processes lead to a concentration of the sample. This can change the quantity and quality of the interactions between the components of the sample (Aiken and Leenheer 1993). As stated before (see page 1), measurements of the adsorption kinetics of pyrene create additional problems due to the very fast adsorption to some water soluble soil components.

2.2 Sorption studies without phase separation

Many authors emphasise the advantages of procedures without soil phase separation, like solid phase micro extraction (Belardi and Pawliszyn 1989, Ohlenbusch et al. 2000), the use of twister (Baltussen et al. 1999, Popp et al. 2001), or fluorescence technics (Backhus and Gschwend 1990, Chen and Bada 1990, Danielsen et al. 1995, Haitzer et al. 2000, Frimmel 2000). One additional advantage of fluorescence measurements is the opportunity of online detection of the fluorescence signal to achieve a continuous environmental monitoring (Marhaba et al. 2000).

One approach to follow the adsorption of hydrophobic compounds to soil material is the dialysis technics. A semipermeable membrane divides the reaction vessel. While the compound of interest should be able to pass through it without delay, the soil material should be confined on one side of the membrane. De Paolis and Kukkonen (1997) used equilibrium dialysis to study the adsorption of benzo(a)pyrene and pentachlorophenol to humic and fulvic acids from sediments. They examined the influence of the pH-value and the aromatic content of the humic material. Rav-Acha and Rebhun (1992) used a two compartment cell, to study the binding of fluoranthene to humic acids. The molecular cut off of the membrane was 1000 Da. It was found adequate to allow the passage of fluoranthene, but not of humic acids. Akkanen et al. (2001) combined the dialysis technics with biotests for Daphnia magna, to study the influence of DOM on the bioavailability of atrazine, pyrene and benzo[a]pyrene. In the presented experiments only the bioavailability of benzo[a]pyrene was effected by DOM. The studies cited above are based on equilibrium dialysis experiments.

The dialysis technics can be used also, to follow the adsorption kinetics of one compound to different surfaces. For this purpose, it is necessary that the compound of interest can pass through the membrane without any hindrance, i.e. the permeability kinetics are much faster than the adsorption kinetics.

2.3 Laser-induced Fluorescence Spectroscopy

2.3.1 Soil-related applications of laser-induced fluorescence spectroscopy

The laser-induced fluorescence spectroscopy (LIF) has some advantages over classical fluorescence measurements. Because the fluorescence signal is proportional to the intensity of the excitation light (Perrin´s equation), the high intensity of the laser beam leads to an increased sensitivity of LIF. A high selectivity and short laser pulse widths (0.5 ns for some nitrogen laser) are further advantages. Richardson and Ando used LIF in 1977 to determine pyrene and four other PAH´s in methanol at concentrations below 1 µg/l.

LIF is widely used in atmospheric and hydrospheric research. Since LIF provides the possibility of in-situ measurements, it is an interesting technique for the study of environmental processes under natural conditions (Löhmannsröben 1997). Todd et al. (1993)

applied in-situ laser-based fluorescence measurements to groundwater monitoring regarding contamination with carbazole and p-cresol. Stevenson and Vo-Dinh (1995) analysed six component mixtures of PAH´s by laser-excited synchronous fluorescence measurements and Rudnick and Chen (1998) determined pyrene in seawater by LIF. Reyes et al. (2000) used LIF for the determination of the pyrene concentration on silica surfaces. Whitcomb et al. (2002) combined LIF with solid phase extraction to measure the concentrations of 15 PAH´s on SPE membranes.

Laser applications in the pedosphere and aquifers systems are rare. Newer investigations of petroleum products in soils have shown that a quantitative determination of oil contaminations is possible directly on soil surfaces with LIF spectroscopy (Schade and Bublitz 1996, Löhmannsröben and Roch 1997). These measurements were carried out on the soil surface or through the glass wall of soil columns. An analysis of compounds in the inner part of soil columns is not reported so far. On a larger scale Apitz et al. (1992) measured petroleum hydrocarbons through a sapphire window on a probe, which is pushed into the ground by a truck-mounted cone penetrometer.

2.3.2 The photobleaching effect in LIF

A challenge for the application of LIF to the analysis of polycyclic aromatic hydrocarbons is the photobleaching effect. Although the effect is known for a long time, the mechanism is still not completely understood.

Zepp and Schlotzhauer (1979) stated that singlet oxygen, an excited form of molecular oxygen, is the key intermediate in photooxygenations. The kinetic data for the direct photochemical reactions of pyrene and other PAH´s in water could be described by a first-order rate equation. Chen et al. (1996) found photolysis processes following pseudo-first-order kinetics. They emphasised that complex phenomena, such as photochemical transformation, result from many, often independent processes. Internal and external factors can be identified which are likely to affect the photochemical transformation. Internal factors are chemical structural features that influence the absorption of light. External factors include exposure parameters such as the proportion of the co-solvent, pH, temperature, salinity and the concentration of dissolved oxygen.

Furthermore Chen et al. (2001) postulated that reactive oxygen species and hydroxyl radicals probably do not contribute to the photolysis mechanism of PAH´s. The initial step in the photodecomposition is most likely a photoionisation which yields the PAH radical cation and a hydrated electron. This is followed by PAH elimination reactions involving water molecules.

Lehto et al. (2000) analysed the photochemical reactions of pyrene and three other PAH´s. The reaction kinetics followed a first order equation. Oxygen concentration had minor or non effect upon the photodegradation rates of PAH´s. According to the authors, it is generally accepted that the photodegradation of PAH´s in solution is an oxidative process which is highly accelerated by the presence of photo-initiators. In general the more polar the solvent, the faster the degradation process of PAH´s.

Sigman et al. (1998) accomplished an extensive study about the mechanisms of pyrene photolysis. In their experiments, the rate of photochemical decomposition was not effected by the addition of $HgCl_2$, a known triplet quencher. The triplet state of pyrene is thus probably not involved in the oxidation mechanism. On the other hand the removal of oxygen by argon purge slowed the photochemical decomposition by approximately a factor of four. These results suggest that in this case oxygen is important for the photochemical degradation of pyrene in water. The authors identified 1-hydroxypyrene as a product of the initial photochemical oxidation. Probably, the first step in the oxidation mechanism involves an electron transfer from the excited singlet state of pyrene to molecular oxygen.

A different situation is given if pyrene is absorbed on surfaces. Reyes et al. (2000) carried out some experiments with pyrene adsorbed on silica. They found, that the pyrene radical cation can be formed either by energy transfer from excited pyrene to molecular oxygen or by photoionisation of adsorbed pyrene. The reaction of radical cations with physisorbed water on silica surfaces can lead to the formation of 1-hydroxypyrene. It is postulated, that 1-hydroxypyrene can undergo secondary photolysis to dihydroxypyrenes. In contact with air, they can be oxidized to diones.

3. Materials and methods

3.1 Preparation of the aqueous pyrene solution

3.1.1 Stability check of an unsaturated stock solution

The fluorescence intensity of pyrene stock solutions of different concentrations was analysed by classic fluorescence spectroscopy (Perkin Elmer LS 30, auto sampler). All samples were compared with and without centrifugation. The stock solution was prepared in 1 l Schott Duran bottles with PTFE caps. 1 ml of an ethanolic pyrene solution was dispersed on the inner surface of the bottle. After the ethanol was evaporated under argon atmosphere, a thin film of pyrene remained. The appropriate amount of water was added and the bottles were shaken for 48 hours on a horizontal shaker at 90 strokes per minute. One of the samples was stirred at 48 °C with a Teflon-coated stir bar, instead. The nominal concentrations of the aqueous pyrene solutions were 50 µg/l, 100 µg/l and 150 µg/l. The centrifugation was carried out at 23 °C for two hours at 10000 rpm. The Corex centrifuge tubes had a volume of 30 ml, the Kontron Instruments centrifuge Centrikon T-324 was equipped with a A 8.24 cat. no. 202100 Rotor. To quantify the adsorption on the Corex glass, one sample was stored in the centrifugation tube for two hours at 23 °C without centrifugation.

3.1.2 Preparation of unsaturated pyrene solutions using ultrasonic

The aqueous 50 µg/l pyrene solution was prepared in 1 l Schott Duran bottles as described before. Afterwards it was treated with ultrasonic to destroy micro crystals, which might have grown during the preparation process. One aliquot of the solution was transferred directly into 50 ml volumetric flasks, a second one into 30 ml Corex tubes without centrifugation and the last one in Corex tubes with centrifugation. All samples were stored at 23 °C in the dark. Centrifugation was carried out for two hours at 10000 rpm and 23 °C. Preliminary to the fluorescence measurements (Perkin Elmer LS 30, auto sampler) all samples were transferred into 50 ml volumetric flasks.

3.1.3 Quantification of wall losses

In this experiment the aqueous pyrene solution was transferred successively into all glass vessels that are used for batch experiments:

1 l Schott Duran bottles with Teflon caps
100 ml Erlenmeyer flasks with Teflon caps
30 ml Corex centrifuge tubes

After each transfer the loss of free pyrene was measured by classic fluorescence measurements (Perkin Elmer LS 30, auto sampler).

3.1.4 Fluorescence spectra of pyrene

The fluorescence spectra of aqueous pyrene solutions were analysed by classic fluorescence measurements with a Perkin Elmer LS 50 equipped with a 1 cm quartz glass cuvette. To yield results which are comparable to measurements with the nitrogen laser the excitation wavelength was set to 337 nm. The width of the excitation slit was 5 nm, the width of the emission slit 2.5 nm. The scan speed of the spectrometer was 100 nm/min and the number of accumulation scans was 2. For the preparation of the aqueous pyrene solution 1 ml of an ethanolic solution was filled in a 1 l Schott Duran bottle. After the ethanol was evaporated under argon atmosphere, the appropriate amount of water was added. The solution was mixed on a horizontal shaker at 90 strokes per minute for 48 hours.

3.2 Validation of fluorescence measurements by comparison with gas chromatography - mass spectroscopy (GC-MS)

To control the quality of the solution preparation and handling and the quality of the fluorescence measurements, the results of classic fluorescence measurements (Perkin Elmer LS 30, auto sampler) were compared with results of the Gas Chromatography - Mass Spectroscopy (GC-MS). The aqueous samples of ascending concentrations were extracted by solid phase extraction (SPE) on C18 cartridges (Chromafix glass cartridges, Macherey-Nagel). Afterwards the samples were transferred to acetonitrile 3:1 toluene and analysed by GC-MS.

An organic standard of 100 mg/l pyrene in acetonitrile 3:1 toluene was prepared for calibration. This solution was analysed by GC-MS, without dilution and in dilution steps at ratios of 1:5, 1:10 and 1:20. 15 ml of the solution were given on C18 cartridges (Cromafix glass cartridges, Macherey-Nagel). The cartridges were dried and extracted with 2.5 ml acetonitrile/toluene. The samples were dried in a nitrogen flow and solved in 100 µl acetonitrile/toluene afterwards. These samples were injected into a Thermo Finnigan GC 9000 / MAT 4500 quadrupole system.

For the analysis of the aqueous pyrene solutions, the C18 cartridges have to be pre-conditioned. For this purpose they were fed with one column volume of acetonitrile, one of methanol and one column volume of distilled water.

For the preparation of the aqueous samples, 2 ml of an ethanolic pyrene solution [200 mg/l] were given into a 5 l flask with glass cap. After evaporation of the ethanol with argon, a thin pyrene film remained on the inner surface of the flask. Three litre of deionised water were added and the flask was shaken for 48 h on a horizontal shaker. The resulting aqueous pyrene solution was filtered through a glass fibre filter (Schleicher & Schuell GF55). Afterwards the stock solution was thinned at different ratios with deionised water to receive the final concentration. Depending on the concentration, ascending volumes of the solution were given on the SPE columns. For the transfer of the samples no pipettes were used to avoid adsorption to the glass material. The samples were poured directly on the SPE cartridges. The effluent of the columns was caught and weighted back.

3.3 Dialysis experiments

In this test an aqueous pyrene solution was dialysed against deionised water. The cellulose dialysis membrane had a 1000 Da molecular weight cut off and a thickness of 50 µm (SpectraPor 6, Spectrum Laboratories). The dialysis bag was fixed on a sinter glass cylinder and filled with 102 ml of a saturated aqueous pyrene solution. The outer compartment with a volume of 168 ml was filled with deionised water. The fluorescence intensity of the solution in the outer compartment was analysed continuously by classic fluorescence measurements (Perkin Elmer LS 50) in a 1 cm quartz cuvette.

3.4 Quenching of pyrene fluorescence by aqueous DOM solutions

3.4.1 Quenching effect of two soil effluents and Aldrich humic acid

The fluorescence intensity of two soil effluents and an aqueous solution of Aldrich humic acid was measured by classic fluorescence measurements (Perkin Elmer LS 50) in a 1 cm quartz cuvette.

A field soil from the test site Krauthausen (pseudogley, average C org. content: 2.3 %) and a forest soil from Jülich (Parabraunerde (pseudogley), C org. content: 6.4 %) were dried in a drying chamber at 40 °C and sieved to two millimetre. Afterwards they were extracted in acrylic glass columns of 25 cm height and a diameter of 7 cm. The columns were packed with the dry soils under constant vibration on the base plate of a sieve shaker. After saturation the soils were irrigated with 60 ml/h. The ceramic frit at the soil bottom had a maximum pore size of 6 µm. The effluent was caught in 1 l Schott Duran bottles with teflon caps. To remove particular soil material the samples were centrifuged for 30 minutes at 10000 rpm. The analytical TOC-concentration of the elutriates was 65 mg/l for the field soil and 36 mg/l for the forest soil (Dohrmann DC-190, Rosemount Analytical). The Aldrich humic acid was dissolved in deionised water at a concentration of 30 mg/l. All solutions were spiked at a ratio of 1:1 with an aqueous pyrene solution (100 µg/l). For analysis the samples were transferred to the quartz cuvette by Pasteur pipettes. The excitation wavelength was 337 nm to yield comparable results to LIF measurements. The width of the excitation slit was 5 nm, the width of the emission slit 2.5 nm.

3.4.2 Impact of the eigen-fluorescence of Aldrich humic acid

The eigen-fluorescence of Aldrich humic acid at different concentrations and its influence on the pyrene fluorescence was analysed in this experiment. For this purpose ascending amounts of the humic acid were given to deionised water and to an aqueous pyrene solution [100 µg/l]. Both series were analysed by classic fluorescence measurements (Perkin Elmer LS 50) in a 1 cm quartz cuvette.

3.4.3 Correction of the inner filter effect

The absorption of the humic acid solution was measured at the excitation and the emission wavelength of pyrene (UVIKON 860, Tegiventa AG), to correct the data for the inner filter effect (according to Lakowicz). The data were also corrected for the eigen-fluorescence of the humic acid. The sample preparation followed the same procedure as in experiment 4.4.2.

3.5 Development of the glass probe head

3.5.1 Technical development of the glass probe head

For the development of the glass probe head the components of the laser system are decisive. Especially the desired time resolution of the measurements is important for the probe head design. Fig. 3 gives an overview of the laser system and the detection unit.

The nitrogen laser MSG 801 SD produced by Lasertechnik Berlin GmbH has a pulse power output of 400 kW and a pulse energy of 200 µJ. The characteristic nitrogen emission wavelength is 337.1 nm. The pulse duration is 500 ps and the outlet beam diameter is 1.5 mm. Over pivoting mirrors, the laser beam can be guided through a dye cuvette or can be coupled directly into the fibre optic cable. The fibre optic cable with a length of 18 m is equipped with a steel coated point, to avoid adsorption of sample material on its surface. It contains one central glass fibre to transmit the excitation light and six glass fibres in a radial arrangement for the fluorescence detection (see Fig. 3).

The detection unit consists of a delay generator, a spectrograph and a charge-coupled device camera. The delay generator (Stanford Research Systems; DG 535) synchronises the laser pulse with the detection time window of the CCD camera. An appropriate definition of the time window opens the opportunity to excludes interfering fluorescence signals. Therefore, the background signal can be reduced considerably. The spectrograph MS 125^{TM,} Type 77400 of LOT-Oriel diffracts the detected fluorescence light. The CCD camera (IntaSpec V, iccd) detects the fluorescence light with a high time resolution which allows the analysis of fast adsorption kinetics. The characteristic mercury wavelength of a spectral calibration lamp (LOT-Oriel, 6035) were used for the calibration of the spectrograph: 365.0 nm; 404.7 nm; 435.8 nm; 546.1 nm; 577.0 nm and 579.1 nm.

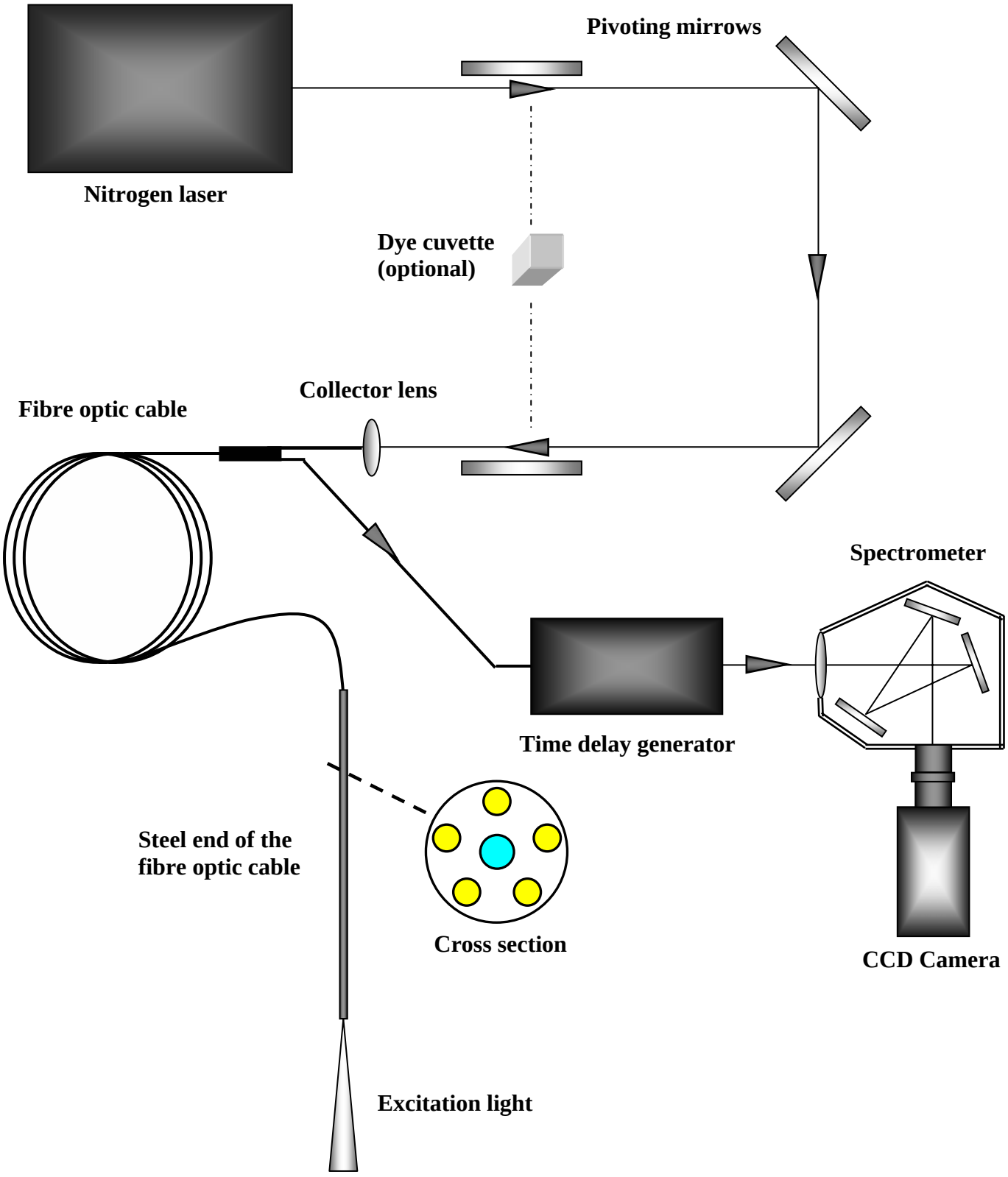

Fig. 3: The components of the laser system and the detection unit composed of the time delay generator, the spectrometer and the CCD camera.

A small test facility was established, to assure reproducible conditions for the measurements of the optical characteristics of each probe head (Fig. 4). The suprasil probe head was fixed vertically in a tripod. To eliminate external light the test solution was measured in a beaker, coated with black pasteboard and the laboratory was completely shaded during the measurements. The steel coated light fibre was coupled into the end of the probe head. The time slot for the detection of the fluorescence was optimised with the delay generator for each probe head design. This was necessary, because the propagation time of the light within the probe head is depending on the geometry of the probe tip.

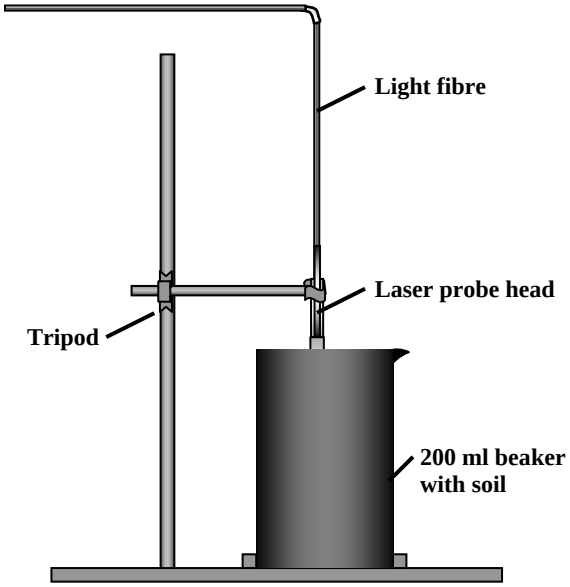

Fig. 4: Test facility for the development of the suprasil probe head.

3.5.2 Scattering of the fluorescence signal by the probe head

To analyse the effects of the suprasil probe head to the pyrene fluorescence spectrum, the fluorescence of an 100 µg/l aqueous pyrene solution was measured with and without the probe head. Both experiments were conducted in the test facility described above. The time gate of the delay generator was set to 247-1000 ns for both tests. All LIF measurements were carried out in a dark room at a constant temperature of 23 °C.

3.6 Spiking of the soil

Three different procedures of adding pyrene to sand were tested in this experiment. To remove all organic compounds, the sand was annealed at 600 °C for 48 hours. The specific surface of the annealed sand was determined by multipoint BET measurements. The results of an elemental composition analysis are given in appendix 2. For all three spiking methods 150 g of annealed sand were spiked in 200 ml Schott Duran beaker. The LIF measurements were conducted in the test facility shown in Fig. 4.

3.7 Influence of the water content on the fluorescence signal

The aim of this experiment was to analyse the influence of the water content on the fluorescence signal of pyrene. For this purpose, annealed sand was spiked 4 mg pyrene per kg sand. Subsequently the fluorescence signal was measured at different water contents. The stock solution contained 50 mg pyrene in 100 ml methanol. Eight millilitre of it were added to 1 kg sand and homogenised well. The sand was spread in a thin layer in an extractor cowl to allow complete evaporation of methanol. Every twenty minutes it was upturned and homogenised. After four hours 150 g aliquots of the sand were placed in 200 ml beaker and moistened with increasing amounts of water. The LIF measurements were conducted in the test facility described above.

3.8 Batch experiments

3.8.1 Adsorption kinetics of pyrene to annealed sand

Several experiments were conducted to collect data about the adsorption kinetics of pyrene. In the first experiment 50 ml solution with increasing pyrene concentrations were given to 100 g of annealed sand in 200 ml Schott Duran beaker. The first test series was analysed by LIF immediately after sample preparation, the second test series after an equilibration time of 14 hours. All sorption and column experiments were conducted at a constant temperature of 23 °C, because temperature has a significant effect on pyrene adsorption (Mader, Goss and Eisenreich 1997).

Based on the results of this experiment, further tests were designed to follow the adsorption kinetics to annealed sand. 100 g of annealed sand were spiked with 50 ml of a 100 µg/l pyrene solution in 200 ml beaker. The LIF measurements were started after an equilibration time of 10 minutes. The irradiation time per measurement was limited to 20 seconds per measurement point, to exclude the photolysis of pyrene. The experiment was kept in the dark at 23 °C over the entire test period of 28 hours. It was repeated under identical conditions.

3.8.2 The photobleaching effect in LIF

For this experiment, a 100 µg/l aqueous pyrene solution was irradiated in intervals in a flow-through cuvette of a fluorescence spectrometer.

The fluorescence spectrometer (Perkin Elmer LS 4) of an HPLC system was used to determine the pyrene fluorescence by a pulsed xenon discharge lamp (output: 8.3 W). The flow-through measurement cell and all in- and outlet capillaries were pre-equilibrated by the 100 µg/l pyrene solution. The pulsed xenon discharge lamp was adjusted to 337 nm for irradiation. After repeated equilibration steps for the steel capillaries, the pyrene solution was injected by a Hamilton Syringe. The measurement volume was irradiated by the pulsed xenon lamp in the intervals specified in “Results”.

In further tests, the photolysis of pyrene was studied in-situ with the nitrogen laser as the excitation source. 60 ml of pyrene solution [100 µg/l] were added to 150 g of annealed sand in 200 ml Duran Schott beaker. The measurements were conducted in the test facility (Fig. 4) and the end of the Suprasil probe head was fixed in the sand as described before. The repetition rate of the laser pulse was 5 Hz for the first 30 min, afterwards it was adjusted to 1 Hz. The gate delay time of the CCD camera was set to 62 ns, the gate width to 600 ns. The camera had a gain of six and the exposure time was 0.034 s. The laser system was switched off over night and before the first measurement on the next day a warm up period of 30 min. guaranteed for full laser energy.

3.8.3 Adsorption kinetics of pyrene to a forest soil

The A-horizon of the forest soil “Jülich”, characterised in appendix 4, was sampled in February 2001. It was homogenised, air-dried and sieved to 2 mm. Until the start of the experiment it was stored in an air-conditioned room at 12 °C in the dark.

At the start of the experiment 80 g of the soil was moistened by 20 ml of deionised water, to allow subsequently instantaneous infiltration of the pyrene solution. The 200 ml Schott Duran beaker was placed in the measuring device (Fig. 4) and the Probe head was fixed in a vertical position. After 30 minutes, 70 ml of the aqueous pyrene solution were added and the LIF detection was started immediately.

Due to the very short in-situ fluorescence signal of pyrene, a second experiment was conducted at a very high water to soil ratio in a classic batch experiment. 80 ml of an aqueous pyrene solution [100 µg/l] and 0.6 g of the soil were placed in 100 ml Erlenmeyer flasks. The samples were shaken overhead in 100 ml Erlenmeyer flasks at 20 °C in the dark. After 0.5; 2.5 ; 5; 24; and 48 hours samples were centrifuged for two hours at 10000 rpm at a constant temperature of 20 °C. Afterwards the free pyrene concentration was detected by a Perkin Elmer LS 30 fluorescence spectrometer with a flow-through cuvette at an excitation wavelength of 337 nm. The width of the excitation slit was 10 nm. Two time steps of the experiment were repeated under identical conditions in a second test.

3.8.4 Adsorption kinetics of pyrene to annealed soils

The A-horizon of both soils, the forest soil “Jülich” and the sandy soil “Kaldenkirchen” (characterised in appendix 3 and 4) were sampled in February 2001. The samples were homogenised, air-dried, sieved to 2 mm and stored at 12 °C in the dark. At the start of the experiment, samples of both soils were annealed for 48 hours at 600 °C to remove all organic substances. The specific surface and the control measurements of the carbon content of the annealed soils are given in appendix 3 and 4.

In the first experiment, 150 g of the sandy soil from Kaldenkirchen were moistened with 50 ml of an aqueous pyrene solution. The reduction of the free pyrene fluorescence over time was analysed by in-situ LIF measurements in the measurement device (Fig. 4). The samples were irradiated only for 20 seconds at each measurement point, to exclude a significant photolysis effect. The reproducibility of the sample preparation and the measurement setup was tested in a second test under identical conditions.

3.9 Soil Column Experiments

The soil column experiments were conducted parallel in three columns, installed in a steel rack. The irrigation and sampling device consisted of an HPLC pump (Knauer, WellChrom K-501), a control PC, a storage container and an irrigation head. All tubes and other materials, in contact with the pyrene solution, were low adsorbing like teflon or Duran glass. Glass frits were smelted in at the bottom of the columns (38 % porosity, max. pore size 1.3 µm). A three way valve at the column outlet offered the possibility to fractionate the percolate. An overview of the arrangement is given in Fig. 5.

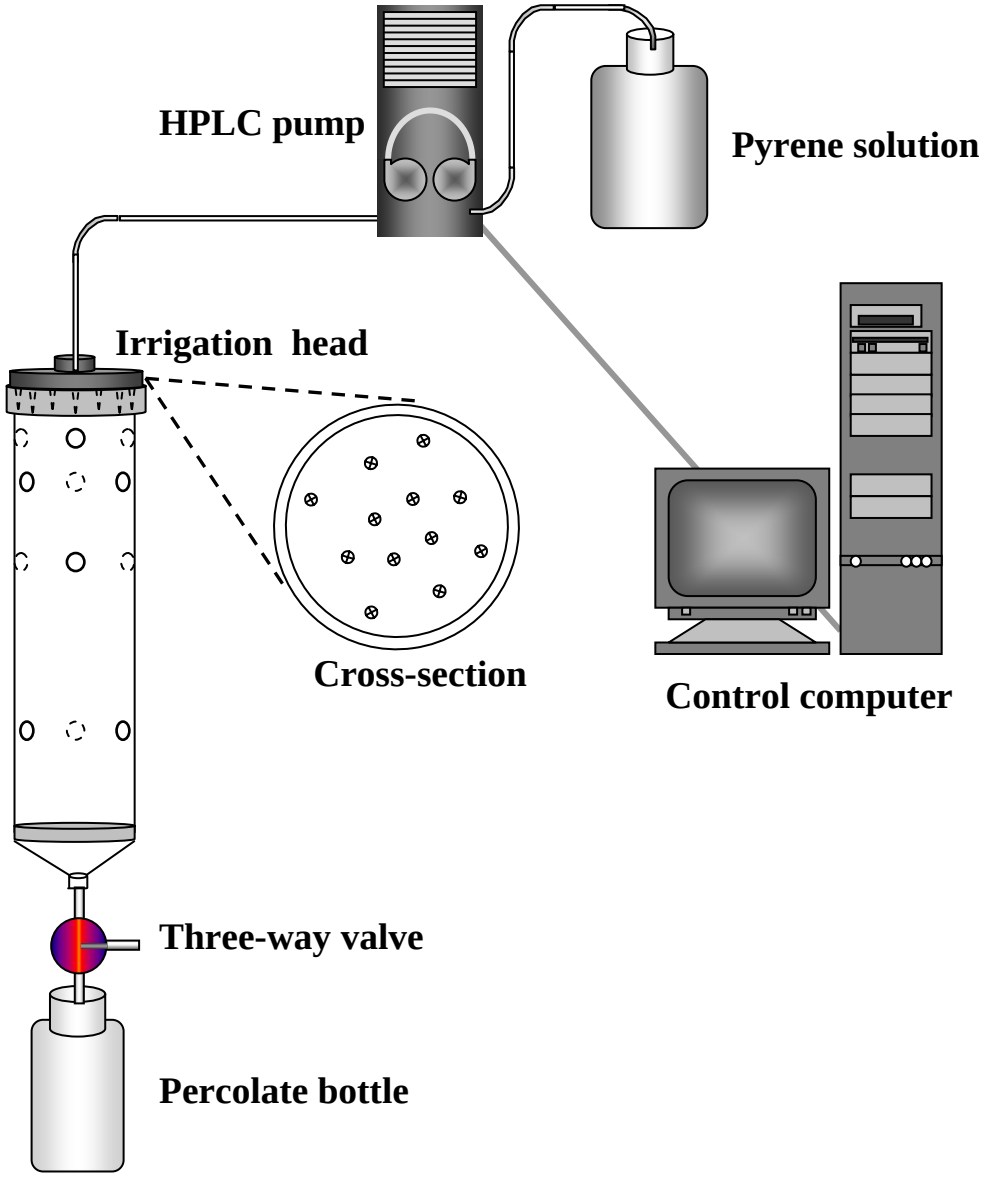

Fig. 5: Schematic configuration of the soil column experiments. The PC-controlled HPLC pump allows a constant irrigation of the soil columns.

The self developed glass columns were designed to avoid adsorption of pyrene as far as possible. Schott Duran GL-14 screwed tube connections were smelted into the column mantel at four different levels. Twelve Suprasil probe heads can be inserted into the GL-14 threads and fixed by perforated teflon caps. The exact dimensions and two photos of the glass columns are given in the figure below.

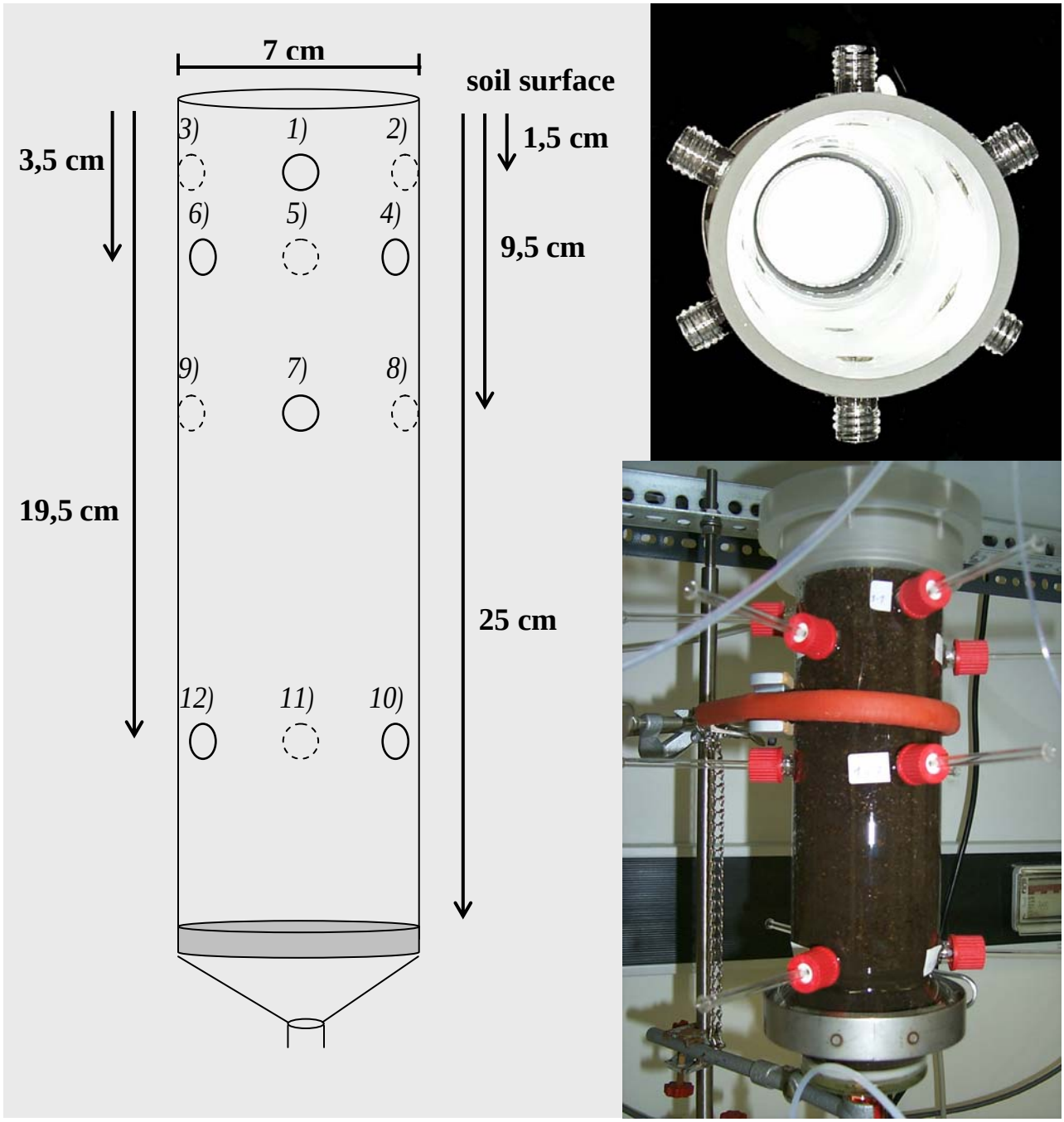

Fig 6: Dimensions of the glass columns, equipped with twelve LIF probe heads on four levels.

4. Results

4.1 Preparation of the aqueous pyrene solution

4.1.1 Stability check of an unsaturated stock solution

The values found in literature for the solubility limit of pyrene in water vary around 130 µg/l. Therefore the stability of three aqueous pyrene solutions was checked at concentrations of 50 µg/l, 100 µg/l and 150 µg/l. The quantification of the free pyrene concentration was accomplished by classic fluorescence measurements. The solutions were shaken on a horizontal shaker at room temperature with 100 strokes per minute. The influence of wall adsorption and the effect of $CaCl_2$ on the free pyrene concentration were tested.

An important aspect of the experiment was to determine the influence of centrifugation on the aqueous solutions. The samples were centrifuged for two hours at 10000 rpm and 15 °C. Centrifugation has been carried out in 30 ml Corex-tubes, all other conditioning steps in 50 ml volumetric flasks. The fluorescence intensities with and without centrifugation are compared in the following diagram.

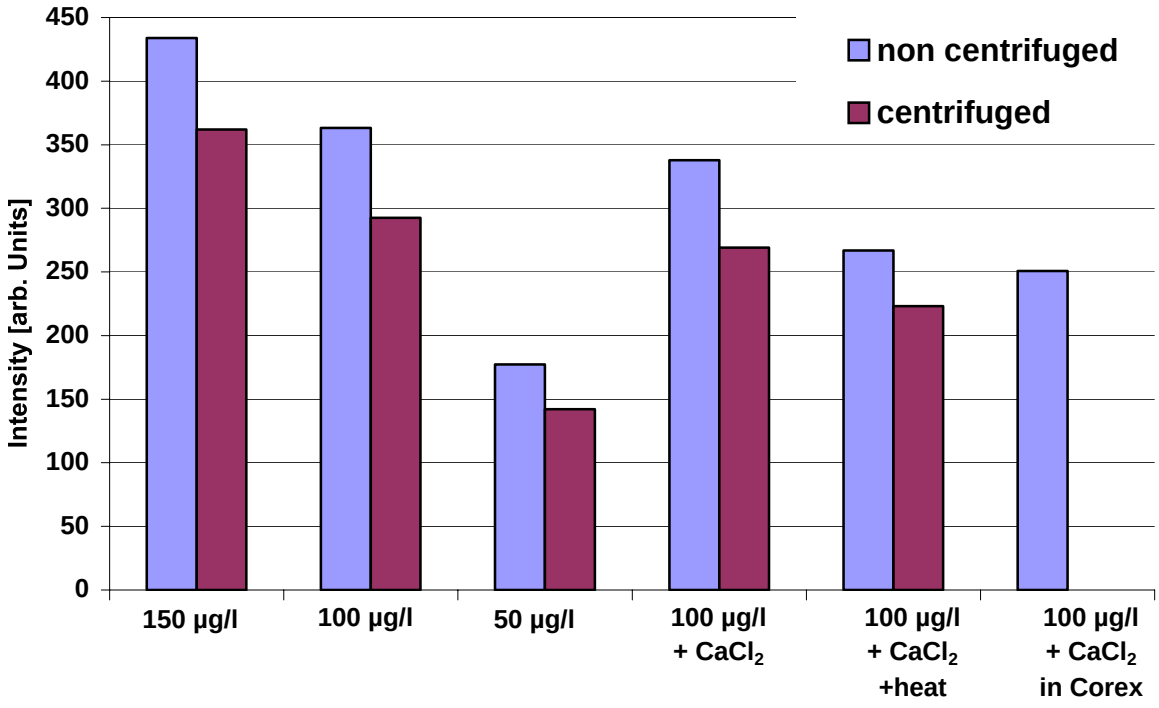

Fig. 7: Effect of centrifugation and the addition of $CaCl_2$ on aqueous pyrene solutions at nominal concentrations of 50 µg/l, 100 µg/l and 150 µg/l.

Different aspects can be observed from the data. First of all, the initial fluorescence intensity of the nominal 100 µg/l solution is twice as high as the intensity of the 50 µg/l solution (factor 2.0). On the other hand the intensity of the 150 µg/l solution is not threefold higher (factor 2.4). The intensity of the centrifuged samples is about 16 % to 20 % lower than the intensity of the uncentrifuged solutions. The addition of $CaCl_2$ leads to a reduction of the fluorescence signal of 8 % in the centrifuged sample and a reduction of 7 % in the non-centrifuged sample. The transfer of the 100 µg/l solution into 30 ml Corex-tubes for two hours without centrifugation leads to a reduction of the fluorescence signal of 25 %.

4.1.2 Preparation of unsaturated pyrene solutions using ultrasonic

An 50 µg/l aqueous pyrene solution was prepared to check the effect of ultrasonification on its stability at room temperature. The contact to the wall of the Corex tubes as well as the centrifugation itself, lead to a decrease of the fluorescence signal. The relative reduction is 5 % and 11 % respectively.

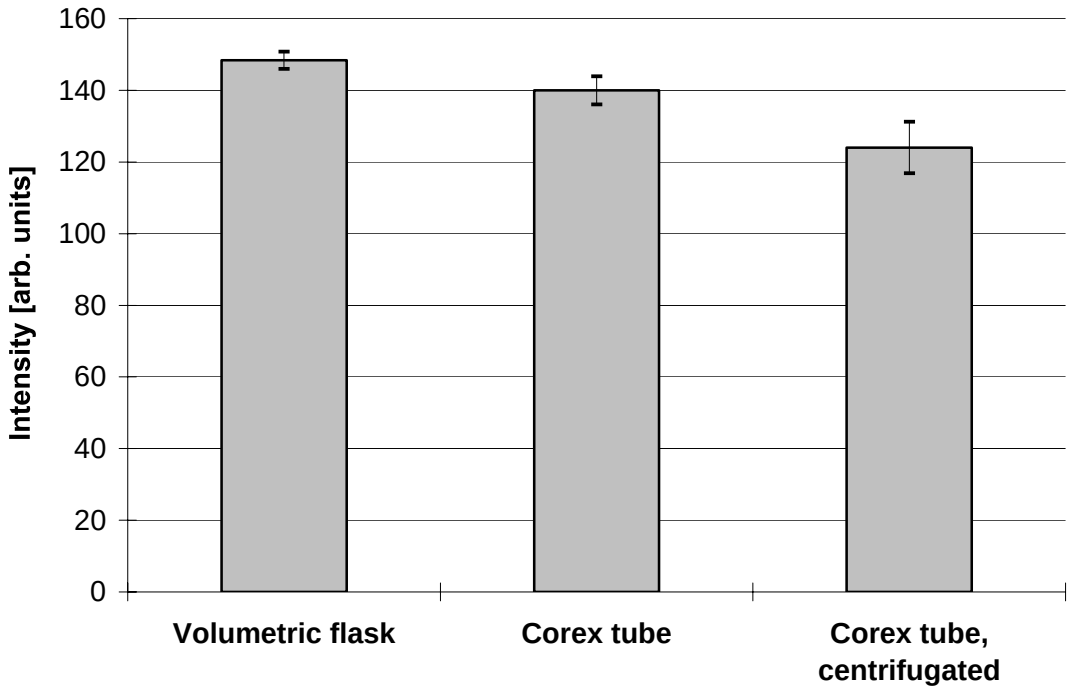

Fig. 8: Quantification of wall losses to Corex centrifuge tubes and centrifugation effects. Presented data are of four parallels, the error bars show the standard deviation.

4.1.3 Quantification of wall losses

To quantify the wall losses, several consecutive conditioning steps have been carried out with the aqueous pyrene solution. Of particular interest were the wall losses relative to the initial concentration. For that reason the pyrene solution was transferred successively into the glass vessels listed below. After an equilibration time of two hours, the fluorescence signal of the solution was measured in a quartz cuvette.

The first result that attracts the attention is the saturation effect at a concentration of 150 µg/l. The fluorescence signal is nearly the same for all conditioning steps similar to a concentration of 100 µg/l. In contrast to this result, the signal of the 50 µg/l solution reproduces clearly the nominal concentration. The values range between 45 % and 53 % of the signal of the 100 µg/l solution. For all nominal concentrations the effective pyrene concentration in solution decreases with the number of conditioning steps. The maximal decrease of the fluorescence signal compared to the stock solution is 24 % at 50 µg/l, 27 % at 100 µg/l and 25 % at 150 µg/l. By adding $CaCl_2$ (10 mmol/l) the concentration of free pyrene in solution is decreased about 3 % and 5 % respectively. The missing values in the last three conditioning steps are due to broken centrifuge tubes during the experiment.

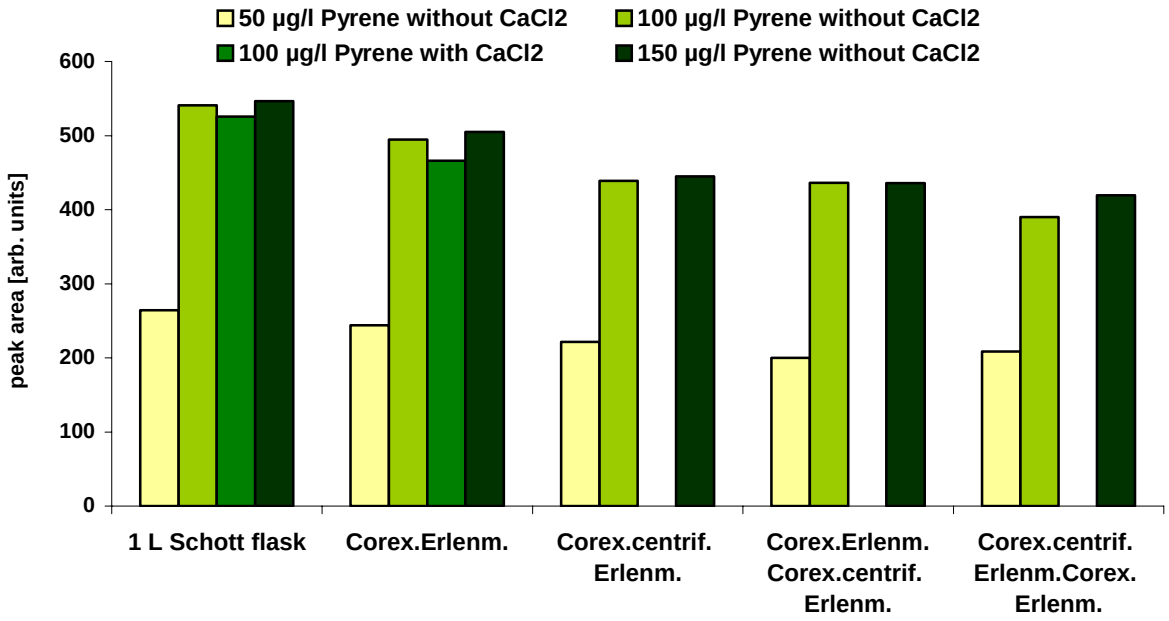

Fig 9: Wall losses of aqueous pyrene solutions of different concentrations in diverse glass vessels.

4.1.4 Fluorescence spectra of pyrene

The question of interest in this test was to define the appropriate range of concentration for aqueous pyrene solutions analysed by fluorescence spectroscopy. The following diagram shows the fluorescence spectra for several initial weights. The characteristic emission bands of pyrene in water at 372 nm, 382.5 nm and 392.5 nm are distinctive.

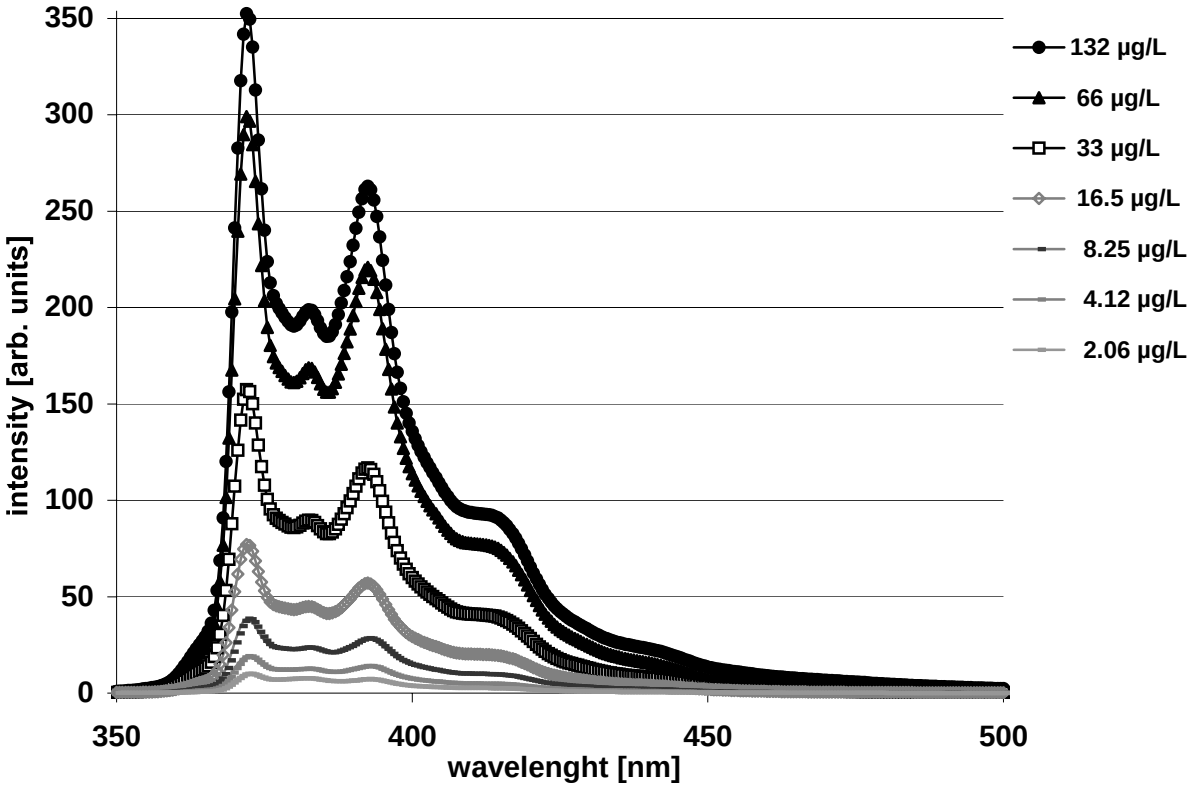

Fig 10: Fluorescence spectra of pyrene in aqueous solution at different nominal concentrations.

The results show a linear correlation between the fluorescence intensity and the nominal concentration, almost about the whole concentration range. Only at the highest concentration of 132 µg/l the fluorescence signal is lowered by saturation effects. To give a better overview of the data, the following graph shows the linear correlation for the three pyrene peaks in water.

The linear regression between the nominal concentration and the intensity of the pyrene fluorescence gives high correlation coefficients between 0.9979 and 0.9991. Corresponding to the characteristic size of the typical pyrene fluorescence peaks in water, the three data series show different slopes. At the excitation wavelength of 337 nm, the fluorescence signal of the solution is not depending on the pyrene concentration.

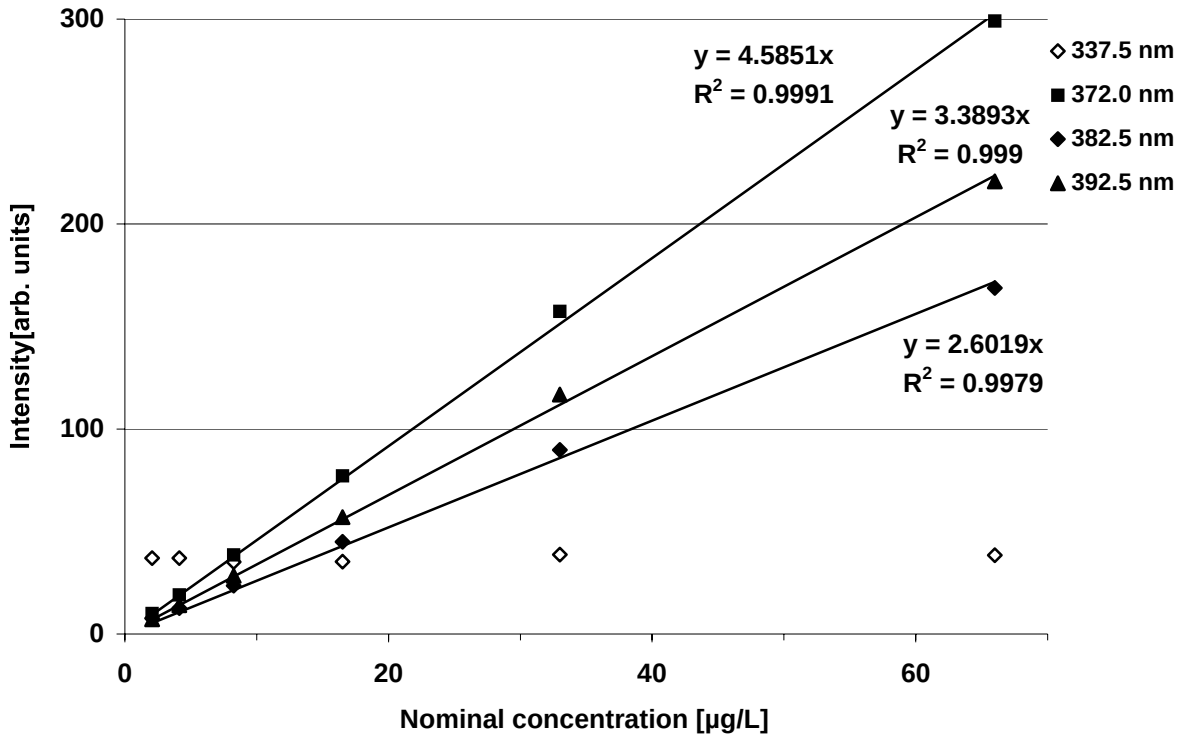

Fig 11: Correlation between nominal concentration and fluorescence intensity of pyrene in aqueous solution. The series above show the fluorescence intensity at the characteristic emission wavelengths of pyrene. The open symbols illustrate the signal at the excitation wavelength (337 nm).

4.2 Validation of fluorescence measurements by comparison with gas chromatography - mass spectroscopy (GC-MS)

This experiment was designed to yield an estimation of the quality of the fluorescence measurements. For this purpose we compared results of the GC-MS with the results of the fluorescence analyser Perkin Elmer LS 30. This unit is equipped with an attenuator, to gain linear concentration to signal ratios over a wider range. The following graph shows the fluorescence signals with and without attenuator.

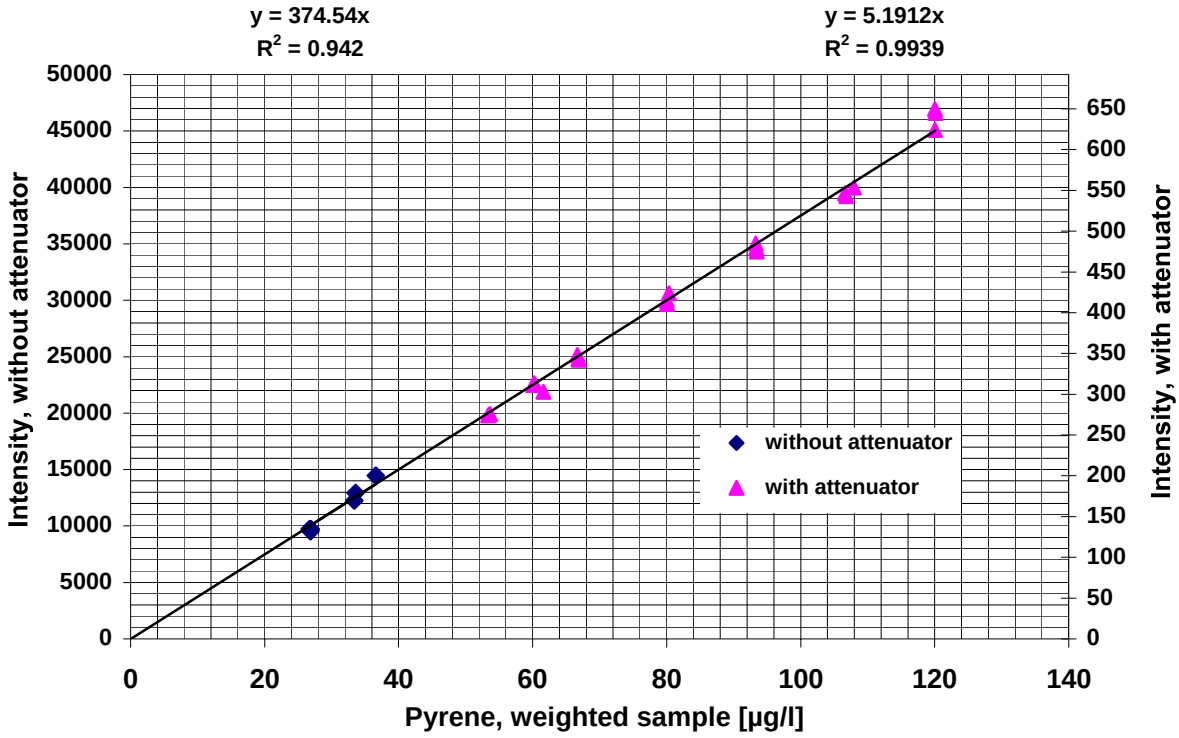

Fig. 12: Fluorescence signal of pyrene depending on the initial weight.

Based on the results above, the fluorescence signals without attenuator have been converted to the analogous values with attenuator. This provides the opportunity, to compare the data with the results of the GC-MS analysis. Results of both methods are shown in the following graph.

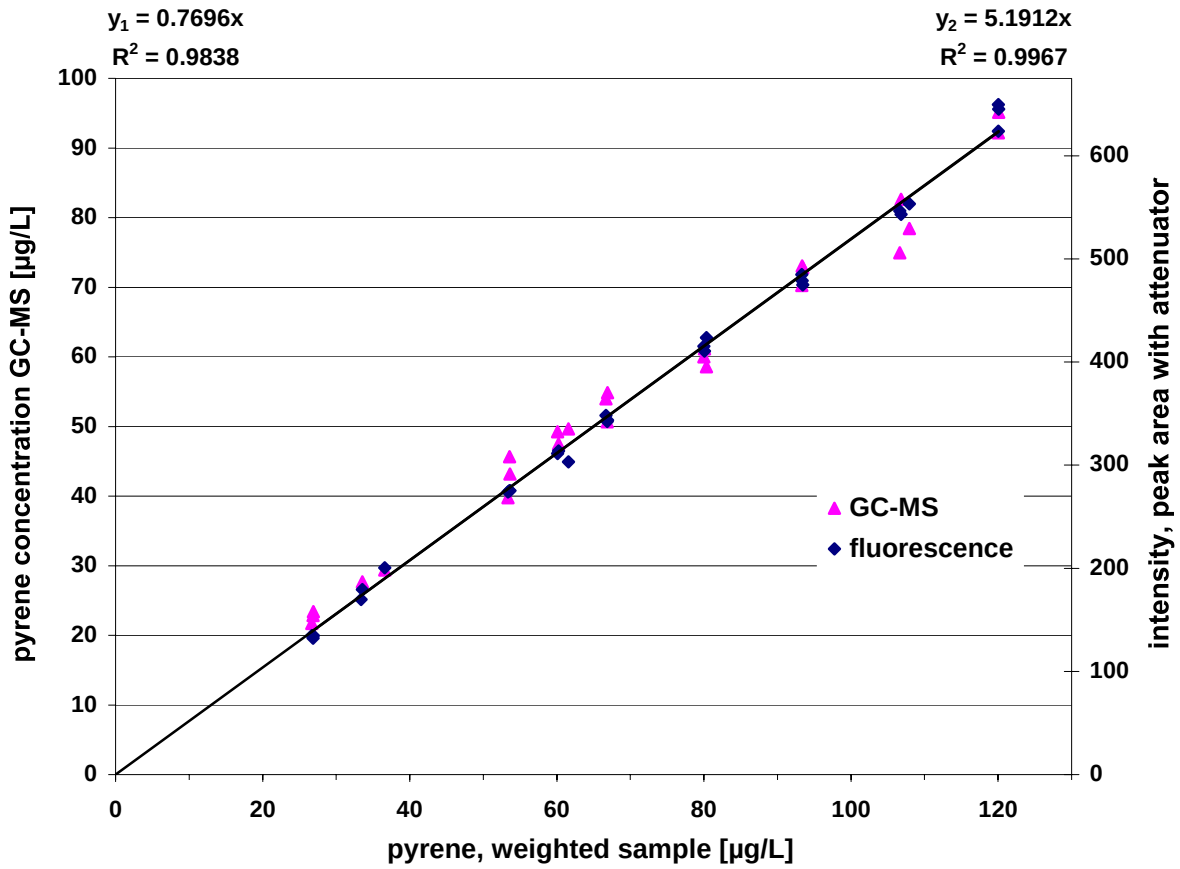

Fig 13: Comparison of fluorescence measurements and GC-MS analysis of aliquots of the same aqueous pyrene solution. The scaling of the fluorescence y axis relative to the GC-MS y axis offers the opportunity to compare both linear regressions y_1 and y_2.

Both analytic methods show a good correlation for the considered concentration range. The correlation factor is with 0.9967 slightly better for fluorescence measurements, compared to 0.9838 for GC-MS analysis.

4.3 Dialysis experiments

This experiment was designed to determine the kinetics of the passage of pyrene through the dialysis membrane. For this purpose the aqueous pyrene solution was dialysed against deionised water. The membrane, characterised by a thickness of 50 µm and a MWCO of 1000 Da, was fixed on a cylinder of sinter glass. The volume of the dialysis bag was 102 ml, the volume of the surrounding water 168 ml. The pyrene fluorescence intensity was measured in the outer compartment.

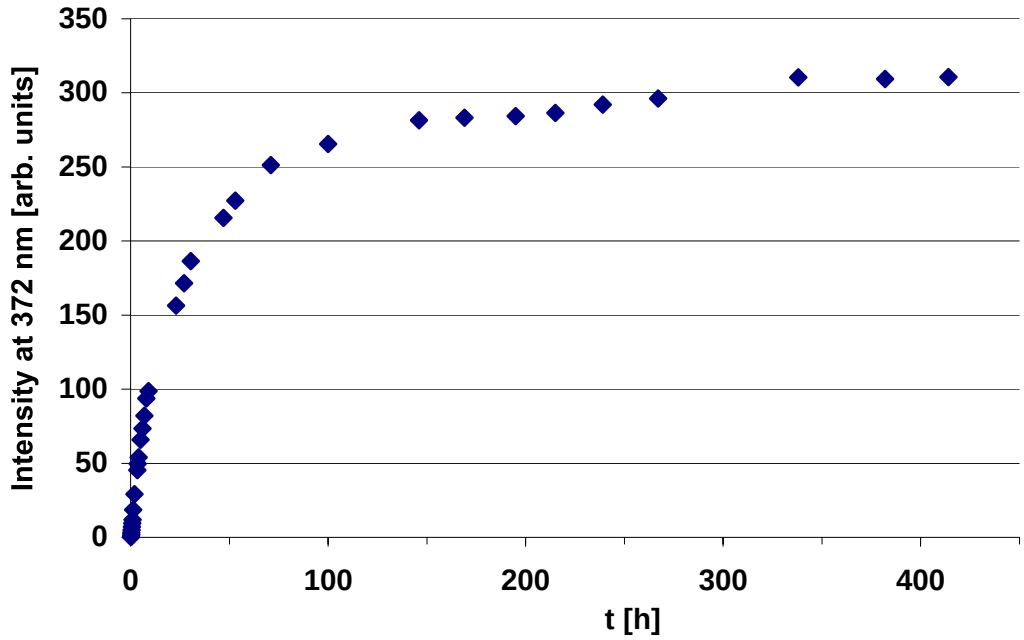

Fig. 14: Pyrene fluorescence intensity over time in the outer dialysis compartment.

The pyrene fluorescence intensity in the outer dialysis compartment shows a rapid initial increase for the first ten hours. During the subsequent 130 hours it slows down constantly. After 338 hours a plateau is reached and no further increase of the fluorescence intensity can be observed.

4.4 Quenching of pyrene fluorescence by aqueous DOM solutions

4.4.1 Quenching effect of two soil effluents and Aldrich humic acid

The quenching capacity of Aldrich humic acid and the effluents of a forest soil from Jülich and a field soil from the Krauthausen test site were analysed in this experiment. The weighted sample of Aldrich humic acid was 30 mg/l. The soil effluents were extracted in columns with a height of 25 cm and a diameter of 7 cm. The ceramic frit had a maximum pore size of 6 µm. The analytical TOC-concentration of the elutriates was 65 mg/l for the field soil and 36 mg/l for the forest soil. They were spiked with an aqueous pyrene solution at a ratio of 1:1. A characterisation of the soils is given in appendix 3 - 5.

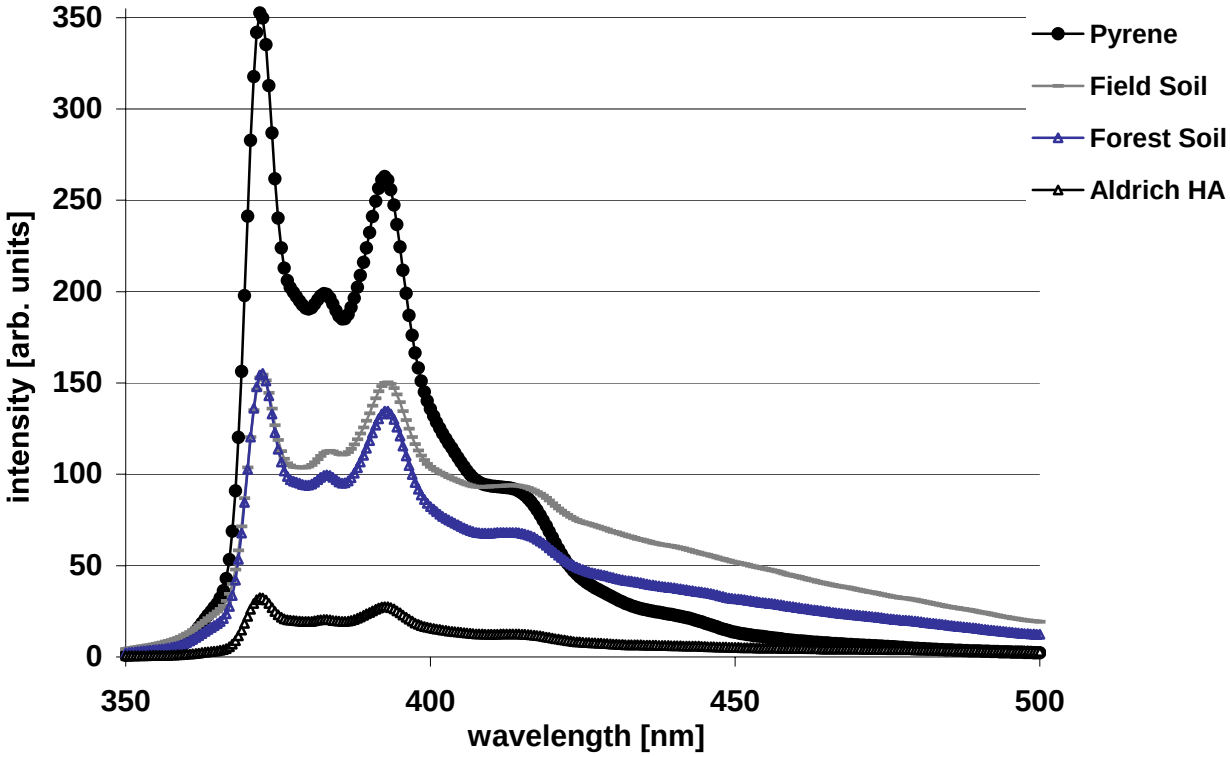

Fig 15: Quenching of the pyrene fluorescence by two soil elutriates and Aldrich humic acid.

As the results show, the fluorescence of pyrene is decreased by all three solutions of humic substances. The strongest decrease of 90 % is caused by Aldrich humic acid. The soil effluents downsize the first pyrene peak about 55 %. An interesting fact is, that the influence of the two soil solutions is nearly the same regarding the first fluorescence peak, whereas the longer wavelength fluorescence is significantly lower in the presence of forest soil organic matter.

4.4.2 Impact of the eigen-fluorescence of Aldrich humic acid

Humic acids show a short eigen-fluorescence for 2 - 4 ns after excitation with ultraviolet light (Panne 1994). To examine the importance of the eigen-fluorescence for the fluorescence quenching method, eight concentrations of Aldrich humic acid were analysed at an excitation wavelength of 337 nm. Different from the LIF measurements, the fluorescence signals were detected immediately after excitation. The pyrene concentration in the first test sequence was 100 µg/l.

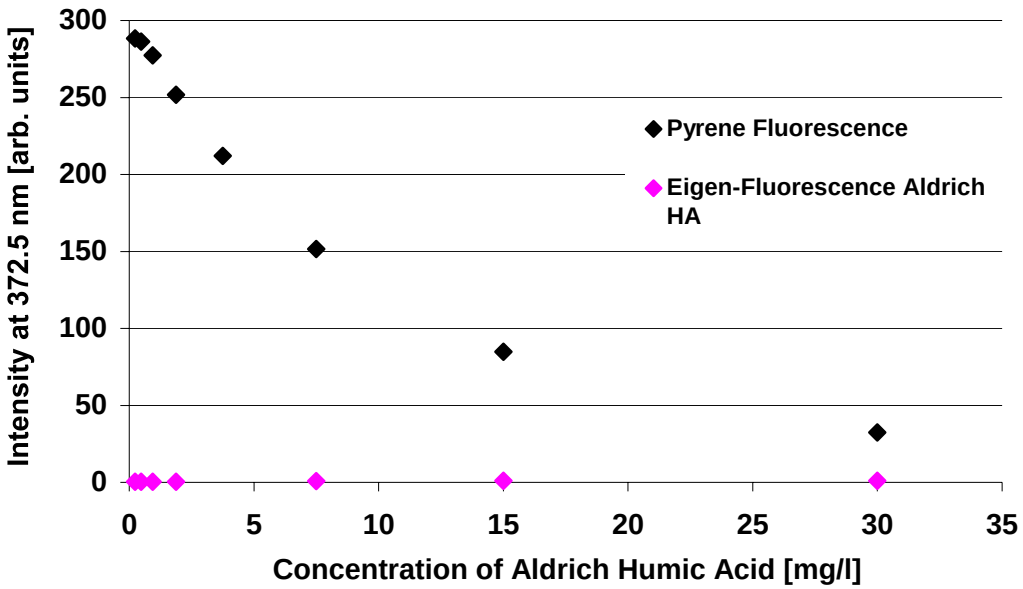

Fig. 16: Quenching of the pyrene fluorescence by Aldrich humic acid. The eigen-fluorescence of Aldrich humic acid is given in the second data set.

The eigen-fluorescence of Aldrich humic acid increases with increasing concentration on a very low level. The maximum value on the arbitrary scale is 1.1 at a concentration of 30 mg/l. The pyrene fluorescence goes back with increasing concentrations of Aldrich humic acid. The ratio between the pyrene fluorescence signal and the eigen-fluorescence becomes smaller with increasing HA concentrations. At a concentration of 0.23 mg/l the eigen-fluorescence of the humic acid is equal to 0.1 % of the pyrene signal, at the highest concentration this percentage rises to 3.4 %.

The following experiment was designed to characterise the inner filter effect of the humic acid solution. Therefore the absorption coefficient of the solution was quantified at the excitation and the emission wavelength.

4.4.3 Correction of the inner filter effect

For the correction of the inner filter effect the light absorption by the humic acid solution was measured at the excitation and the detection wavelength. The fluorescence data were corrected for the inner filter effect according to the Lakowicz equation (18).

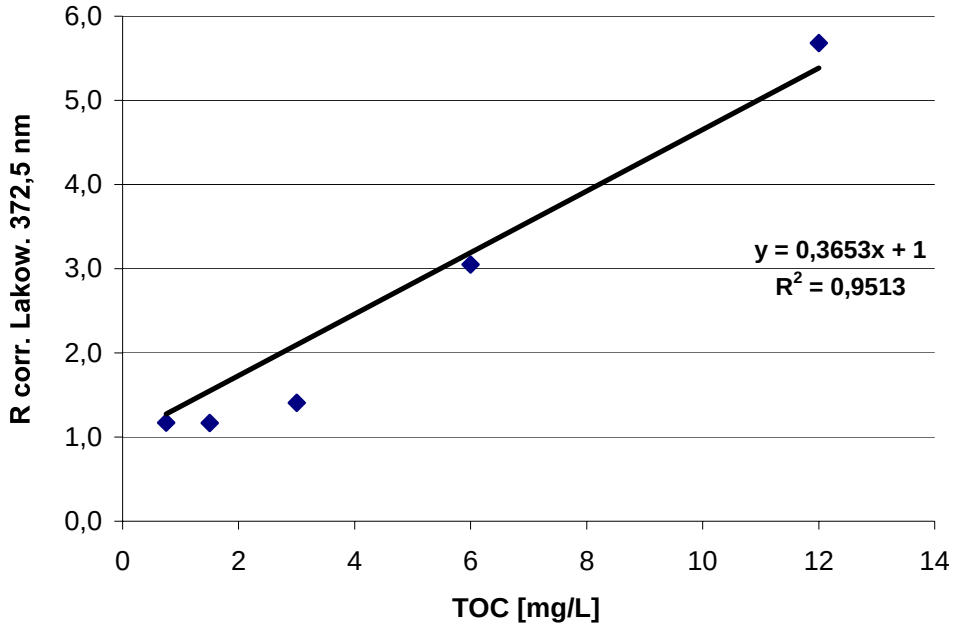

Fig. 17: Fluorescence signal ratio of pyrene at different concentrations of Aldrich humic acid in aqueous solution. The values are corrected for the eigen-fluorescence of the humic acid and the inner filter effect (equation 19) of the solution.

According to the fluorescence quenching method (see chapter 1.5.2), the slope of the linear regression gives the K_{OC}-value (equation 20) for the sorption of pyrene to Aldrich humic acid:

$$K_{OC} = 3.6 \cdot 10^5 \, l / kg$$

The correlation coefficient for the linear regression is 0.951.

The K_{OC}-value for the effluent of the field soil and pyrene was determined in the same way. The effluent of a soil column was mixed with the same volume of an aqueous pyrene solution of the concentration 100 µg/l. The initial TOC concentration of the elutriate was 65.7 mg/l. The slope of the linear regression gives the K_{OC}-value of $1.1 \cdot 10^4$ l/kg. The correlation coefficient for the linear regression is 0.982.

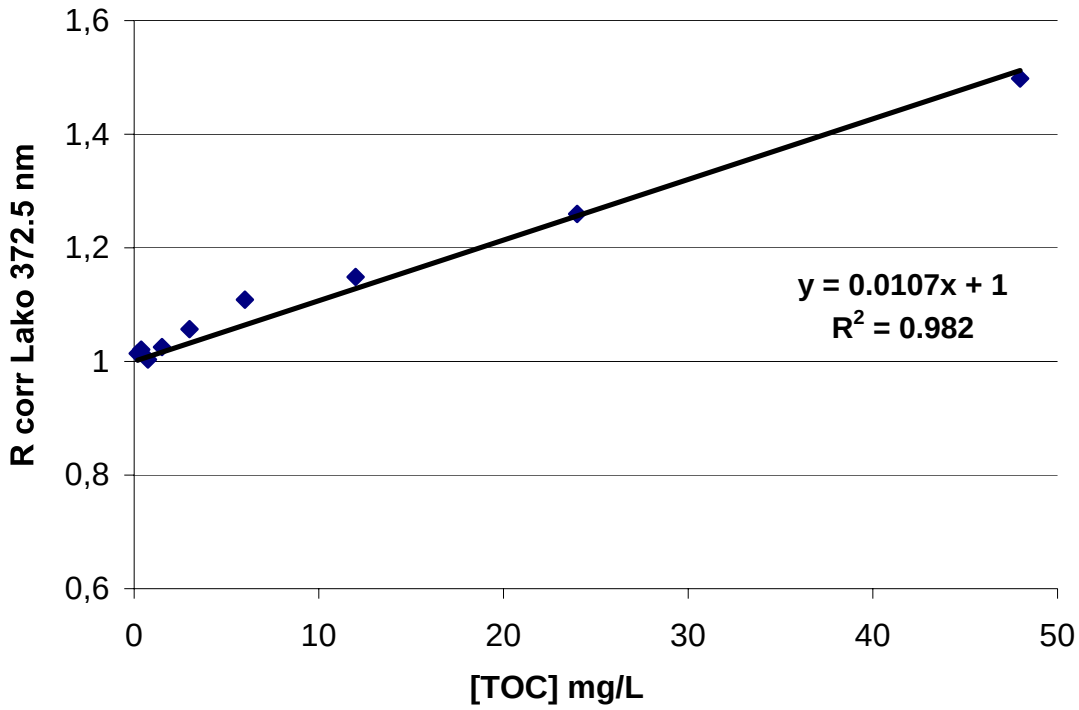

Fig. 18: Quenching of pyrene fluorescence by the elutriate of a field soil, characterised in appendix 5. The fluorescence signal is corrected for the eigen-fluorescence and the inner filter effect (equation 19).

4.5 Development of the glass probe head

4.5.1 Technical development of the glass probe head

The main problem for the application of the laser-induced fluorescence spectroscopy in soils is to obtain representative fluorescence data. The direct use of the light fibre in soils would be very sensitive for inhomogeneities. Due to the narrow point of emission of the excitation light, small soil particles or microcrystals of pyrene could lead to exceptional low or high values, which do not reflect the average concentration. For this reason it is necessary to spread the excitation light over a larger surface to yield significant data. Therefore, an optical probe head has been developed, which offers the opportunity to measure the average fluorescence intensity of the surrounding medium.

In a first step, probe heads made out of glass tubes were compared with probe heads out of glass rods. The results (not presented here) show, that the reflection of excitation light is higher for the probe heads out of glass tubes. During the production process, the glass tubes are melted off at the end of the probe. This leads to a convex surface on the inner side. Due to the unequal refraction index of glass and air, a major part of the excitation light is reflected which leads to undesirable high excitation peaks in the emission spectrum. For this reason all further probes have been produced out of glass rods. To fix the light fibre in front of the glass rod, a glass tube of higher diameter was glued on the rod as a guide rail (UV hardening adhesive, Bohle 665).

The repeated use of the probe heads led to a higher background signal. Fluorescence measurements showed, that capillary attraction in very small interstices results in pyrene accumulation. Cleaning the probe heads with organic solvents or NaOH does not solve this problem.

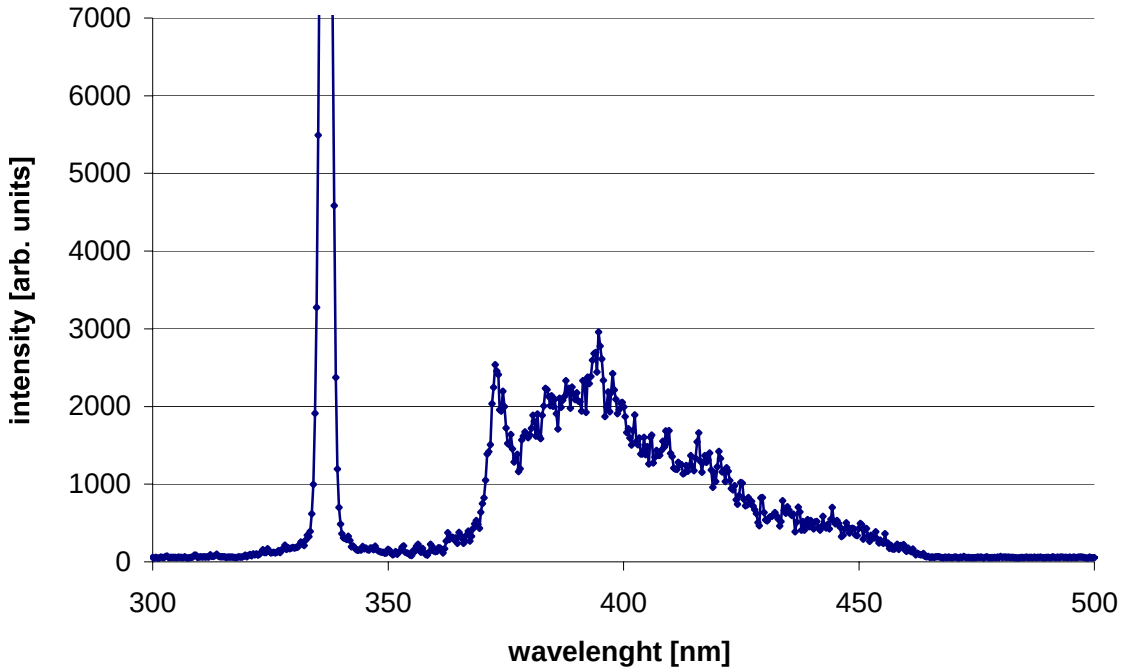

Fig. 19: Fluorescence signal of the adhesive between the glass rod and the glass tube after five measurements in a saturated aqueous solution of pyrene.

Due to these results, the production of the probe heads was changed. The outer glass tube was shrunken on the inner rod without any adhesive. These probe heads can be cleaned easily with pulp cloth and hexane.

The influence of different probe head geometries on the eigen signal and the fluorescence signal of the surrounding material was studied in several tests. The aim of all geometries was, to scatter the light to a larger surface of the probe head. In soil, the excitation light is stopped in the space of one or two millimetres. For this reason it is important, that the excitation light leaves the probe head also through the flank, to obtain a representative fluorescence signal of the surrounding soil. The geometries tested are shown in the following plan:

The last type was filed of at different angles. To obtain a preferably high scattering of the excitation light, the first prototypes of the probe heads have been used with the rough abraded surface. Further test showed, that it is impossible to remove all pyrene from the rough surface

just by cleaning it with solutes like methanol or hexane. For this reason all further probe heads have been fire polished. The scattering of the excitation light is still sufficiently high, and the probes can be cleaned easily by hexane and pulp cloth. The following diagrams show the eigen-signal and the fluorescence signal in aqueous pyrene solution for some probe heads.

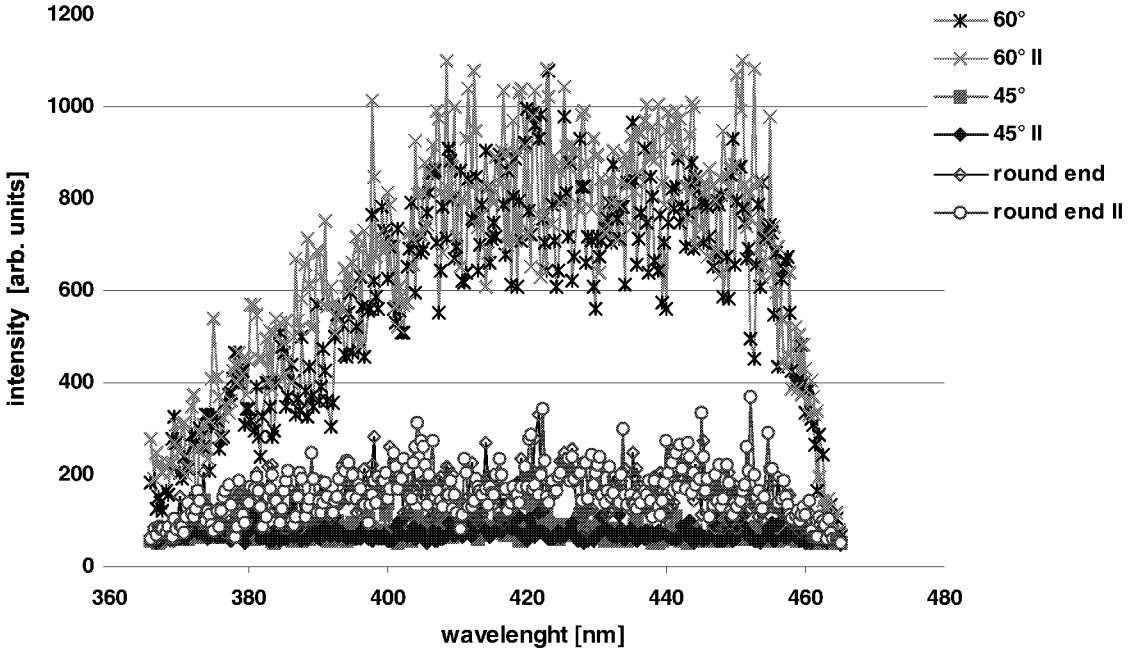

Fig. 20: Eigen-signal of three different probe heads in water. The probe heads have been used before in concentrated pyrene solutions. They were simply cleaned with hexane and pulp cloth to test their cleaning characteristics. The signal of each probe head was determined in duplicate.

The eigen-signals of the 45° abraded probe head and the round end probe are sufficiently low, whereas the eigen-signal of the 60° abraded probe would superimpose the pyrene fluorescence at low concentrations.

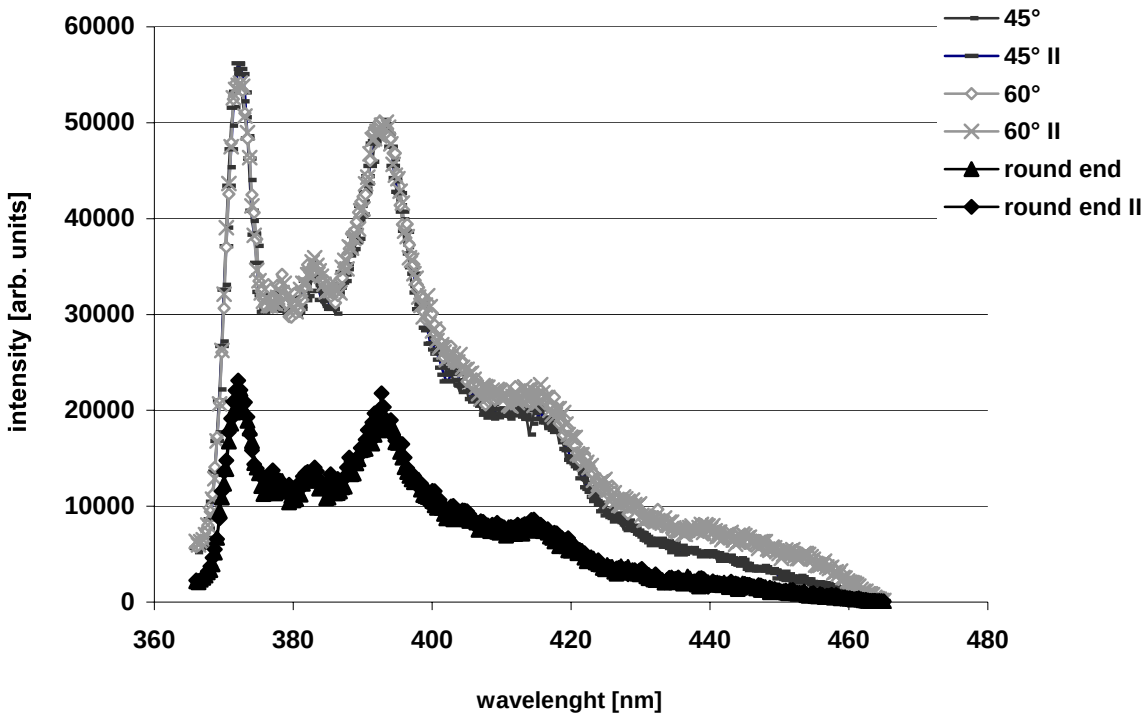

Fig. 21: Fluorescence signal of three probe heads with different geometries in an aqueous pyrene solution of 100 µg/l. The end of the probe heads have been rounded off or abraded in the given angle.

The round end probe head detects only a small fluorescence signal in the aqueous pyrene solution, because a significant part of the 337 nm excitation light is reflected inside of the probe head. Obviously the reflected light is not available for pyrene detection. Furthermore the reflected light causes a big flat top peak in the emission spectrum and may lead to the destruction of the sensitive CCD camera. The pyrene spectra detected by the abraded probe heads are more than two times higher. Almost all of the excitation light passes through the probe head into the surrounding medium and causes an intense pyrene fluorescence. Due to the higher eigen-signal of the 60° probe head all further measurements were carried out with the fire polished 45° probe head. The following sketch illustrates the final form:

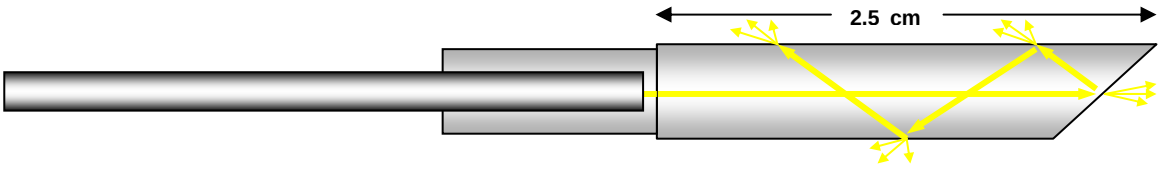

Fig. 22: Conceptual diagram of the final geometry of the 45° glass probe head.

4.5.2 Scattering of the fluorescence signal by the probe head

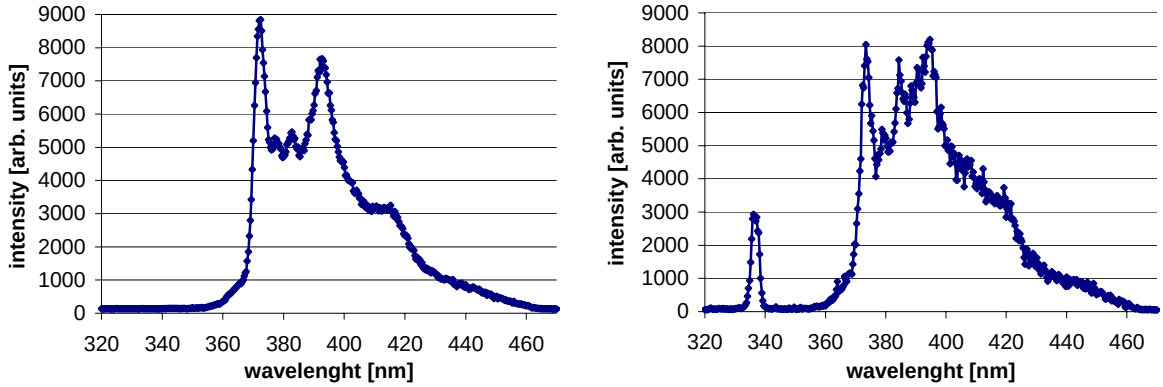

Fig. 23: Fluorescence signal of an 100 µg/l aqueous pyrene solution. The first diagram shows the spectrum directly measured with the light fibre in the solution, the second one the spectrum measured with the 45° probe head.

In this experiment, the loss of intensity and changes in the fluorescence spectrum caused by the probe head were characterised. The intended scattering of the excitation light, to irradiate a larger surface of the sample, leads inevitably to distortion of the detected fluorescence spectrum. This distortion should be kept to a minimum. The comparison of both spectra shows that all characteristics of the pyrene fluorescence spectrum are still distinguishable. All peaks at 372 nm, 382.5 nm, 392.5 nm and the shoulder around 415 nm are distinctive. The main difference between both spectra are the small peaks which are randomly spread over the curve. They are caused by the diverse propagation times of the light, that passes the probe head at different angles. The peak at 337 nm is caused by reflected excitation light from the 5 ns laser pulse. This peak also appears in spectra directly measured with the optical fibre. The difference lies once again in the propagation time of the light within the probe head. In the left spectrum the excitation light was blinded out as the time gater of the CCD camera opened not until 247 ns. In the right spectrum, the propagation time of a minor part of the excitation light was long enough to fall into this time window.

4.6 Spiking of the soil

One problem for experiments with pyrene in solid media is the addition of pyrene itself. To stay close to reality, it is desirable to dissolve pyrene in an aqueous solution. Because of the low solubility of pyrene in water this is only possible for concentrations up to 100 µg/l. In principle, there are two ways for obtaining concentrations above this limit.

The first one is to add more water than the solid medium can take up. The surplus of water can be evaporated. In this case, micro crystals of pyrene might accrue on the solid phase.
The second possibility to exceed the solubility limit is to add pyrene solved in organic solutes like methanol, hexane or ethyl alcohol to the dry matrix (Amellal et al. 2001). The solvent can be evaporated and the spiked soil will remain. In a second step the desired volume of water can be added. One advantage of this method are the relative small volumina of the solute and the fast evaporation. Disadvantages might be caused by a non-uniform evaporation which may lead to higher heterogeneities in the allocation of pyrene. Residuals of the organic solute may change the phase equilibrium and the adsorption characteristics of pyrene.

To determine the impact of the solution preparation, measurements have been carried out in three different ways. First of all, pyrene was added in aqueous solution and the free pyrene concentration was measured directly in the sand (Fig. 24). Secondly the concentration of free pyrene was measured in the supernatant after adding a surplus of pyrene solution (Fig. 25). In a last variant the pyrene concentration was measured directly in the sand after organic spiking with methanol, as described above (Fig. 26). All three methods were conducted in 200 ml beaker. The optical probe head was fixed in a tripod. After moistening the sand, the in-situ fluorescence intensity of pyrene was analysed.

Both, the in-situ fluorescence measurements in the sand with ascending volumes of the aqueous pyrene solution and the measurements in the two phase system, show a linear correlation between concentration and fluorescence intensity. Because it is impossible to gain higher concentrations for the in-situ measurements using aqueous pyrene solutions, these measurements were carried out in the concentration range between 5 µg/l and 80 µg/l. The fluorescence measurements in the aqueous phase covered the range from 80 µg/l to 166 µg/l. The correlation coefficient for the in-situ-measurements in the sand is 0.977 and for the fluorescence measurements in the aqueous phase it is 0.985.

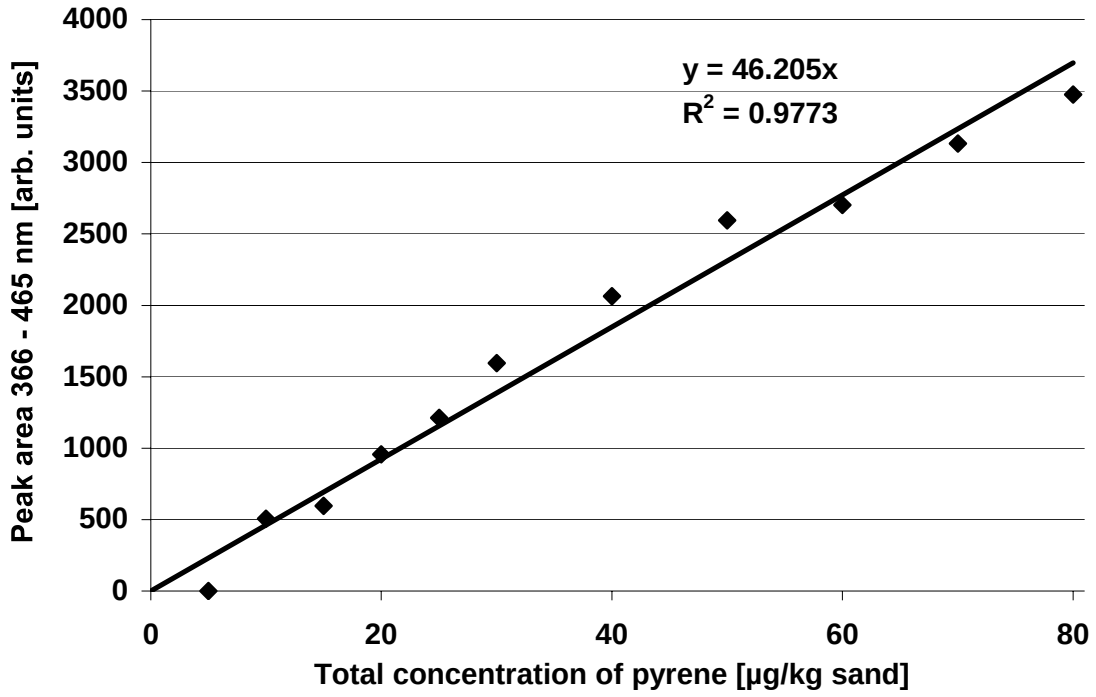

Fig. 24: Pyrene fluorescence signal in annealed sand. Ascending volumes of an aqueous 100 µg/l pyrene solution were added to 150 g sand.

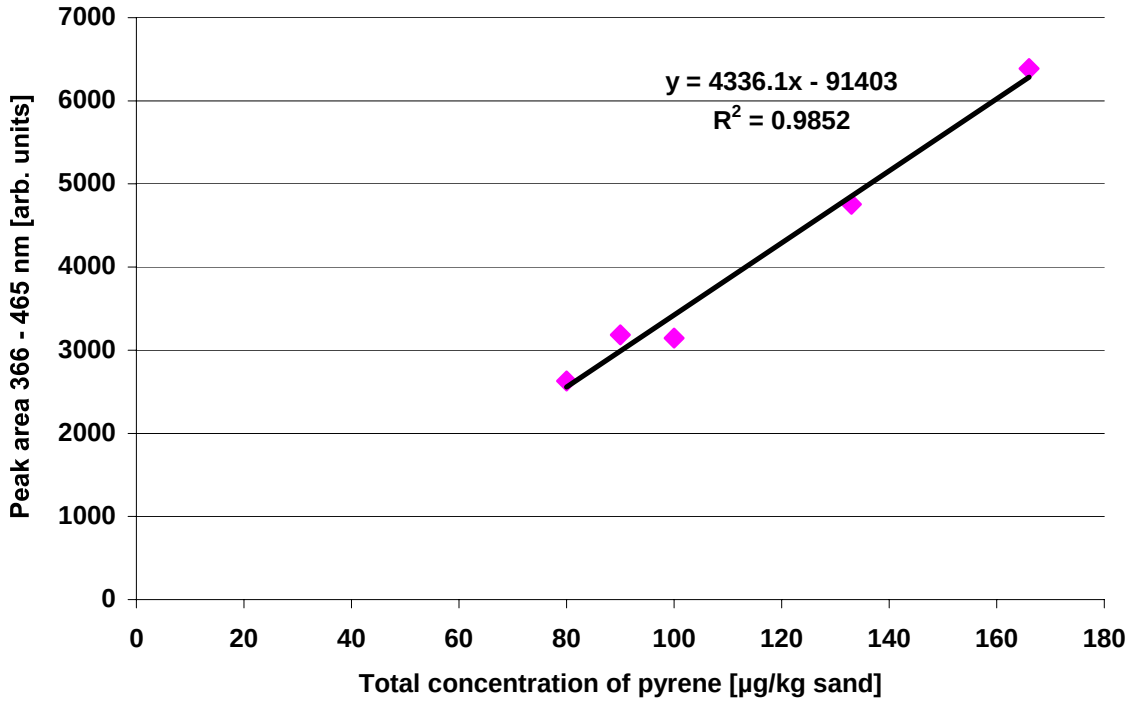

Fig. 25: Pyrene fluorescence measurements in the supernatant of a two phase system with annealed sand. Increasing volumes of an aqueous 100 µg/l pyrene solution were added to 150 g sand.

For the organic spiking, 8 ml of methanol with increasing pyrene concentrations were added to 200 g of annealed sand. After homogenisation the methanol was evaporated at room temperature in an extractor hood for four hours. Test series with different sand to water ratios were tested. After moistening the sand, the samples were allowed to equilibrate for one hour.

The test series of the annealed sand spiked with methanol, show no linear signal to concentration ratio. With rising concentrations, the slope of the curve decreases and the fluorescence intensity reaches a plateau. There is no systematic effect of the mass ratio of water and soil. The fluctuation range of the data is relative high. The variation coefficient increases with pyrene concentration and reaches 40 % for the highest concentration.

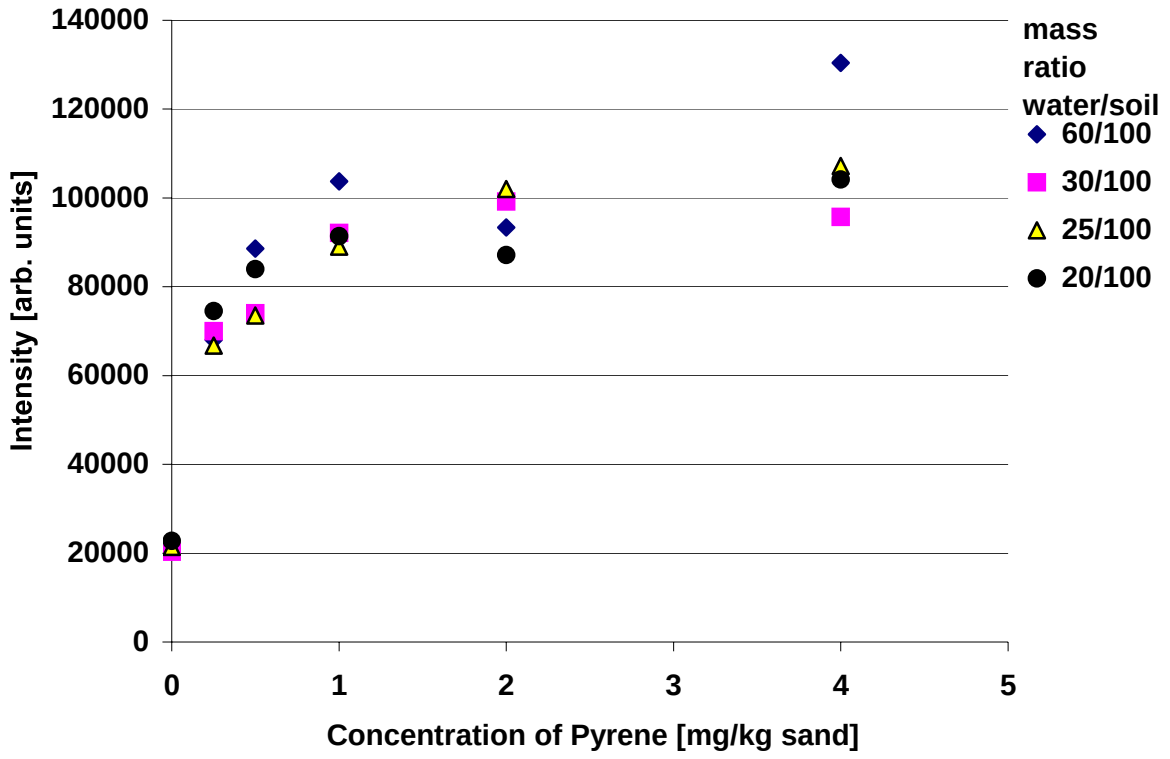

Abb. 26: Fluorescence signal of annealed sand, spiked with a methanolic pyrene solution at different water contents.

4.7 Influence of the water content on the fluorescence signal

Due to different refraction indices of air and water, it is important to quantify the influence of the water content of the surrounding medium on the fluorescence signal. In this experiment annealed sand with a pyrene concentration of 4 mg/l was analysed at different water contents. For each test row, 8 ml of a methanolic pyrene solution were added to the sand. The methanol was ablated at room temperature in an extractor cowl for four hours. Subsequently the quoted amount of water was added.

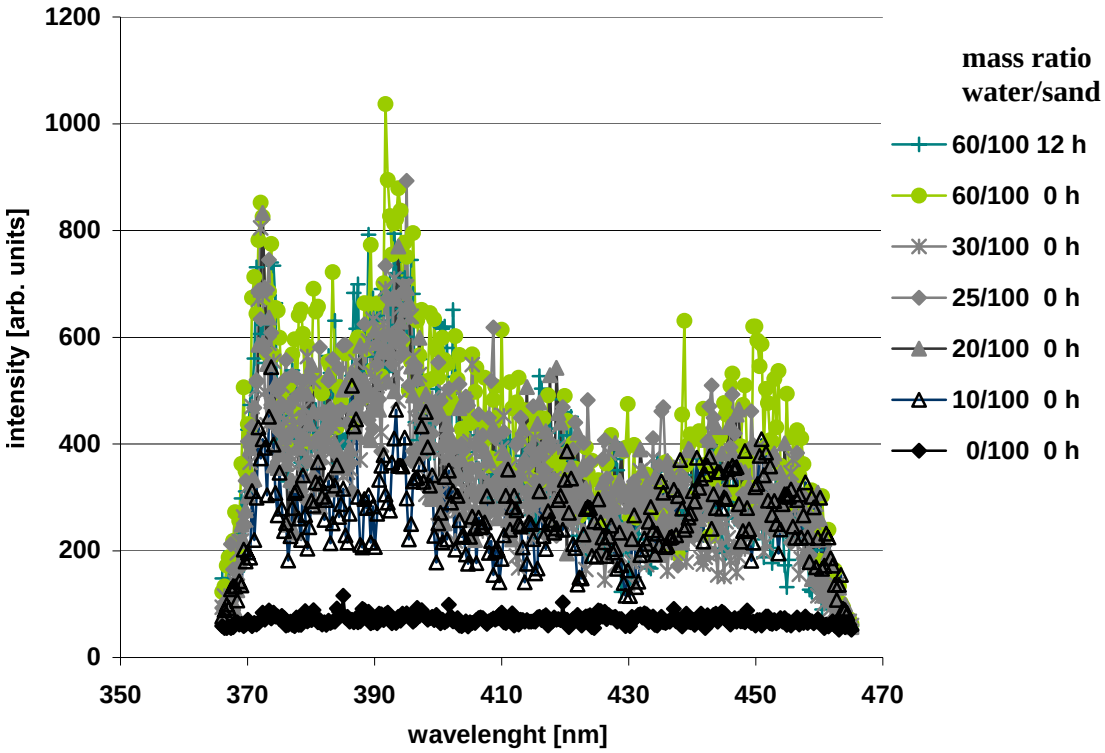

Fig. 27: Fluorescence signal of annealed sand spiked with 4 ppm pyrene at different water contents.

The mass ratio of water and sand shows a strong influence on the fluorescence signal of pyrene at a concentration of 4 mg/kg sand. The fluorescence signal in dry sand (mass ratio 0/100) is 80 % lower than in the sample with a mass ratio of 60/100 after twelve hours. At a mass ratio of 10/100 the fluorescence signal is still 27 % lower. For all other samples the fluorescence signal is nearly the same. The area under the curve varies about 3.3 %. An exception is the sample with a mass ratio of 60/100 which was measured instantaneously. The fluorescence signal of this sample is about 21 % higher.

4.8 Batch experiments

4.8.1 Adsorption kinetics of pyrene to annealed sand

This experiment was the first one in a test series about the adsorption kinetics of pyrene. Samples with increasing concentrations of pyrene were analysed immediately after sample preparation and, in a second test series, after 14 hours equilibration time. In the first test, the fluorescence signal increases constantly with higher pyrene concentrations. After the equilibration of the system for 14 hours, this relation cannot be observed anymore.

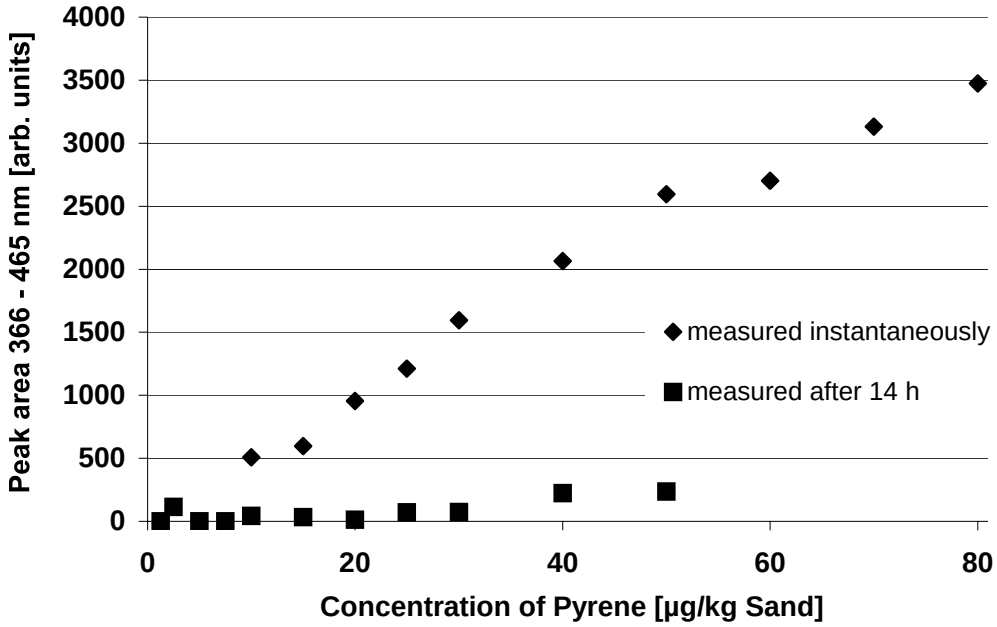

Fig. 28: Fluorescence signal of 100g samples of annealed sand, each moistened with 50 ml of pyrene solution with increasing concentrations. The fluorescence intensity in the sand was measured by the LIF probe head immediately after sample preparation and, in the second series, after an equilibration time of 14 hours.

Based on the results of this test, the following experiment (Fig. 29) was designed to follow in-situ the adsorption kinetics of pyrene over time. For this purpose, 100 g of annealed sand were spiked with 50 ml of a 100 µg/l pyrene solution. The samples were allowed to equilibrate for 10 minutes before the first measurement. As a test for the reproducibility of the method, the experiment was repeated under identical conditions. Photolysis of pyrene can be excluded, because all samples were kept in the dark and the irradiation time was limited to 20 seconds per measurement.

The results of the first experiment show, that the fluorescence intensity of pyrene diminished about 70 %, compared to the fluorescence signal after 10 minutes. After a steep initial decline of the fluorescence signal during the first 500 minutes, no further reduction of the fluorescence signal can be observed. In the second experiment, the first data point was recorded after 30 minutes. The fluorescence intensity was comparable to the fluorescence signal in the first test. Only after 300 and 600 hours some deviations in the fluorescence intensity can be observed between both tests. For the longest equilibration times, the same value is detected for both experiments.

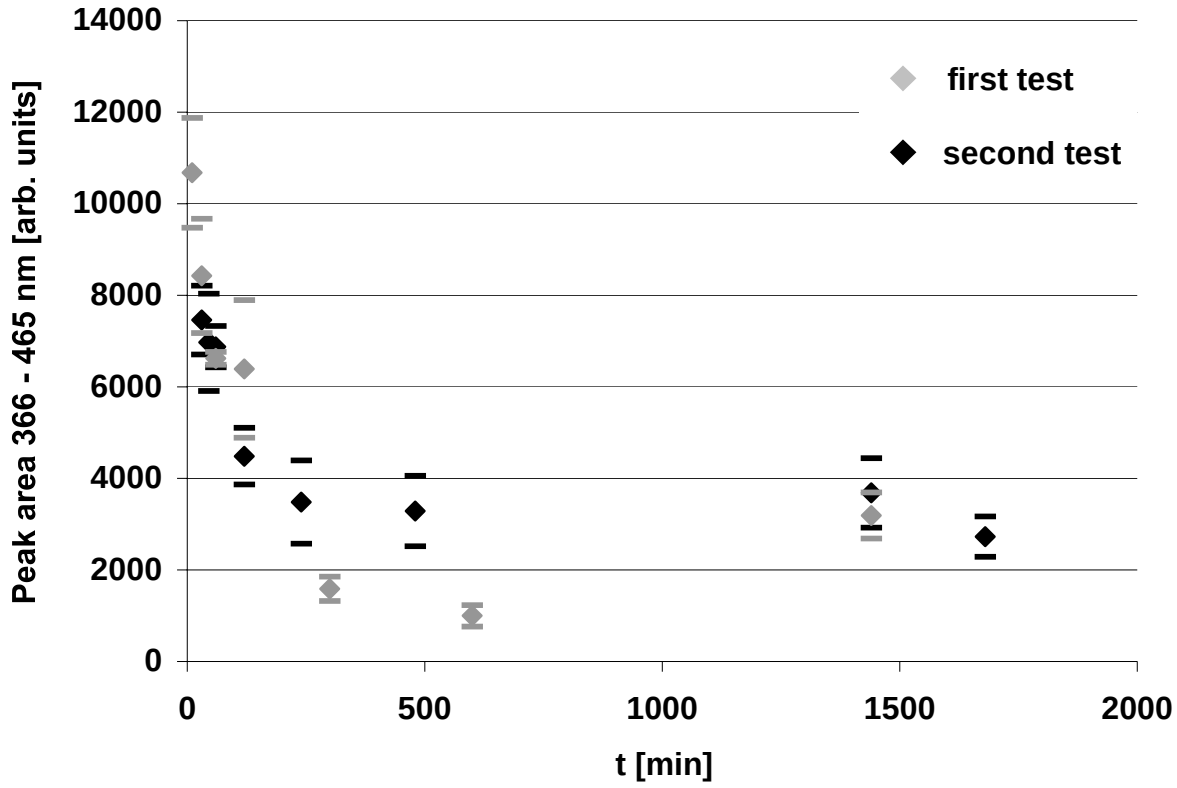

Fig. 29: Pyrene [50 µg/kg sand] fluorescence signal in annealed sand over time. The values represent the mean of three parallels, the error bars show the standard deviation. To prove the reproducibility, the test was repeated under the same conditions.

4.8.2 The photobleaching effect in LIF

The short pulse duration of the laser source and the fast detection device offer the opportunity of highly time resolved measurements. Unfortunately, the high intensity irradiation of the sample can also lead to the destruction of pyrene molecules. To quantify the extent of the photolysis effect, a volume of 3 µl pyrene solution was irradiated by a pulsed xenon discharge lamp in the measurement cuvette of an HPLC system. The integrated fluorescence spectrometer was the Perkin Elmer LS 4 system. The excitation light was adjusted 337 nm to yield results which are comparable to experiments with the nitrogen laser. The flow through cuvette is an open system with steel capillaries for supply and dissipation of the solution. The irradiation intervals of two hours were intermitted by intervals without irradiation.

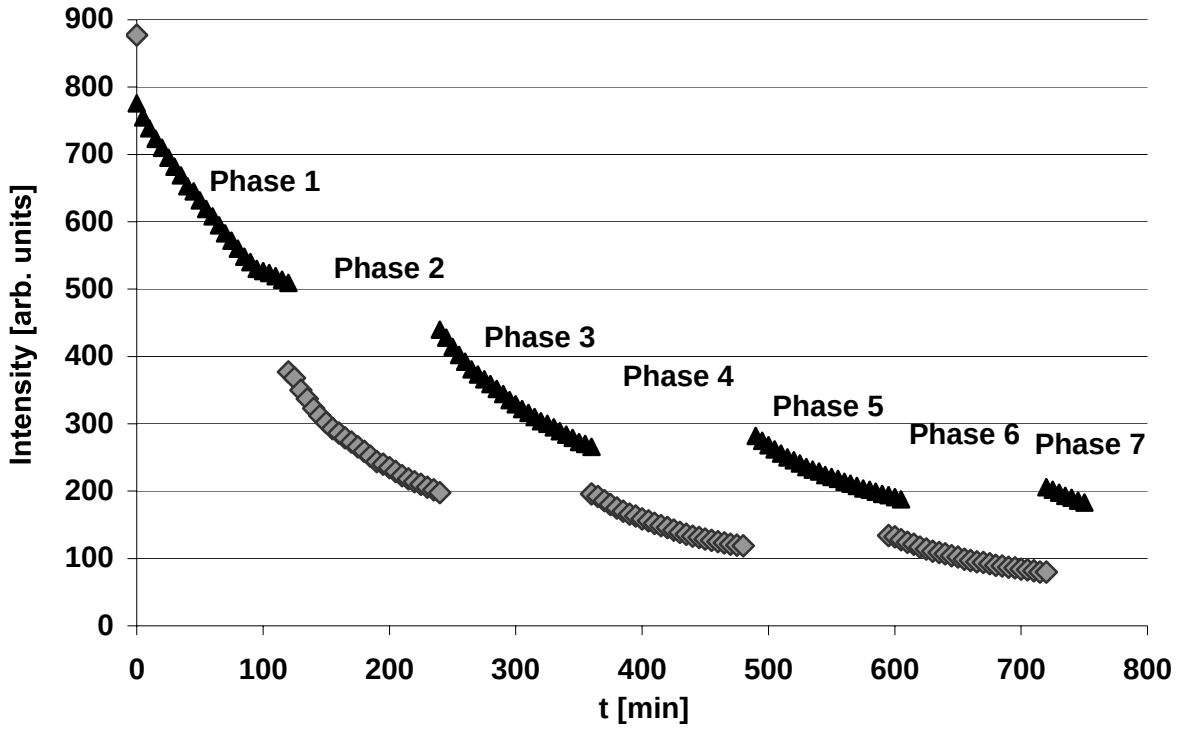

Fig. 30: Photolysis of pyrene at 337 nm in a 3 µl flow through cuvette in two test series. The samples were irradiated by a pulsed xenon discharge lamp.

In both series, the fluorescence intensity of the 100 µg/l pyrene solution declines over the entire test period. The sharp fall of the fluorescence signal at the beginning of the test slows down and passes into a slow and constant decline at the end of the experiment. In phase 1 and phase 2 the fluorescence signal falls even without irradiation of the sample. In all further phases the fluorescence declines only in the irradiated samples. In the dark the fluorescence signal remains constant or shows a marginal increase.

Photolysis of pyrene on mineral surfaces can differ from photolysis of dissolved pyrene molecules. For this reason, in-situ measurements in annealed sand were conducted with the optical laser probe head at an initial pyrene concentration of 40 µg/kg sand. The repetition rate of the laser pulse was 5 Hz for the first 30 min, then it was adjusted to 1 Hz. The periods without data points represent the night intervals when the laser was switched off.

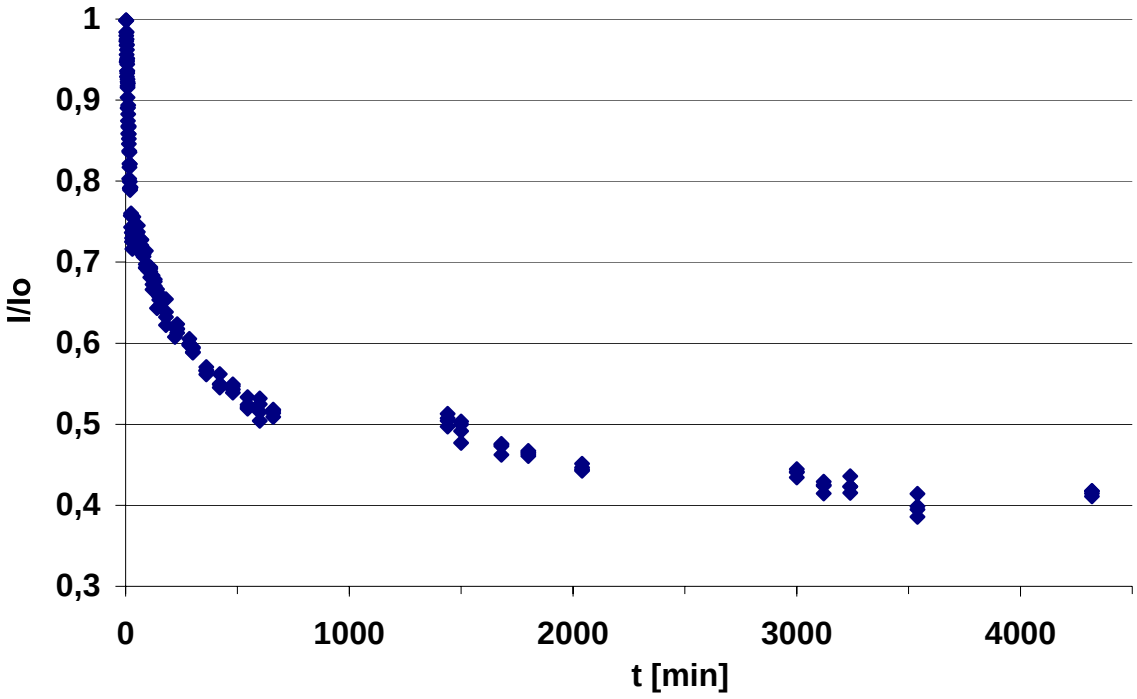

Fig. 31: Pyrene fluorescence in annealed sand over time divided by the initial fluorescence. The sample was irradiated constantly at a repetition rate of 5 Hz during the first 30 minutes and 1 Hz for the remaining time.

The fluorescence intensity shows a strong initial decline over the first 30 minutes. After that, the ratio of the current fluorescence intensity to the initial fluorescence diminished with a lower rate. The slope of the test curve abates constantly until the end of the experiment. Without irradiation of the sample during the night, no further reduction of the fluorescence intensity can be observed. The relative reduction of the fluorescence signal during the first 30 minutes is 38 % and for the entire test time it is 58 %.

4.8.3 Adsorption Kinetics of pyrene to a forest soil

To analyse the adsorption kinetics of pyrene to a forest soil (Parabraunerde, Luvisol), the pyrene fluorescence signal was detected in-situ by the laser probe head. The forest soil from Jülich, characterised in appendix 4 has an organic carbon content of 6.4 %. 70 ml of the aqueous pyrene solution [100 µg/l] were added to 80 g of the air-dried, sieved [2 mm] soil. To avoid buoyancy of the dry soil, it was pre-moistened with 20 ml deionised water.

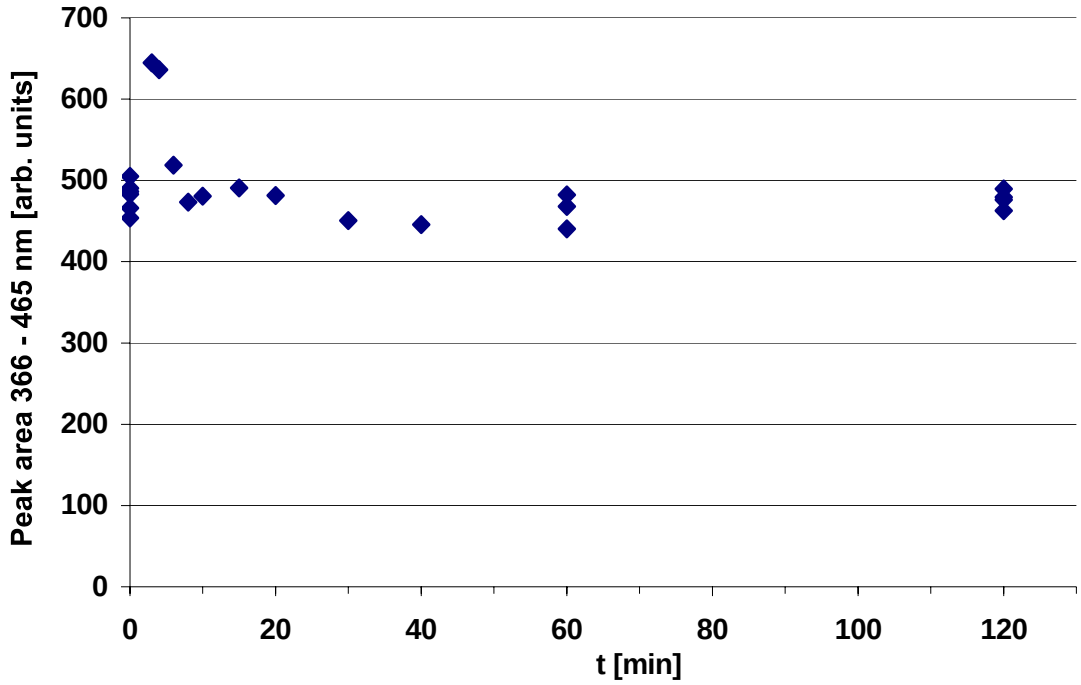

Fig. 33: Fluorescence signal over time of the forest soil “Jülich” spiked with pyrene [875 µg/kg soil].

After a short initial rise of the in-situ fluorescence signal, the fluorescence intensity returns to the start value after eight minutes. Until the end of the test the signal stabilises at a peak area of 470 units.

Due to the very high adsorption capacity of the forest soil, free pyrene can only be detected during the first few minutes. To obtain more data about the adsorption characteristics of the soil, batch experiments were accomplished at a very high water to soil ratio. 0.6 g of the air-dried, sieved [2 mm] forest soil were added to 80 ml of a 100 µg/l pyrene solution. The samples were shaken overhead in 100 ml Erlenmeyer flasks at 20 °C in the dark. After centrifugation for two hours at 10000 rpm, the free pyrene concentration was detected by classic fluorescence measurements. The error bars show the standard deviation of three replicates. To prove the reproducibility of the method, two time steps were repeated in a second test.

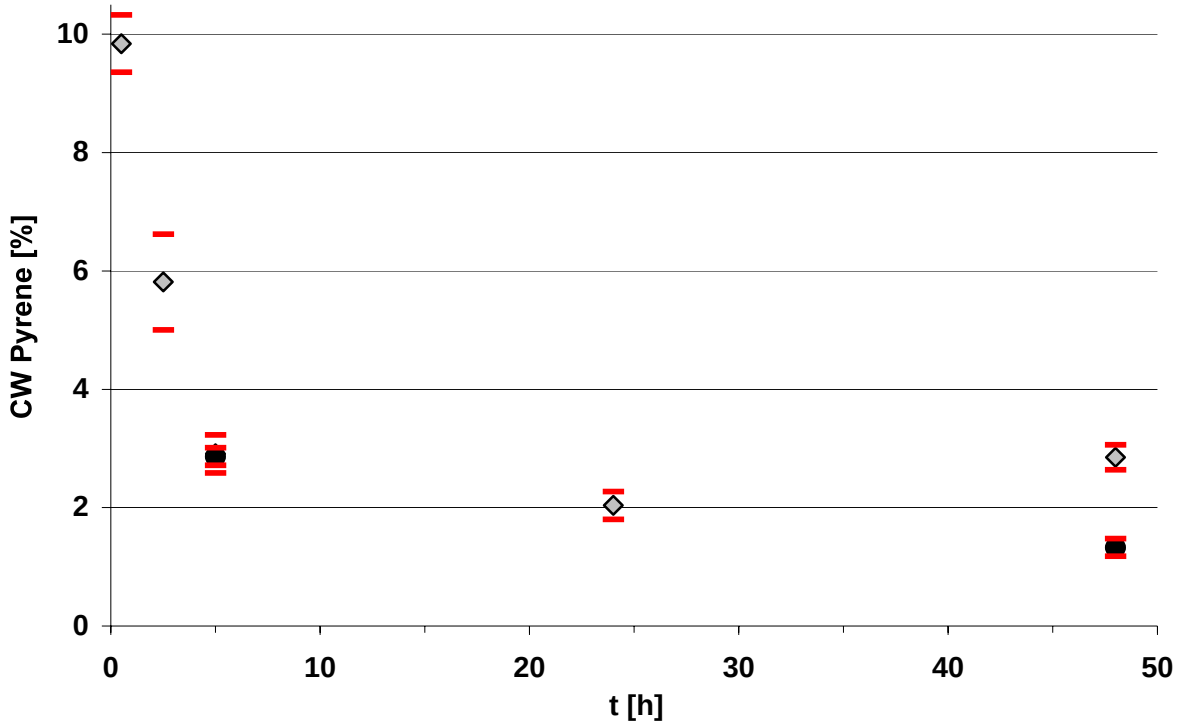

Fig. 34: Concentration of dissolved pyrene over time in a suspension of 0.6 g forest soil and 80 ml pyrene solution.

In spite of the very high water to soil ratio, most pyrene is adsorbed by the soil material within the first 30 minutes. The fraction of dissolved pyrene goes back to 9.8 % after 0.5 hours and 2.9 % after five hours. After 24 to 48 hours, only about 2 % of the pyrene mass is still dissolved (2.0 %, 2.8 % and 1.2 %). The standard deviation is sufficiently low for all measurement points, the coefficient of variation is 6.1 % at maximum. The data were background corrected for the eigen-fluorescence of the humic material (according to Lakowicz) and for the inner filter effect.

4.8.4 Adsorption Kinetics of pyrene to annealed soils

To prove the applicability of the laser probe head to adsorption kinetic measurements, several experiments with pyrene and annealed soils were conducted. The soils were heated at 600 °C for 48 hours to remove all organic compounds. In this first experiment, 150 g of a sandy reference soil from Kaldenkirchen (for characterisation see appendix 3) were moistened with 50 ml of an aqueous pyrene solution. The reduction of the free pyrene fluorescence over time was analysed by in-situ LIF measurements. The samples were irradiated only for 30 seconds at each measurement time, so that significant photolysis can be excluded. To prove the reproducibility of the sample preparation and the measurement setup, the first time segment of the experiment was repeated under identical conditions.

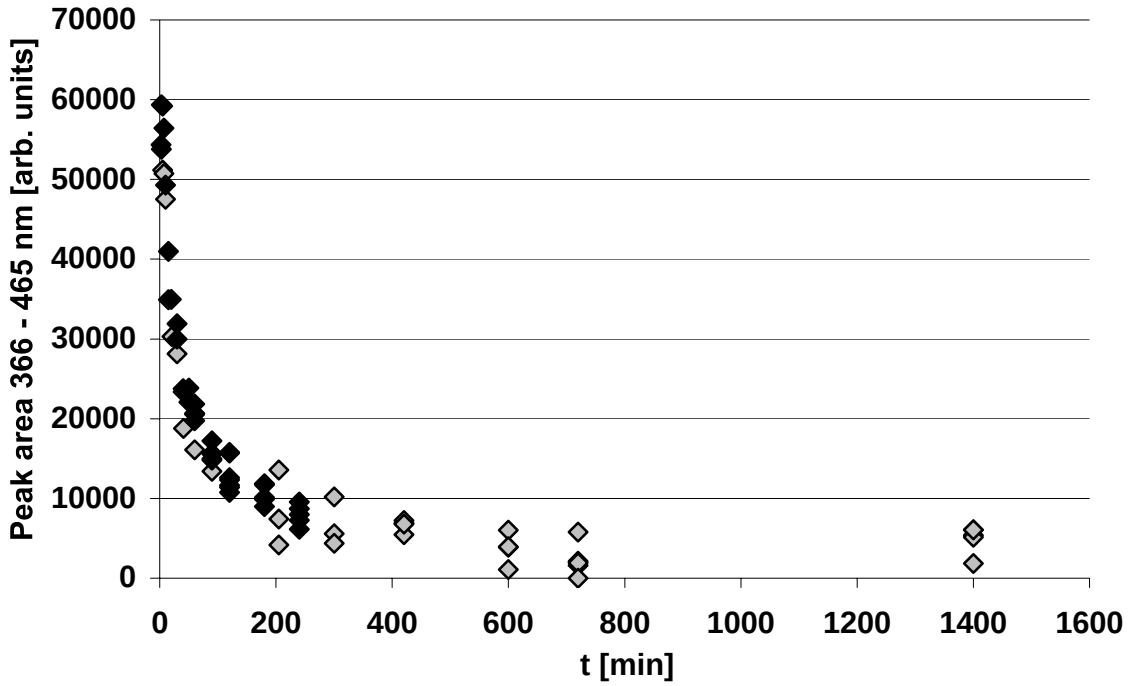

Fig. 35: Pyrene fluorescence over time in the annealed sandy reference soil Kaldenkirchen.

Within the first 30 minutes, the free pyrene fluorescence drops to the half of the initial intensity. Afterwards the decrease becomes slower and the values converge to the final level which is attained after 600 minutes. Until the end of the experiment no further decline of the fluorescence signal can be observed. The final fluorescence signal equals 5 % to 10 % of the initial fluorescence. The deviation between the parallels is sufficiently low and the reproducibility of both tests is excellent.

The purpose of this test was to compare the sorption characteristics of the annealed sandy soil from Kaldenkirchen with the sorption capacity of the annealed forest soil (Parabraunerde, Luvisol). Therefore the sorption of pyrene to the forest soil was measured with the experimental setup of the previous test. Due to the diverse specific water retention of the two soils, 150 g of the forest soil were spiked with 80 ml of the pyrene solution [150 µg/l].

A general problem for in-situ measurements in soil is the quantification of free pyrene at the time t_0. It represents the fluorescence signal of free pyrene before any pyrene molecules attach to the soil matrix. Obviously it is impossible to measure the free pyrene concentration in a spiked matrix before any interaction between the pyrene molecules and the matrix takes place. To deal with this problem, the in-situ measurements were set into correlation with ex-situ measurements. These analyses were carried out with the laser system and standard 1 cm quartz cuvettes. The light fibre was fixed in front of the cuvette to ensure reproducible measurements. Both, the initial pyrene solution and the equilibrated solution at the end of the experiment were measured with this experimental setup. The ex-situ measurement values were used to scale the initial in-situ data.

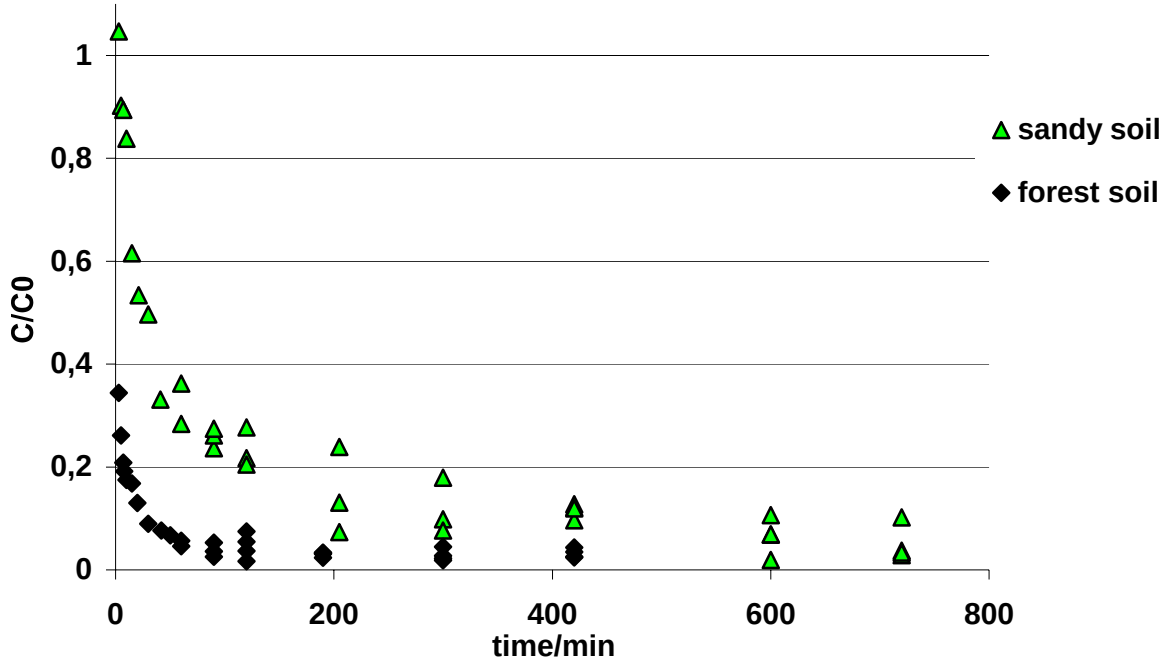

Fig. 36: Comparison between in-situ pyrene fluorescence measurements in a sandy soil from Kaldenkirchen and a forest soil from Jülich.

The trend of the pyrene fluorescence signal differs fundamentally in the two soils. In the sandy soil, the fluorescence signal at the first measurement time is equal to the initial

fluorescence. In the forest soil over 60 % of the initial pyrene fluorescence disappear, due to adsorption, after the first three minutes. After 30 minutes only 10 percent of the initial fluorescence signal can still be observed. The equilibrium level, which is reached after 190 minutes, equals three percent of the initial fluorescence intensity. In the sandy soil, the fluorescence signal takes much longer to reach the equilibrium level. After 30 minutes the fluorescence intensity still equals 50 % of the initial value.

4.9 Soil Column Experiments

4.9.1 Bromide breakthrough curves

Column experiments are an important instrument to derive information about the adsorption behaviour of hydrophobic compounds to soil components. In this test the adsorption characteristics of three different soils were compared. The forest soil from Jülich was tested with and without combustion of the organic material and the sandy soil from Kaldenkirchen was tested only in the annealed condition. For hydraulic equilibration, the three columns were irrigated with a 5 mmol $CaCl_2$ solution for 24 hours. At the start of the experiment, this solution was exchanged for an aqueous 100 µg/l pyrene solution, which contained 5 mmol of $CaBr_2$ as a conservative tracer. The columns with the annealed soils were fed with the pyrene solution until the pyrene fluorescence signal of the effluent was the same as the signal of the stock solution. Afterwards, the desorption phase was started. The pyrene/$CaBr_2$ solution was changed once again for the 5 mmol $CaCl_2$ solution. Thus, the irrigation with the conservative tracer Br^- ranged over the same time period as the irrigation with pyrene.

In combination with the known irrigation rate, the conservative tracer can be used to calculate the effective pore volume of the soil column. Samples of the effluent were taken at least every twelve hours. The concentration of bromide was analysed by ion chromatography. The figure below shows the breakthrough curve of bromide in the annealed Kaldenkirchen soil. The 10 mmol Br^- solution was exchanged for a 10 mmol Cl^- solution after 312 hours.

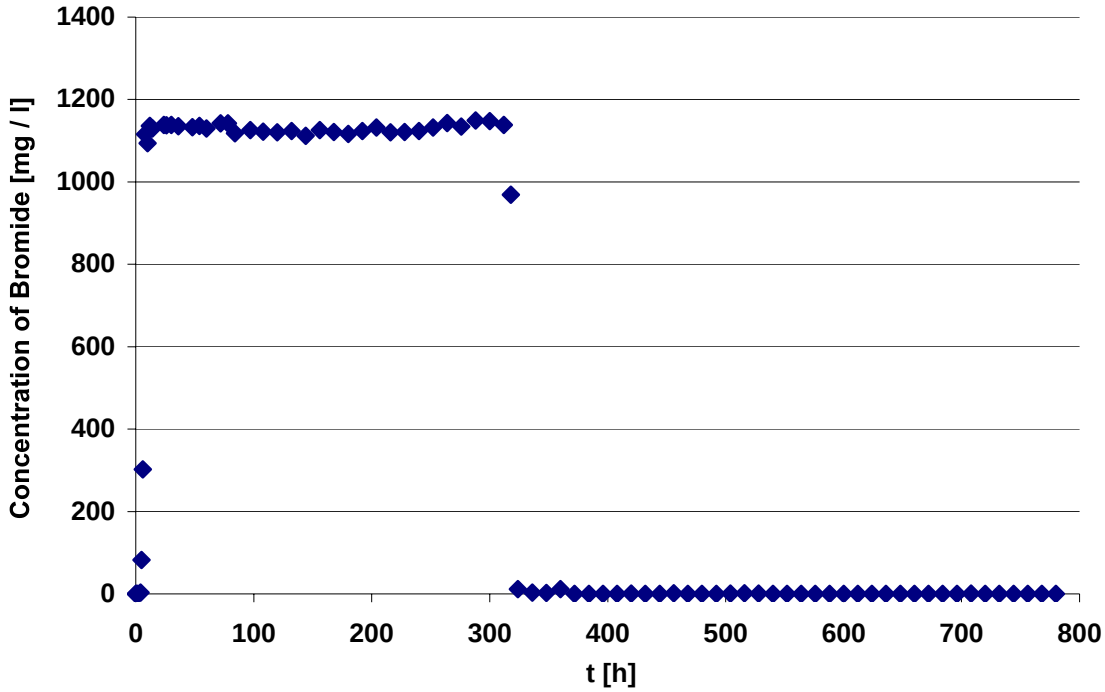

Fig. 37: Bromide breakthrough in the effluent of an annealed sandy soil from Kaldenkirchen.

At the start of the experiment, the bromide concentration in the effluent of the annealed Kaldenkirchen soil is below the detection limit. After four hours it begins to rise and after 26 hours the concentration of bromide reaches the equilibrium level of 1137 mg/l. During the following 286 hours only minor fluctuations of the effluent bromide level can be observed and at the measurement time 312 h, the concentration is 1138 mg/l. At this time the $CaBr_2$ solution containing pyrene was exchanged for a $CaCl_2$ solution without pyrene to analyse the desorption characteristics of the soil. The effluent concentration of bromide starts to fall after four hours and equals 11.7 mg/l at the measurement time 324 h. Afterwards the bromide concentration in the effluent shows a continuous decline and after 672 hours, it falls below the detection limit of 0.02 mg/l.

The breakthrough of bromide in the annealed forest soil was examined under the same experimental conditions. The shape of the breakthrough curves of both soils is similar, whereas in detail some differences can be observed. The fluctuations around the plateau value are slightly higher for the Jülich forest soil than for the Kaldenkirchen soil and the bromide breakthrough takes longer in the forest soil. The first increase of the bromide concentration can be observed after six hours. After twelve hours the concentration exceeds 1000 mg/l. It takes 48 hours from the start of the experiment, until the equilibrium concentration of

1182 mg/l is reached. After 312 hours, when the $CaBr_2$ solution is exchanged for a $CaCl_2$ solution, the effluent concentration of bromide is 1171 mg/l. From that time it takes 24 hours until the bromide concentration drops to 0.64 mg/l. After an overall time of 540 hours, the concentration of bromide falls below the detection limit of 0.02 mg/l.

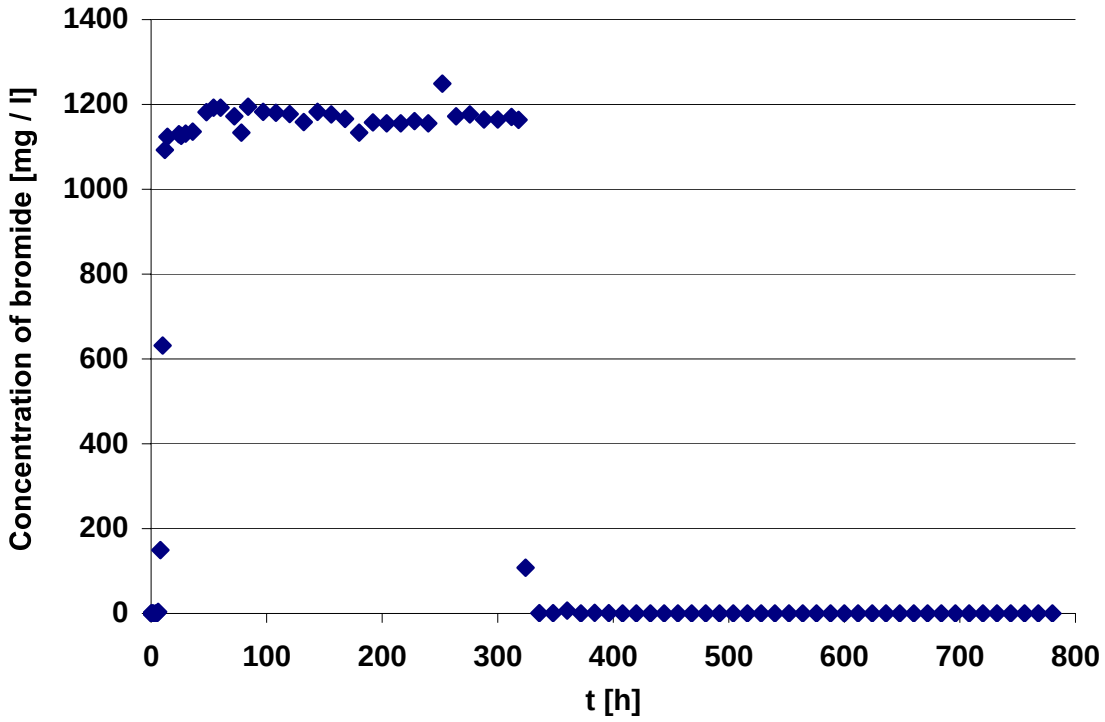

Fig. 38: Bromide breakthrough in the effluent of an annealed forest soil from Jülich

4.9.2 Column experiment with sieved natural forest soil

Due to the low water solubility of pyrene, it is impossible to analyse its adsorption characteristics in-situ at realistic water to soil ratios, in soils with a very high carbon content (see chapter 4.11). Due to the constant irrigation of the soil in column experiments, it should be possible to apply a surplus of pyrene, even if it is applied solely in aqueous solutions. After all pyrene binding sites are occupied, it should be possible to measure free pyrene, even if the binding capacity of the soil is very high.

The experimental setup for this test was the same as for the column experiments with the annealed soils. The soil column was fed constantly with 60 ml/h of a 100 µg/l pyrene solution, containing 5 mmol of $CaBr_2$. The laser probe heads were integrated in the glass column at soil

depths of 1.5 cm, 4.5 cm, 9.5 cm and 19.5 cm (see Fig. 6). The following diagram shows the concentration of bromide in the effluent (25 cm) over time. The black symbols show the pyrene fluorescence signal 1.5 cm below the soil surface.

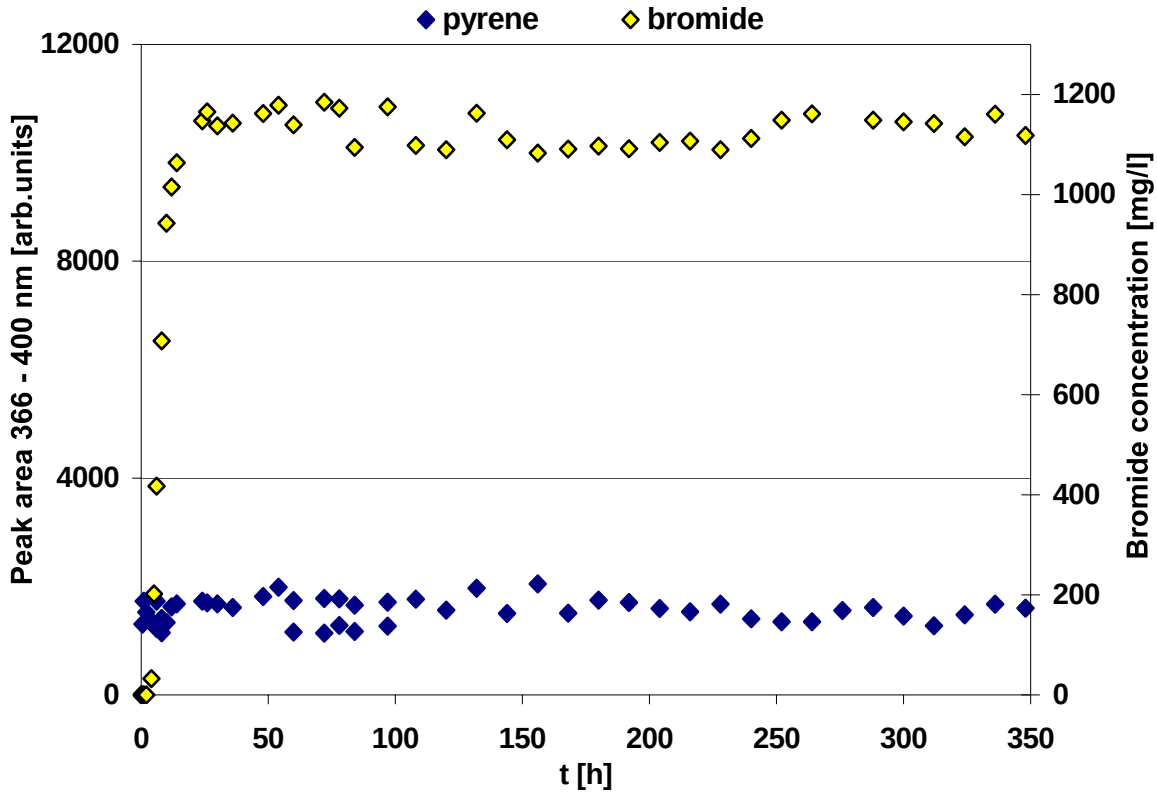

Fig. 39: Bromide concentration in the Jülich forest soil effluent over time. The second data series shows the pyrene fluorescence signal 1.5 cm below the soil surface.

The breakthrough of bromide in the sieved natural forest soil is similar to the breakthrough in the annealed forest soil. The increase of the effluent bromide concentration starts after four hours. After 14 hours the concentration of bromide exceeds 1000 mg/l and after 24 hours the equilibrium level of 1147 mg/l is reached. The effluent concentration of bromide shows higher fluctuations than in the annealed soil. At the end of the test after 348 hours it is 1118 mg/l.

The fluorescence signal measured by the laser probe heads 1.5 cm below the soil surface is constant over the entire test period. Even after 348 hours, no increase of the fluorescence intensity can be observed.

4.9.3 Column experiment with annealed soils: The sandy soil “Kaldenkirchen” and the “Jülich” forest soil.

Fig. 40 gives an overview of the fluorescence signals of all LIF probe heads in the annealed soil Kaldenkirchen over time. The probe heads are arranged in four levels at 1.5 cm, 4.5 cm, 9.5 cm and 19.5 cm soil depth (see Fig. 6). The three probe heads of one level are equidistant and displaced against the adjacent levels. The addition of pyrene was started at the beginning of the test and the fluorescence signal of the effluent (25 cm) is plotted in the central figure at the bottom of the page.

One thread (Schott GL 14) of the glass column was not complying with the standard, so that it was impossible to insert a probe head. The other probe heads of the 1.5 cm and the 3.5 cm level show a significant initial increase of the fluorescence signal. It is remarkable that the fluorescence signal drops before the pyrene solution is exchanged after 288 hours. In the 9.5 cm level, only one probe head (no. 8) shows a strong increase of the fluorescence signal. The other two probes show a similar curve shape but on lower levels. The decline of the fluorescence intensity starts still before the start of the desorption phase.

In the 19.5 cm level, two probe heads show high fluorescence signals and the third probe shows a moderate increase of the fluorescence intensity. The fluorescence intensity starts to rise after 69 hours and reaches the highest value after 116 hours. Afterwards a slow decline of the signal can be observed. From the start of the desorption phase the drop of the fluorescence signal accelerates. The background fluorescence level is reached after 536 hours at probe no.10, after 692 hours at no.11 and after 680 hours at no.12.

The trend of the free pyrene fluorescence in the effluent is similar to the probe heads on the 19.5 cm level. The start of the fluorescence increase is shifted for 80 hours and the highest signal is detected after 104 hours. A slow drop of the fluorescence intensity during the constant irrigation with pyrene solution can be observed, too. The dual peak, which also can be observed in the 19.5 cm level, shows the same shape in the effluent measurements. After the desorption phase is initiated, the fluorescence signal drops continuously. Although the fluorescence intensity is very low, it does not reach the background level until the end of the test.

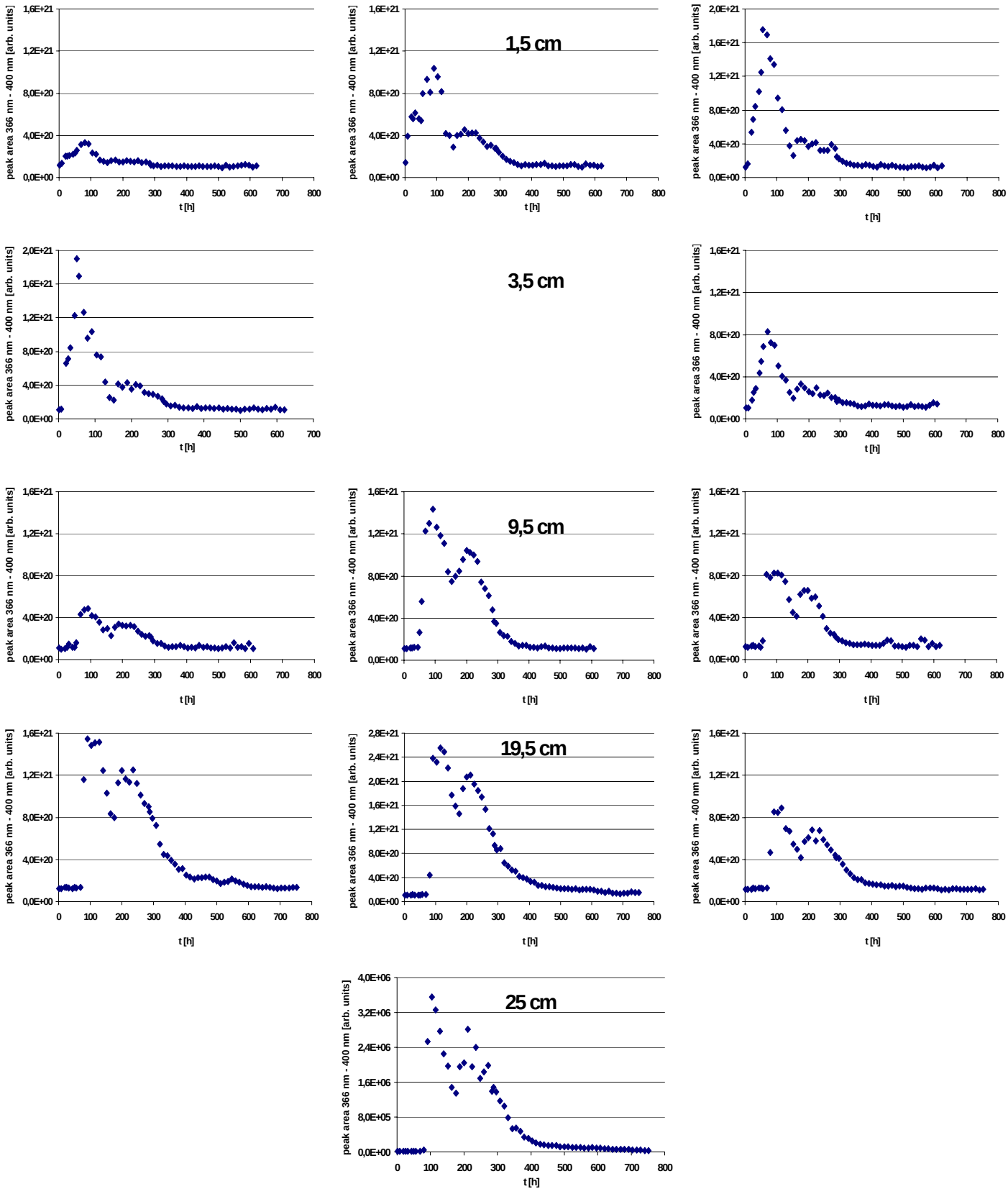

Fig. 40: Synopsis of the in-situ fluorescence signals over time of all probe heads in the sandy soil Kaldenkirchen. The diagram at the bottom shows the ex-situ fluorescence signal of the leakage measured in a 1 cm quartz cuvette.

Fig. 41 shows the fluorescence signals of all LIF probe heads in annealed forest soil over time. Obviously probe head no. 1 is defect and detects no expedient fluorescence signals. The other probe heads show the breakthrough of free pyrene through the soil column.

In the 1.5 cm level, the increase of the free pyrene fluorescence can be observed after 20 hours. The maximal fluorescence intensity is detected after 69 hours. Afterwards the fluorescence signal shows a significant decrease even before the addition of pyrene solution is stopped. The shape of the curve shows the same dual peak as the measurements in the sandy soil. After the addition of pyrene is stopped, the fluorescence intensity declines constantly without reaching the background level until the end of the experiment.

In the 3.5 cm level, the increase of the fluorescence signal starts between 26 and 54 hours and therefore, a little bit later than in the upmost level. Until the maximum level is reached at the three LIF probes, it takes between 69 and 97 hours. The dual peak shape of the curve is similar to the 1.5 cm level and after the start of the desorption phase it takes between 116 h and 252 h until the signal of the three probe heads reaches the background level.

The probe heads in the 9.5 cm level show heterogeneous data of the fluorescence intensity. The signal of probe no.7 is higher than the signals of all other probes in this soil column whereas the signals of the probes no.8 and no.9 are relative low. The increase of the fluorescence intensity takes longer than on the 3.5 cm level. During the first 69 hours of the experiment the signal remains constant. Afterwards a strong increase at probe no.7 can be observed, which is completed after 92 hours. The time curve shows the same dual peak shape as the probe heads of the upper levels. At the start of the desorption phase after 289 hours, the fluorescence signal drops constantly and traces back to the background level after 704 hours.

In the 19.5 cm level, the shape of the breakthrough curves differs from the curves discussed so far. Only probe no.12 shows two peaks which are less significant. Probe no.11 shows overall a very low intensity and probe no.10 detects only one distinct peak. Between 152 and 188 hours the fluorescence signal begins to rise. The maximum fluorescence intensity is reached after 236 hours, respectively after 260 hours. The curves show a pronounced tailing and the signal does not fall to the background level until the end of the test.

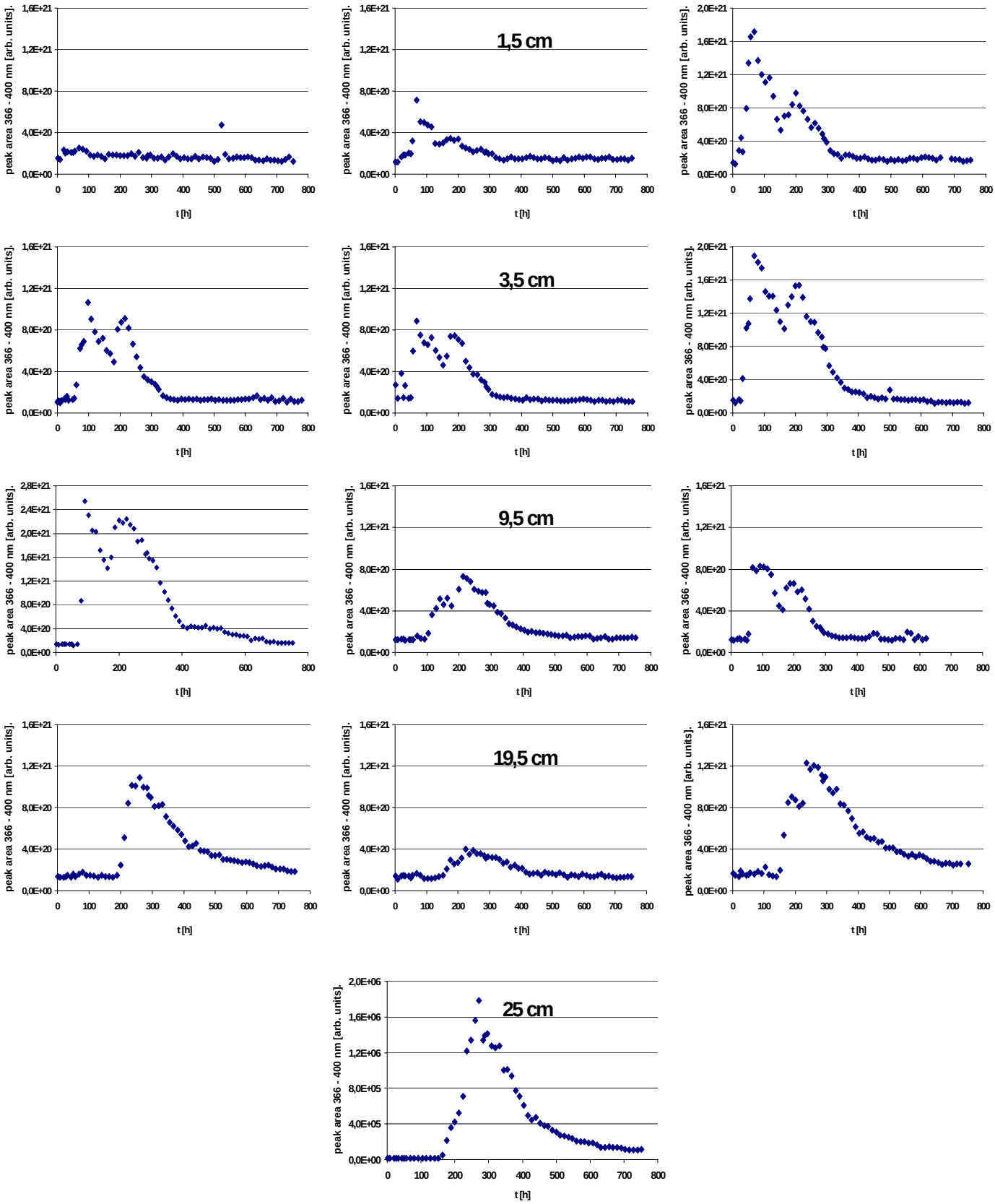

Fig. 41: Synopsis of the in-situ fluorescence signals over time of all probe heads in the forest soil. The diagram at the bottom shows the ex-situ fluorescence signal of the leakage measured in a 1 cm quartz cuvette.

The effluent breakthrough curve shows the same characteristics as the curves of the 19.5 cm level. Only one distinct peak with a steep increase of the fluorescence intensity can be observed. It starts after 164 hours and exhibits a maximum after 272 hours. Ten hours after the start of the desorption phase the fluorescence shows a constant decline. The slope of the curve decelerates so that a pronounced tailing occurs. The fluorescence signal remains above the background level until the end of the test.

5. Discussion

5.1 Preparation of the aqueous pyrene solution

The preparation and handling of aqueous pyrene solutions holds some challenges due to the very low water solubility of pyrene and its high affinity to nonpolar surfaces. Several experiments were carried out to optimise the different preparation steps.

One important question was the influence of centrifugation, because it is the classic procedure for phase separation for all ex-situ sorption studies. In all experiments (the data presented here are representative examples) centrifugation leads to a reduction of the free pyrene concentration between 11 % and 20 %. This observation also holds true for very low pyrene concentrations of 50 µg/l, which equals less than 50 % of its solubility limit. These results offer no obvious interpretation. The sample preparation, as well as the centrifugation, were carried out at 23 °C. Therefore any temperature effect can be excluded. The formation of microcrystals could be an explanation, but it would be astonishing at low pyrene concentrations like 50 µg/l (Billington et al. 1988).

The most supposable mechanism could be a kind of “facilitated wall adsorption” of pyrene molecules. Even without centrifugation a certain amount of pyrene molecules attaches to the glass surface (see Corex tube control in Fig. 8). It is conceivable that, facilitated by the application of centrifugation energy, more pyrene molecules attach to the glass surface or to other pyrene molecules. These molecules would be excluded from fluorescence measurements in the aqueous phase. Unfortunately no literature data are available about this mechanism.

The second aspect that can be derived from the data is an advisable concentration range for pyrene up to a concentration of 100 µg/l. Within this range, the aqueous pyrene solution shows a sufficient stability and a linear correlation between fluorescence measurements and the free pyrene concentration can be assured (see Fig. 11). The addition of 10 mmol $CaCl_2$ per litre causes a slight reduction of the free pyrene concentration. This outsalting effect is well known from literature (Lee et al. 2000) but for a nonpolar substance like pyrene it is weak.

Conditioning the pyrene solution by ultrasonic does not solve the problem of free pyrene reduction by centrifugation, but it leads to smaller standard deviations between sample parallels (see Fig. 8). This effect is based on a better homogenisation of the pyrene solution. Based on these findings, pyrene stock solutions for all further measurements were conditioned by ultrasonic.

In all experiments, the contact of the pyrene solution with any vessel lead to a reduced free pyrene concentration. Even if only low-adsorbing materials like glass or teflon are used this effect can be observed. Even the Corex centrifugation tubes lead to a small but measurable reduction of the free pyrene concentration (see Fig. 8,9).

Based on these results, three general rules were established for all further measurements:

- only low-adsorbing materials like glass or teflon were used (e.g. glass columns)
- sample preparation steps were kept to a minimum
- materials used for constant pyrene concentrations (e.g. teflon HPLC tubes) were pre-equilibrated

Different parameter can be considered for the quantification of the pyrene fluorescence intensity: the height of one of the main peaks (372 nm, 382.5 nm, 392.5 nm), the area under the whole curve or under a defined section. To determine the appropriate parameter, the fluorescence spectra of an aqueous pyrene solution was recorded at seven concentrations. Only at the highest concentration of 132 µg/l, a solubility limit effect for the free pyrene concentration can be observed. For all lower concentrations linear correlations between peak heights and the nominal pyrene concentration can be observed. Correlation factors between 0.998 and 0.999 affirm that all three peaks can be used for the quantification of the free pyrene concentration. Because the ratio between the peaks is constant, it is reasonable to assume, that it is also possible to analyse the area under the curve. The shape of the curve is in good agreement with spectra from literature (Löhmannsröben and Roch 1997, Mackenzie et al. 2002), affirming that the experimental parameter are appropriate and the pyrene solution is free of disturbing traces.

5.2 Validation of fluorescence measurements by comparison with gas chromatography – mass spectroscopy (GC-MS)

The experimental comparison between the GC-MS analysis and the fluorescence analysis was designed to check the preparation and handling of the aqueous pyrene solution. Moreover, the organic standard offers the opportunity to quantify the loss of pyrene during the sample preparation for the GC-MS analysis. The use of an organic standard is not possible for the fluorescence measurements, because the fluorescence spectrum of pyrene in organic solvents differs fundamentally from its spectrum in water. For this reason we decided to check the quality of the fluorescence measurements on the basis of the comparison with the GC-MS analysis.

The slope of the GC-MS curve in Fig. 13 is 0.77, which corresponds to a loss of 23 % of the pyrene mass, due to wall losses and pyrene adsorption on the SPE cartridge (The manufacturer of the SPE cartridges, Macherey und Nagel, indicates a relative loss of pyrene on the cartridge of 10 %; company catalogue 2003). This result emphasises the advantages of in-situ measurements, the more so as losses during sample preparation are even more pronounced in complex matrices like soils.

5.3 Dialysis

It has been shown, that the dialysis technique is a powerful tool for equilibrium adsorption analysis (Höllrigl-Rosta et al. 2003). The aim of our work was to combine dialysis experiments and the fluorescence quenching method, to follow the adsorption kinetics of pyrene in a two compartment system. One compartment with the sorbent of interest and a second compartment with aqueous pyrene solution. The rate of the pyrene diffusion from one compartment into the other allows the calculation of the pyrene adsorption rate. Unfortunately the results of the first experiments showed, that the diffusion of pyrene across the dialysis membrane was the rate limiting step for adsorption kinetic experiments.

Dialysis kinetics have been followed along the time by measuring the escape of pyrene from the dialysis bag with fluorescence spectroscopy. It can be shown that I_F values are satisfactory

modelled by equation (3). A permeation rate constant (*k*) can be calculated as well as the corresponding effective diffusion time (τ_{eff}) through the membrane. In the case of a dialysis membrane with a MWCO of 1000, only τ_{eff} values $\geq$ 24 hours can be estimated accurately. This limits the application of this approach for the binding kinetics of pyrene to humic substances.

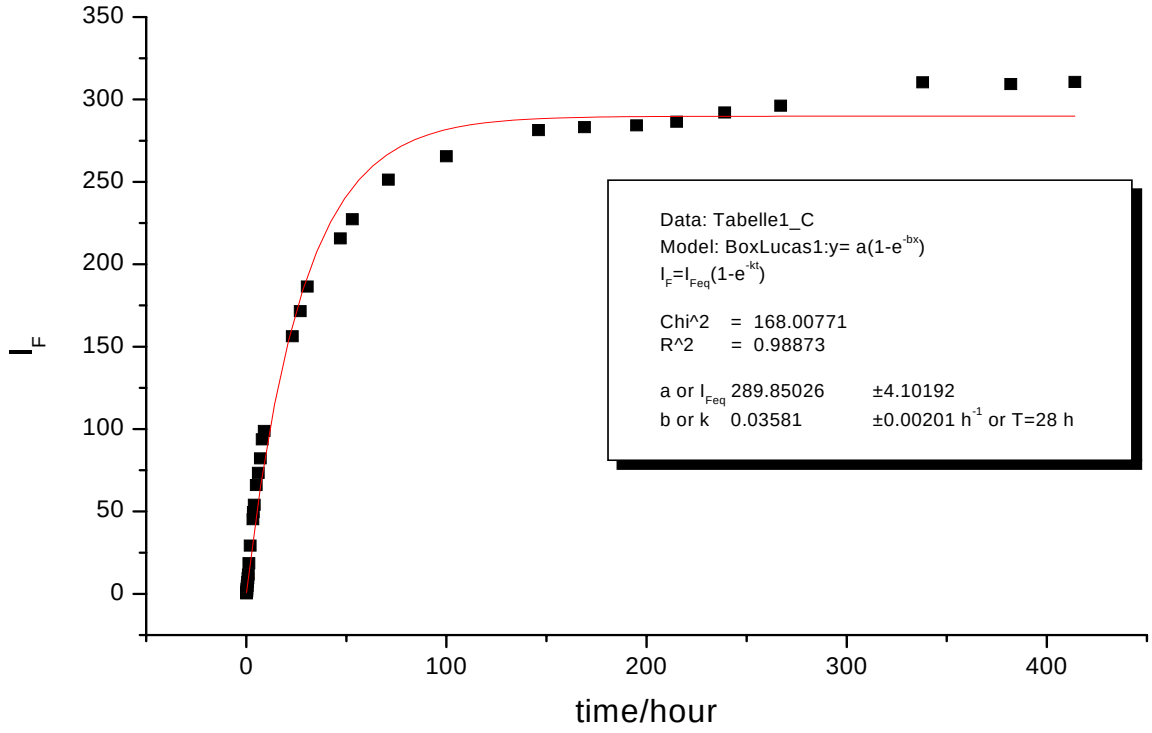

Fig. 42: Pyrene fluorescence intensity over time in the outer dialysis compartment.

Indeed, many authors describe a fast initial sorption step for PAH´s (Johnson 2000, Shor et al. 2003), which cannot be measured at low effective diffusion times. In fluorescence quenching experiments Schlautman and Morgan (1993) were able to show, that the fast initial sorption step (considered as instantaneous sorption) of pyrene to several humic acids, is completed within 20 seconds.

Similar results were reported for the adsorption kinetics of other compounds like tri-n-butyltin to humic acids. In dialysis experiments O`Loughlin, Traina and Chin (2000) found, that the diffusion of TBT across the dialysis membrane was the rate-limiting step. An estimation of the effective diffusion coefficient through the membrane pore (MWCO 1000) can be made for pyrene molecules according to the Renkin equation (5-8). Pore radius (rp) and pyrene molecule hydrodynamic radius (a) are calculated from

$$\frac{M_W}{N_A} = \frac{4}{3}\pi a^3 \rho \qquad (39)$$

with Mw: molecular weight, N_A: Avogadro number; ρ: density and a: molecule radius. For the pyrene molecule, radius a is calculated with Mw = 202.26 g and ρ = 1.271 g cm^{-3}. For the dialysis membrane, the calculation of r_p is based on a maximum Mw of 1000 and the specific density of water, ρ = 1 g cm^{-3}.

A pore radius (r_p) of 0.7 nm and a pyrene molecule hydrodynamic radius (a) of 0.4 nm are thus calculated.
It follows with (5-8) and $a/r_p = 0.57$ that
$D_{eff} = D_{water}\ 0.025$

From the Stoke-Einstein equation

$$D = \frac{k_B T}{6\pi\eta a} \qquad (40)$$

with k_B, Boltzmann constant, T, absolute temperature, η, water viscosity and a, the molecule radius, a diffusion coefficient D_{water} of $5.36*10^{-10}$ m^2s^{-1} for pyrene in water is calculated. From (8), an effective diffusion coefficient of $D_{eff} = 1.07*10^{-11}$ m^2s^{-1} is estimated for the diffusion through the membrane pore. For that reason, the approach to use the dialysis technique for kinetic analyses was not pursued further in this study.

5.4 Quenching of pyrene fluorescence by aqueous DOM solutions

5.4.1 Quenching effect of two soil effluents and Aldrich humic acid

In accordance with the fluorescence quenching method, established by Gauthier et al. 1986, all three samples of humic material show a pronounced effect on the pyrene fluorescence. At the given concentration, the soil effluents diminish the pyrene fluorescence to a half of the original signal. This effect is sufficiently high to quantify the concentration of the organic material by fluorescence measurements. The highest fluorescence quenching capacity can be observed for Aldrich humic acid (AHA). The calculated K_{OC} value of $3.65 \cdot 10^5$ l/kg is higher than literature data of Laor and Rebhun (1997): $1.19 \cdot 10^5$ l/kg or Perminova et al. (1999): $2.3 \cdot 10^5$ l/kg. An explanation for the diverting values could be the preparation method of the test solution. Perminova et al. used up to 60 µl acetonitrile and Laor and Rebhun used up to 800 µl of methanol for the preparation of one litre test solution. All our experiments have been carried out without any solvents, because they might disturb the sorption equilibrium.

Although the absolute TOC concentration in the AHA solution was lower than in the soil elutriates, the quenching effect was much more pronounced. There are some remarks in literature, that AHA solution is not representative for soil humic acids, although it is often used as a reference material (Laor et al. 1998). The quenching properties of AHA support this point of view.

The characteristics of the pyrene fluorescence spectrum maintain during the quenching process by AHA and the forest soil elutriate. The effluent of the field soil from Krauthausen changes the ratio between the fluorescence intensity at shorter and longer wavelength. The explanation for this observation is a significant eigen-fluorescence of the field soil effluent around 420 nm. The impact of the eigen fluorescence of humic acids on laser experiments will be discussed in the following paragraph.

5.4.2 Impact of the eigen-fluorescence of Aldrich humic acid

For a better understanding of the presented results, a fundamental difference between classic fluorescence and LIF measurements should be mentioned again. The fluorescence spectrograph LS 50 (Perkin Elmer) is equipped with a pulsed xenon lamp. Its pulse duration is approximately 20 µs. The fluorescence signal is integrated over the whole time period.

For LIF measurements, a very short light pulse of only 5 ns is used for sample excitation. The following detection interval can be controlled by a delay generator. To suppress all disturbing fluorescence signals, the time gate is opened not until 60 ns. The fluorescence lifetimes of all humic acids fall into this period.

For the accuracy of the classic fluorescence measurements, the extent of the humic acid eigen-fluorescence was determined. At the excitation wavelength of 337 nm and in the concentration range between 0.2 mg/l and 15 mg/l, the eigen-fluorescence of Aldrich humic acid is negligible. It becomes only relevant at the highest humic acid concentration, where approximately 90 % of the pyrene fluorescence (100 µg/l) are quenched.

For the determination of the K_{OC}-values by classic fluorescence measurements in chapter 4.4.3 and 4.4.4 all data are corrected for the eigen-fluorescence. For all LIF experiments in this work, the eigen-signal of the organic material is eliminated by the time delay generator.

For the correction of the second disturbance variable, the inner filter effect, the light absorption by humic acid solution is measured at the excitation and at the emission wavelength. All data presented in chapter 4.4.3 and 4.4.4 are corrected for the inner filter effect by the Lakowicz equation (18). The resulting K_{OC}-value for pyrene and the Krauthausen field soil is $1.1 * 10^4$ l/kg. It is slightly lower than literature data. Chiou, McGroddy and Kile (1998) reported K_{OC} values for pyrene and five different soils between $9.12 * 10^4$ l/kg and $9.77 * 10^4$ l/kg from classic batch experiments and HPLC analysis.

5.5 Development of the glass probe head

The development of the glass probe head was accomplished consecutively. Beforehand, the technical demands were defined. The main requirements are:

- high efficiency for the emission of the excitation light
- high efficiency for the collection of the fluorescence light of the surrounding medium
- emission of the excitation light over the whole spike surface
- low eigen-signal
- the distortion of the fluorescence spectra should be kept to a minimum
- no aging effect of the probe head due to adsorption of fluorescing material
- facile cleaning of the probe head

The suprasil probe head shown in Fig. 22 complies with these requirements and has been used for all further measurements.

5.6 Spiking of the soil

The different methods of spiking a soil with poorly water soluble substances like pyrene are described in chapter 4.6. The results show the principal feasibility of all three methods, but highlights also some disadvantages.

The main disadvantage of adding an aqueous pyrene solution to soils is the limited achievable concentration range. The low water solubility of pyrene (132 µg/l at 25 °C, Dabestani and Ivanov 1999) and problems of solution stability near the solubility limit, narrows this method down to a concentration range below 100 µg/l. Working within this concentration range it is the most appropriate method, because all test parameter (water to soil ratio, phase equilibration, wetting of the soil) stay close to reality. The test results (Fig. 24) show a linear correlation between the nominal concentration and the fluorescence intensity over the whole concentration range. Considering that these are results of in-situ measurements, the correlation factor of 0.977 is sufficiently high, even at very low concentrations.

Adding a surplus of water to the soil might cause some problems. First of all, it has to be assured that the pore water is in true equilibrium with the supernatant. Only if this condition is fulfilled, the transfer of results from supernatant measurements to the equilibrated pore water concentration is admissible. Secondly, the high water to soil ratio can lead to a different state of aggregation of soil particles than under natural conditions. This might have an effect, especially on the adsorption/desorption rate constants.

If these critical aspects are taken into account for the data interpretation, adding a surplus of water is an adequate method for adsorption studies at higher pyrene concentrations. The test results (Fig. 25) show a linear correlation between the fluorescence intensity and the nominal pyrene concentration between 80 µg/kg and 160 µg/kg sand. The correlation coefficient of 0.985 is sufficiently high.

Spiking the soil with an organic pyrene solution is the most problematic procedure. The great advantage of this method is the possibility to achieve very high pyrene concentrations that equal a multiple of the water solubility limit. Due to theoretical considerations and based on our test results, there are also some important disadvantages.

After adding pyrene, solved in methanol to the soil, the methanol is ablated at room temperature in an extractor cowl. If the solvent can be evaporated completely under these conditions, depends on the soil characteristics.

Besides this aspect, there are some intrinsic elements of uncertainty for this method. For the calculation of the optimal amount of methanol, two contradictory aspects have to be considered. The smaller the amount of solute, the worse the achieved distribution of pyrene in the soil. On the other hand, a higher volume of methanol will cause permanent changes in the soil matrix, which will lead to non-representative sorption characteristics of the soil.

Our results show, that the concentration range, where the in-situ fluorescence signal is proportional to the free pyrene concentration, cannot be extended significantly by organic spiking of the soil. There are some indications that pyrene concentrations above 100 µg/l lead to microcrystals or bilayer on the soil surface (Lochmüller and Wenzel 1990). Under these conditions no linear correlation between the pyrene concentration and the fluorescence signal

can be expected. In our experiments, these uncertainties lead to a higher variation coefficient, especially at higher concentrations.

In this context, it should be mentioned that all our experiments with aqueous pyrene solutions were conducted without any detergents or organic solutes, to guarantee for an unaffected phase equilibration.

5.7 Influence of the water content on the fluorescence signal

Due to different refraction indices of air and water, the water content of the soil is an important parameter for optical in-situ measurements. Because LIF fluorescence measurements in soils are new, the data available in literature are rare. Our own measurements show a critical threshold value for the mass ratio of water to sand. Up to a ratio of 10:100, the optical transition of the light from the surrounding medium into the probe head is hindered. Therefore the intensity of the fluorescence signal is highly depending on the sample water content. At water to sand ratios above 20:100, all signals are at the same level. Once the optical transition between the probe head and the medium is possible, the water content shows only a minor influence on the detected fluorescence intensity.

5.8 Batch experiments

5.8.1 Adsorption kinetics of pyrene to annealed sand

The first kinetic experiments were conducted in annealed sand, to analyse the pyrene adsorption to a carbon-free system with a relative small specific surface (0.570 m^2g^{-1}). For that purpose annealed sand was spiked with increasing pyrene concentrations. The fluorescence activity of the samples was detected by the laser probe head immediately after sample preparation. Under these conditions a linear correlation (R^2 = 0.977) between the applied pyrene concentration and the fluorescence signal can be observed, even at low concentrations. This observation confirms the expectation, that annealed sand without any organic compounds and with a relative small specific surface would adsorb pyrene only to a minor extent.

After 14 hours, the measurement results deviate strongly from this assumption. Over the whole concentration range the observed fluorescence intensity is close to the background level. At a pyrene concentration of 50 µg/kg sand, the fluorescence signal at 14 hours is reduced to 9 % of the original signal. From these results two conclusion can be derived. First of all, pyrene is bound to a large amount to annealed sand, although the specific surface of the sand is relative low. In this context Mader et al. (1997) reported that not only the sorbent surface area accounts for the sorption capacity of mineral surfaces, but also the type of the mineral. The second important result of this experiment is the observation, that even in annealed sand, most sorption places for pyrene are not accessible instantaneously. According to this Piatt et al. (1996) found pyrene equilibration times of 30 hours in batch experiments with aquifer sediments.

5.8.2 The photobleaching effect in LIF

The photolysis effect of pyrene has been discussed in literature in several publications (Zepp and Schlotzhauer (1979), Chen et al. (1996), Lehto et al. (2000), Chen et al. (2001)). The conclusions of these publications are contradictory (see chapter 2.3.2), and indeed there are many disruptive factors that can influence the detection of the photolysis effect.

Therefore our experiments had two defined aims:

- To detect the photolysis effect in a system that allows for a conservative estimation of its extent. For this purpose we used the flow-through cuvette of a HPLC system with a pulsed xenon lamp, fixed at the nitrogen laser wavelength.
- To detect the photolysis effect of pyrene in-situ by the laser probe head.

The results of the experiments in the HPLC flow-through cuvette are shown in Fig. 30. The test design of both experiments was the same. The first one started with the photolysis phase, the other one with the dark control phase. The interpretation of the data is based on the following assumption: Under constant adsorption conditions, it is reasonable to assume, that the slope of the light intensity curve of a sample – with or without irradiation – would constantly decrease over time. Based on this assumption it is possible, to compare a time phase with irradiation with the preceding time phase without irradiation. According to the assumption, a stronger decrease of the fluorescence intensity during the light phase can be led back exclusively on the photolysis effect.

Comparing this way phase 2 and phase 3 of the upper curve one obtains 69 arbitrary units versus 174 arbitrary units of fluorescence intensity. Therefore 105 units can be led back on the photolysis effect. Referring to 550 arbitrary units at the irradiation start, this value is equal to a decrease of the fluorescence intensity of 19.1 %. Comparing the same way time phase 4 and 5 one obtains a relative value of 24.0 %.

In phase 4, a marginal increase of the fluorescence intensity can be observed. The most reasonable explanation for this observation is back diffusion from the steel capillaries into the measurement cell. The pyrene concentration in the cuvette was lowered by photolysis in time phase 3, while the concentration in the steel capillaries remained constant. In phase 4 a partly equilibration of the concentration gradient can be observed. Considering the back-diffusion effect for the photolysis rate, the relative decrease due to photolysis is 28.1 % of the initial concentration.

The comparison of phase 3 and 4 of the second experiment gives a value of 25.2 % photolysis and between time phase 5 and 6 a value of 22.1 %. Considering the back diffusion during phase 5, one obtains a relative photolysis effect of 28.3 % for phase 6.

Summarising these data shows the pronounced effect of pyrene photolysis in aqueous solutions. For the interpretation of the data it is necessary to keep in mind, that the light source was a pulsed xenon lamp. The pulsed light source of the detection unit is designed to avoid photolysis effects as far as possible. In common HPLC systems, if pyrene solution is pumped constantly through the cuvette, one would not expect a significant photolysis effect. For online applications in soils, the situation is different. Constant fluorescence analysis of the same pyrene solution will cause significant artefacts due to the photolysis effect.

The data of the in-situ measurements in annealed sand by the LIF probe head show similar results as the HPLC system. The variation of the laser repetition rate and the alternation between phases with and without irradiation of the sample show similar effects on the pyrene fluorescence signal. To avoid a photolysis effect as far as possible, all further measurements with the LIF probe head were conducted without constant irradiation. Although the laser system was kept on during the whole experiment to ensure a constant operating temperature, laser pulses were only emitted during the measurement time. This means, that the sample

irrigation time was below twenty seconds for each measurement point at a repetition rate of 1 Hz.

5.8.3 Adsorption kinetics of pyrene to a forest soil

At natural water to soil ratios, no significant fluorescence signals of pyrene can be observed in the natural forest soil Jülich. Although there is a reproducible signal for the first six minutes, the signal to noise ratio does not allow a substantiated interpretation of the data (Fig. 33). Because fluorescence measurements can only detect free pyrene, they show some limitations for soils with high organic carbon contents (> 5 %). In these soils all pyrene is sorbed immediately by solid and dissolved organic matter.

Due to these experimental limitations, experiments were conducted at very high water to soil ratios, to collect data about the sorption kinetics of pyrene to natural organic matter. The data confirm the very high sorption capacity of the forest soil. Based on these data, it is unlikely to detect free pyrene at natural water to soil ratios in soils with high carbon contents. These findings are important for the interpretation of the soil column experiment with the forest soil Jülich.

5.8.4 Adsorption kinetics of pyrene to annealed soils

The batch experiments with the LIF probe head offer the opportunity to follow in-situ the adsorption kinetics of pyrene to annealed soils. Even after removing the organic material, both soils show very diverse sorption characteristics. For the sandy soil Kaldenkirchen, the instantaneous sorption of pyrene is insignificant. At the beginning of the LIF measurements (t = 3 min), it is still possible to detect the whole amount of pyrene added. The sorption characteristics of the annealed forest soil Jülich are quite different. At the first measurement point, one minute after the addition of pyrene, already 60 % of the pyrene mass are adsorbed. The instantaneous sorption sites contribute fundamentally to the overall pyrene adsorption capacity. The data of both soils were fitted by the bicontinuum model.

The equation $y = a + be^{-kx}$ was fitted to the data shown in Fig. 43, were x is the time and a, b and k are defined by the following equations:

$$a = \frac{Pyr^{I}_{free}}{k'_{ads}/k_{des} + 1} \qquad b = \frac{(k'_{ads}/k_{des})}{k'_{ads}/k_{des} + 1} \qquad k = (k'_{ads} + k_{des})$$

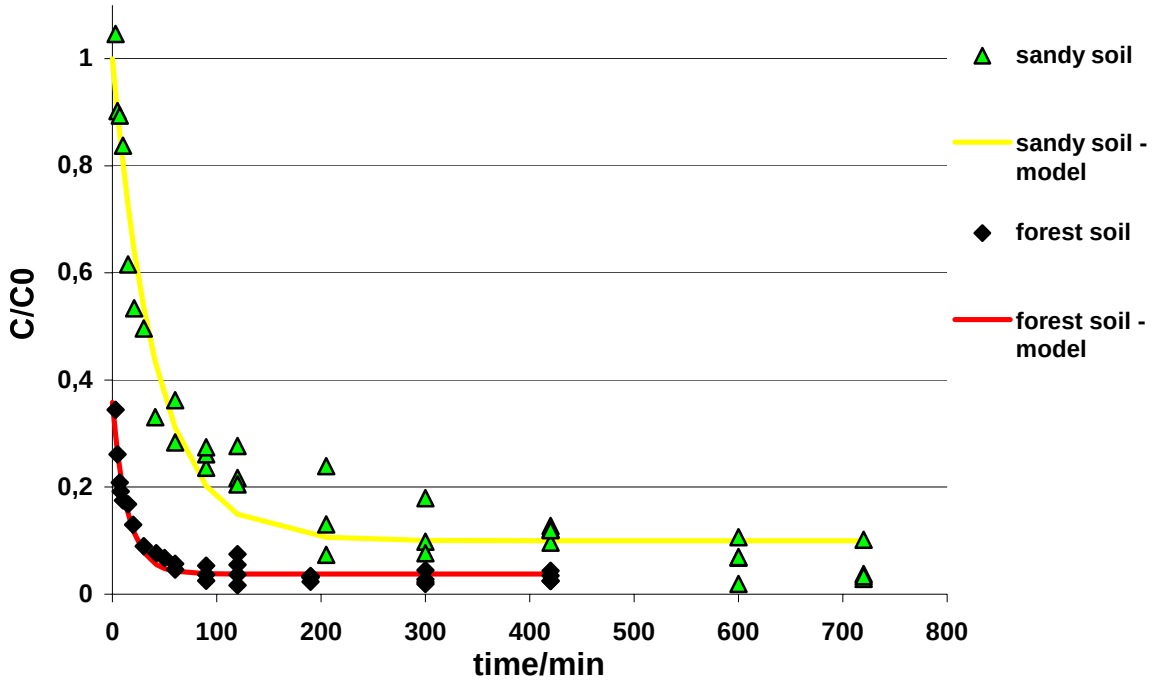

Fig. 43: Adsorption kinetics of pyrene over time in annealed soils measured by LIF.

Modelling the data of the sandy soil Kaldenkirchen by the bicontinuum model, one obtains a K_d value of 4.5 l*kg^{-1}. This result is in good accordance with results of Piatt et al. (1996), who reported K_d values between 7.2 l*kg^{-1} and 9.3 l*kg^{-1} for pyrene and uncontaminated aquifer material. The fraction of instantaneous sorption sites is f = 0, which means that all sorption sites in the annealed soil Kaldenkirchen are rate limited. The calculated desorption rate for pyrene is k_{des} = 0.145 h^{-1}.

The modelling of the forest soil data yields a distribution coefficient of K_d = 25.7 l*kg^{-1}. Considering the annealing process, this value is relative high, compared to literature data of K_d values for inorganic surfaces (K_d = 0.84 l*kg^{-1} for Fe_2O_3 and Pyrene, Mader et al. 1997).

There are two factors that might explain the high value. The first reason for the relative high adsorption capacity is the high specific surface area of 7.4 m^2 g^{-1} which is much higher than the specific surface area of the sandy soil: 2.6 m^2 g^{-1}. This can be directly related to the clay fractions (f_{clay}) in sandy soil and forest soil which are 0.036 and 0.14 respectively (see annex 3 and 4). Indeed, distribution coefficients normalised by the clay fraction: K_d/f_{clay} are of the same order. K_d/f_{clay} values of 125 (l kg^{-1}) and 183 (l kg^{-1}) are respectively found for the

sandy soil and the forest soil which demonstrate the importance of the mineral phase in the sorption capacity of annealed soils.

Nevertheless, a second reason for the observed higher K_d or K_d/f_{clay} values of forest soil is the OC content. Although the forest soil was glowed in a thin layer and homogenized several times during the annealing process, the removal of the organic substance was incomplete. The subsequent analysis shows a TOC value of 0.011 % (see appendix 4).

The fraction of instantaneous sorption sites is f = 0.1 for the forest soil and the desorption rate is k_{des} = 0.45 h^{-1}. The modelled data show a good correlation with the measurement results. The reproducibility of the in-situ laser induced fluorescence measurements is excellent (see Fig. 35).

5.9 Soil Column Experiments

5.9.1 Hydrodynamic characterisation of the soil columns by breakthrough measurements of the conservative tracer bromide.

For the optimisation of the experimental conditions, a forward simulation of the bromide breakthrough in the soil columns was calculated. Based on these results, the following initial and boundary conditions were defined:

Soil surface area:	36.4 cm²
Bulk density Kaldenkirchen, annealed:	1515 g/l
Bulk density forest soil, annealed:	950 g/l
Bulk density forest soil, air dried:	625 g/l
Irrigation rate:	60.0 cm³/h
pore water velocity for Kaldenkirchen:	v = 3.81 cm/h
pore water velocity for the forest soil:	v = 2.53 cm/h

The effective dispersion of a substance in the soil column depends on the molecular dispersion, which is a property of the substance, and the hydrodynamic dispersion, which depends on the flow characteristics of the soil column.

Bromide diffusion coefficient in water:

$$D^w = 0.0738 \text{ cm}^2/\text{h}$$

Effective dispersion coefficient of bromide in the sandy soil :

$$D = 0.516 \text{ cm}^2/\text{h}$$

Effective dispersion coefficient of bromide in the forest soil :

$$D = 0.813 \text{ cm}^2/\text{h}$$

The dispersivity can be calculated by the quotient of the effective dispersion coefficient and the pore water velocity.

For Kaldenkirchen one obtains:

$$Disp. = \frac{D}{v} = \frac{0.561 cm^2 h^{-1}}{3.81 cm h^{-1}} = 0.135 cm$$

The dispersivity of the annealed forest soil is 0.306 cm.

The quotient of the irrigation rate and the soil surface area is Darcy´s flux, which is Jw = 1.648 for our experiments.

The actual solute flux across the soil surface [$ML^{-2}t^{-1}$] during the sorption phase was:

cv_{Top} = 1860 mg/cm^2h

(product of the solution concentration [ML^{-3}], which was c = 1130 mg/l for a time period of 312 h, and c = 0 mg/l during the desorption phase, and the average pore water velocity v [Lt^{-1}].

The bromide concentration at the soil column outlet over time cv_{Bottom} [$ML^{-2}t^{-1}$] was modelled by Hydrus 1D.

For the annealed sandy soil Kaldenkirchen, the model results correspond well to the concentration flux, measured at the column outlet. The bromide equilibrium concentration is reached after 12 hours and no significant fluctuation of the maximum level can be observed. The results were calculated on the assumptions, that the soil column is in hydrodynamic equilibrium and all contained water does contribute to the solute transport. Adsorption of bromide was set to zero, because it has been shown in numerous experiments before, that in most soils bromide behaves like a conservative tracer (Dunnivant et al. 1992, Vereecken et al. 2001).

Both, the increase of the bromide concentration and the concentration drop after 312 hours can be simulated well by Hydrus 1D. The coefficient of model efficiency (Nash and Sutcliffe 1970) of 0.9996 shows that it is the appropriate model.

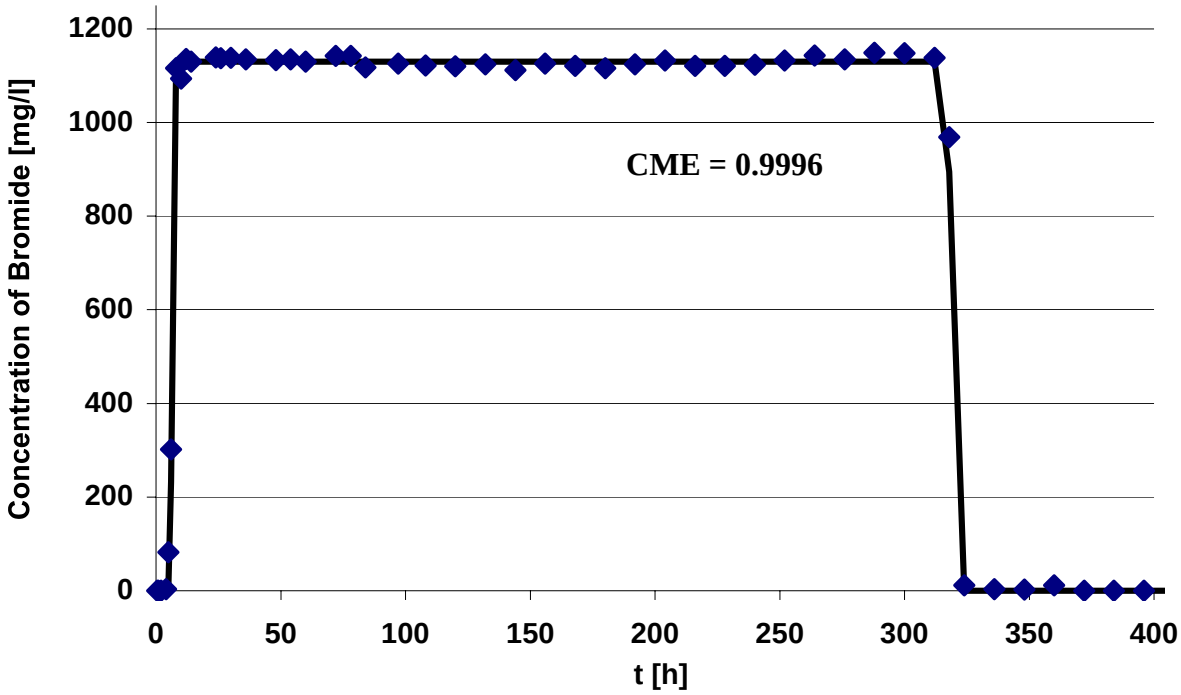

Fig. 44: Modelled and experimental results of the bromide breakthrough in the annealed sandy soil Kaldenkirchen at the bottom of a 25 cm soil column.

The results of the soil column with the annealed forest soil Jülich show a similar characteristic. One slight difference to the results for Kaldenkirchen are the small fluctuations around the bromide equilibrium concentration. Because they are within the uncertainty range of the method, and the experimental results can be still modelled accurately (CME = 0.9993) with the boundary conditions described before, an over-interpretation of the results should be

avoided. The increase as well as the decrease of the bromide concentration in the soil column outlet can be modelled precisely.

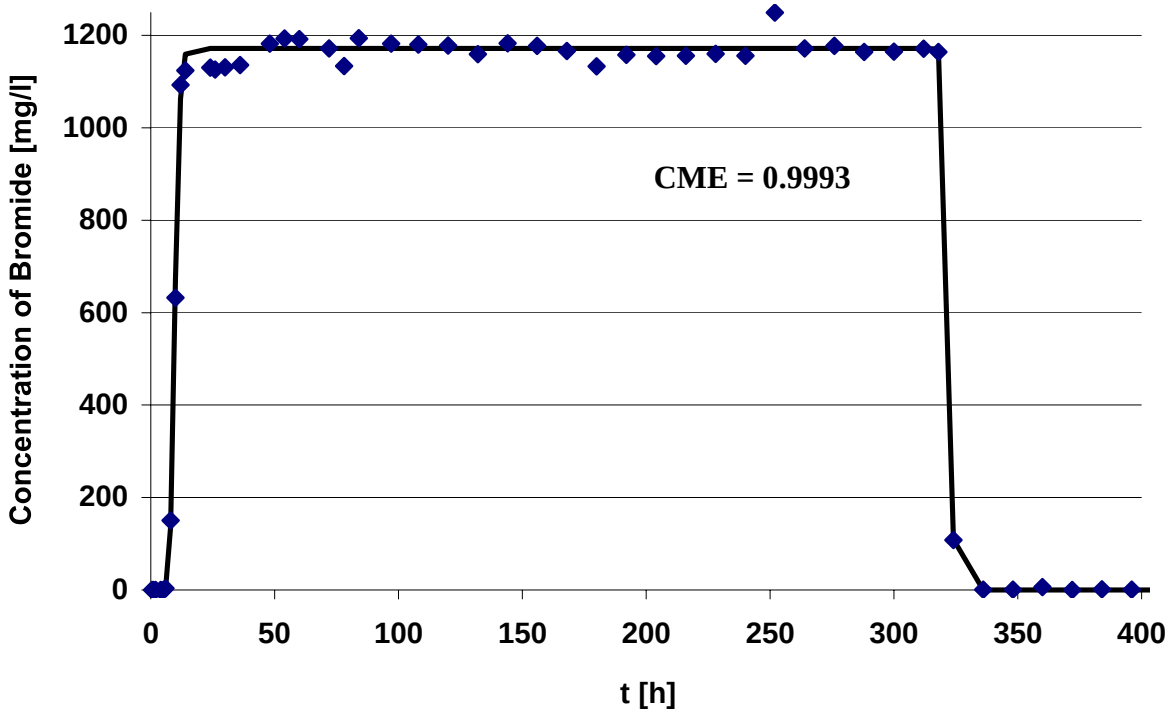

Fig. 45: Bromide breakthrough concentration over time in the annealed forest soil Jülich. The length of the column is 25 cm.

5.9.2 Pyrene transport in the annealed sandy soil Kaldenkirchen

As described before, the pyrene concentration was measured by laser probe heads in 1.5 cm, 3.5 cm, 9.5 cm and 19.5 cm below the soil surface. Additionally the outflow concentration of pyrene was analysed by LIF measurements in a 1 cm quartz cuvette.

The values for f, K_d, ϖ (in Hydrus defined as α) and β, fitted to the outflow data, were used for a Hydrus 1D forward calculation of the pyrene concentration over time for different soil depths. Afterwards the results of the forward calculation were compared with the probe head data without any further fit of the model results.

In the natural forest soil, all pyrene is adsorbed to the soil matrix or to dissolved organic matter. There is no free pyrene in the soil solution, even at a soil depth of 1,5 cm and an

irrigation time of 348 hours (see Fig. 39). The comparison with the annealed soil shows the enormous binding capacity of the soil organic matter.

The results correspond well to the batch experiment results with the natural forest soil (see chapter 4.10). In the batch experiments, free pyrene can be only detected at unnaturally high water to soil ratios. And even at a ratio of 80 ml pyrene solution to 0.6 g forest soil, all free pyrene is adsorbed completely after 10 hours. In literature, many authors worked with unnatural high pyrene loads on natural soils to avoid this problem. Hwang and Cutright (2002) for example, used a sandy loam with initial pyrene concentrations of 15 mg/l.

In the sandy soil Kaldenkirchen, the breakthrough of pyrene at the soil column outlet shows several interesting effects (Fig. 46). First of all, the pyrene concentration shows a very steep increase after 80 hours. Starting from the background level, it takes only 24 hours until the maximum concentration of the experiment is reached. Therefore the free pyrene breakthrough in the soil column shows a very sharp front with high concentrations of truly dissolved pyrene. Once the concentration of the stock solution is reached in the column outlet, the breakthrough curve shows pronounced fluctuations around the equilibrium concentration. An explanation of this phenomenon is not easy, because the bromide tracer shows a homogeneous flow regime. For this reason a hydrodynamic heterogeneity is not plausible. The reasons for the observed effect will be discussed below, together with the model results. Brusseau and Rao (1989) observed similar breakthrough curves in their experiments with organo-bromide compounds in aquifer material. The curves showed also a very sharp front and two successive peaks.

After the start of the desorption phase, the drop of the pyrene concentration begins almost immediately, but it slows down soon and goes over into a pronounced tailing that is not completed until the end of the test. The Hydrus 1D model also shows a pronounced tailing under chemical non-equilibrium conditions, but the model predicts an earlier decline to the background concentration. The reason for this discrepancy might be effects, that are not integrated in the Hydrus 1D model. For example, it has been postulated that slow desorption of organic compounds may be controlled by hindered diffusion through micropores (Shor et al. 2003). An effect like this could lead to an additional delay in pyrene sorption, which is not predicted by the model.

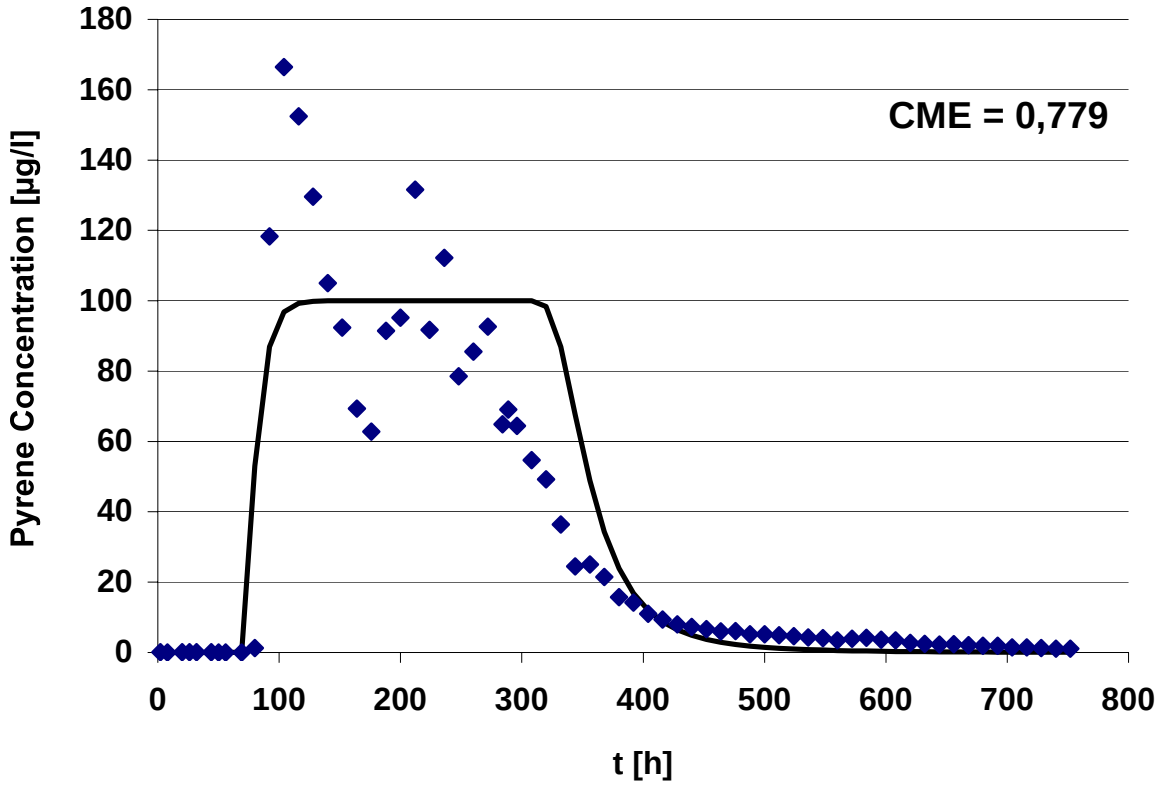

Fig. 46: Pyrene outflow concentration over time for the sandy soil Kaldenkirchen. The LIF results were measured in a 1 cm quartz cuvette.

The table below shows the modelled K_d value and the optimised fitting parameter for the Hydrus 1D model (Fig. 46). The initial values for the model run are given in brackets. The number of iterations for the least squares analysis was six.

Least squares analysis	Initial value
K_d = 19.0	(4.5)
f = 0.470	(0.700)
ϖ = 0.273	(0.04)
β = 0.720	(1.0)

As a result of the least squares analysis, the pyrene breakthrough data can not be fitted adequately by a Freundlich isotherm. A value of $\beta = 0.720$ shows clearly a deviation from the Freundlich adsorption model.

The fitted parameter were used for the forward calculation of the probe-head data at different soil depth (Fig 47). With increasing depth, the calculated data show a more pronounced tailing of the breakthrough curve and the speed of the initial pyrene breakthrough decreases.

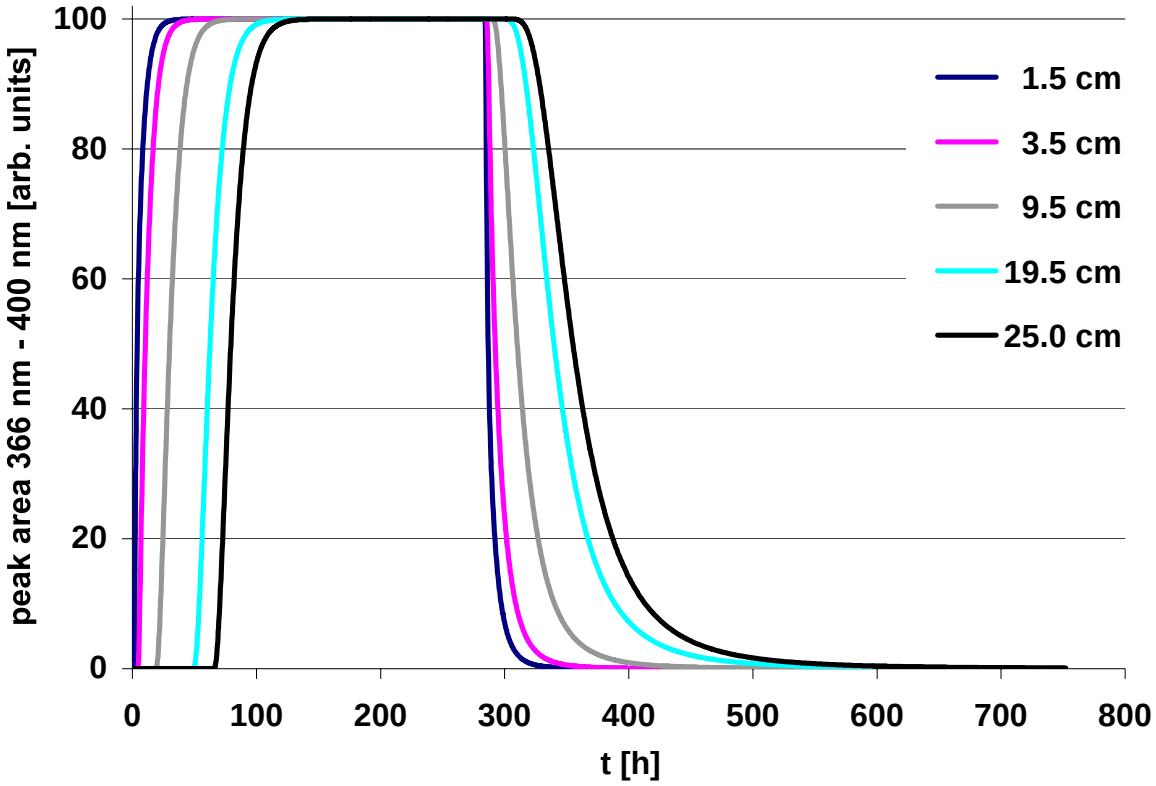

Fig. 47: Forward calculation of the pyrene concentration over time at different soil depths for the sandy soil Kaldenkirchen.

The breakthrough curves of the forward calculation are compared with the probe head data at different soil depths. Therefore, the outflow data of the soil column were transferred to different soil depths and afterwards directly compared to the in-situ fluorescence data of probe heads on the same level.

Figure 48 shows the comparison of the model results for probe head no. 12 on the 19.5 cm level and the in-situ measured LIF data.

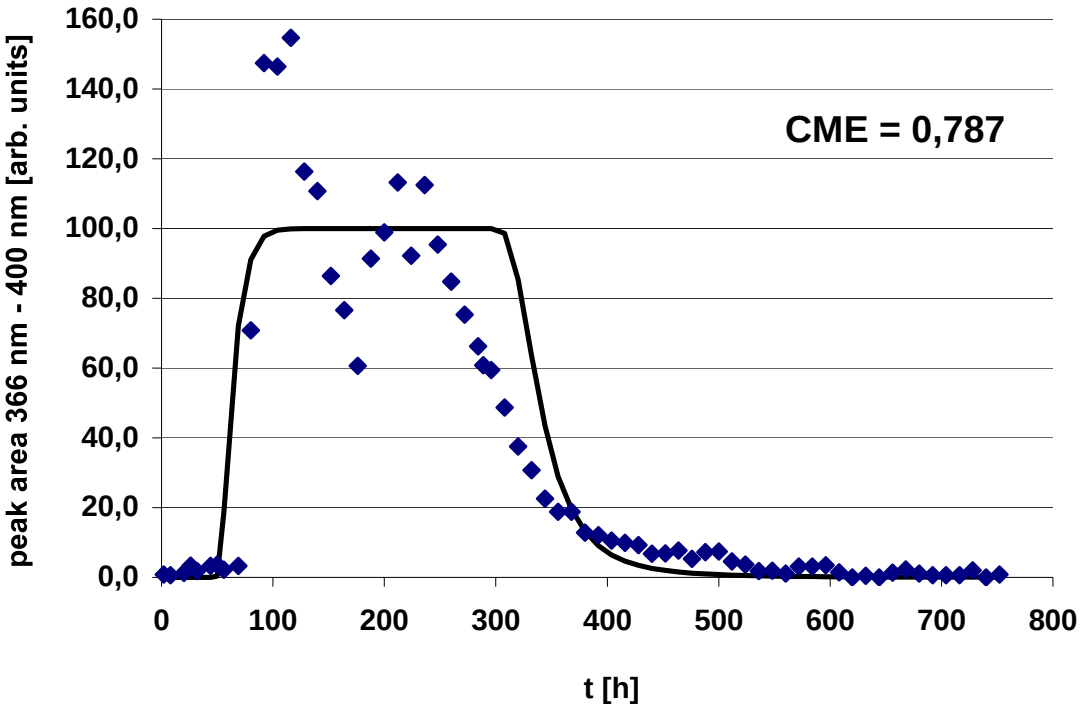

Fig. 48: Free pyrene concentration at LIF probe head No. 12 (19.5 cm) over time.

The model results can simulate well some important phases of the pyrene breakthrough curve, but emphasise also some unexpected characteristics of the experimental data. The steep increase of the free pyrene concentration after 70 hours is simulated well by Hydrus 1D. However, the experimental data show an overshoot of the pyrene concentration to a very high level and subsequently a kind of compensation, before the expected equilibrium concentration is reached. There are two aspects that might contribute to the explanation of this effect. First of all, a kind of facilitated transport by inorganic colloids may contribute to the strong initial release of pyrene out of the soil column. Although this explanation is reasonable, it is hard to proof. Until know, there are no unambiguous data in literature about the correlation of the binding type of pyrene to inorganic colloids and its photochemical properties. Mackenzie et al. (2002) also regret the lack of a definition for the type or strength of interaction which classifies a solute as being “sorbed” or “freely dissolved”. To answer this problematic will be of particular interest for further LIF studies.

The second approach to explain the observed data is the experimental set-up for the soil column irrigation. The soil columns were saturated at the start of the experiment. Afterwards, they were irrigated for 24 hours with a $CaCl_2$ solution at a rate of 60 ml per hour to reach

hydraulic equilibrium. The exchange of this solution against the aqueous pyrene solution with $CaBr_2$ at a constant irrigation rate, marks the starting point (t = 0) of all our experimental results. If 24 hours were to short to transfer the soil columns into a hydrodynamic equilibrium, the high initial pyrene concentrations could go back to temporary higher pore water velocities. The following decrease of the pore water velocity and therefore higher contact time to the soil matrix could explain the relative low pyrene values before the pyrene concentration reaches the “true equilibrium”. This explanation should be understood as one possible explanation. To proof it, further experiments and model results are essential. There are also some aspects against this hypothesis. If the changes in pore water velocity are sufficiently high to influence the sorption equilibrium of pyrene, these changes should be visible in the bromide breakthrough curves.

To summarise the different aspects of the high initial pyrene breakthrough and the subsequent drop of the pyrene concentration, the following facts should be kept in mind:

- The observed effect is no artefact of the LIF probe head, because the effect is clearly visible in the soil column outlet.
- The effects can be observed at several LIF probe heads
- The irrigation rate was constant over time (precise HPLC pumps and regular checks of the solution containers).
- Due to the relative low irrigation rate, the water content might have decreased in the upper part of the soil column

The drop of the free pyrene concentration during the desorption phase is steeper for the modelled data. In the experiment, it starts earlier and takes longer than simulated by Hydrus 1D. Both, the measured pyrene concentration and the modelled data reach the background level approximately after 600 hours. The high sensitivity of the laser probe head allows the detection of pyrene concentrations close to the background signal. This opportunity is essential, because Altfelder et al. (2001) emphasise that analytical methods often fail for detecting the whole time period of the tailing of non-equilibrium breakthrough curves.

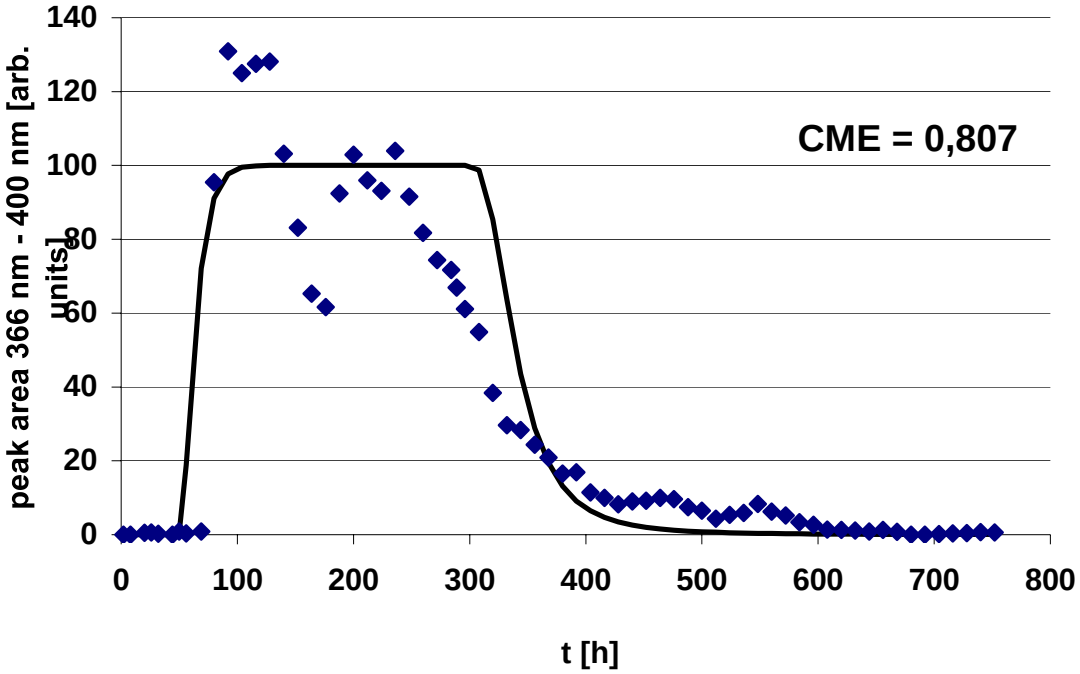

Fig. 49: Free pyrene concentration at LIF probe head No. 10 (19.5 cm) over time.

The experimental and simulated data at probe head no. 10 show similar effects than probe head no. 12, but the deviations from the equilibrium concentration are less pronounced. Anyway, the shape of the curve is the same for all three probe heads and for the free pyrene concentration in the soil column outlet (Fig. 46).

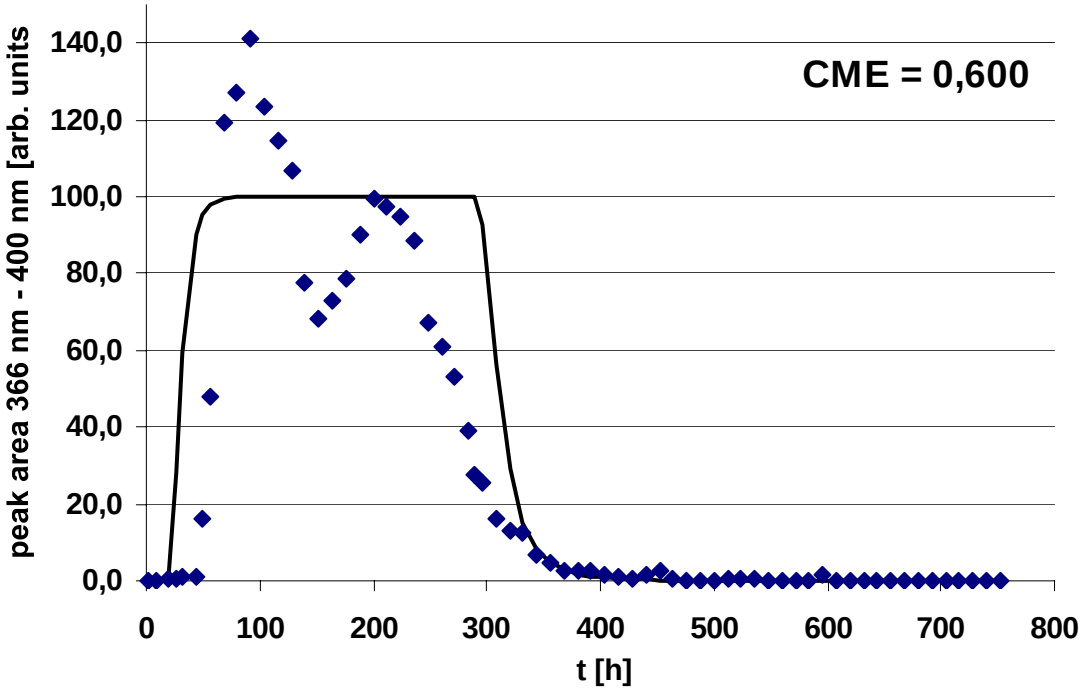

Fig. 50: Free pyrene concentration at LIF probe head No. 8 (9.5 cm) over time.

The measurement results of the 9.5 cm level show an effect, that can be observed also, but less pronounced on the 19.5 cm level. The pyrene fluorescence goes already back before the start of the desorption phase. The explanation for this observation is a decrease of the water content and therefore a disturbance of the transition of fluorescence light into the probe head. This drying effect is the same effect as described in chapter 5.7 for very low water contents. For some reason, the effect was stronger in our soil column experiments. The drying effect is the reason for the unreliable results of the probe heads on the 1.5 cm and 3.5 cm level. Because the Hydrus 1D forward calculation is based on fluorescence measurements in a quartz cuvette, an influence on the model data can be excluded. The comparison with the modelled data and the time of the fluorescence drop shows, that the probe heads no. 10 and 12 gave realistic results.

Based on these results, two general requirements for the use of the LIF probe heads in soils can be derived. The LIF probe heads should only be applied to saturated soils and sediments or it must be assured, that the system is in hydraulic equilibrium at the begin of the experiment. If the water content at the probe head is constant, the method can be also applied to unsaturated soils.

5.9.3 Pyrene transport in the annealed forest soil Jülich

The fluorescence data of the column outlet for the forest soil Jülich were fitted in the same way. The figure below shows parallels and differences of the measurement results and the fitted values.

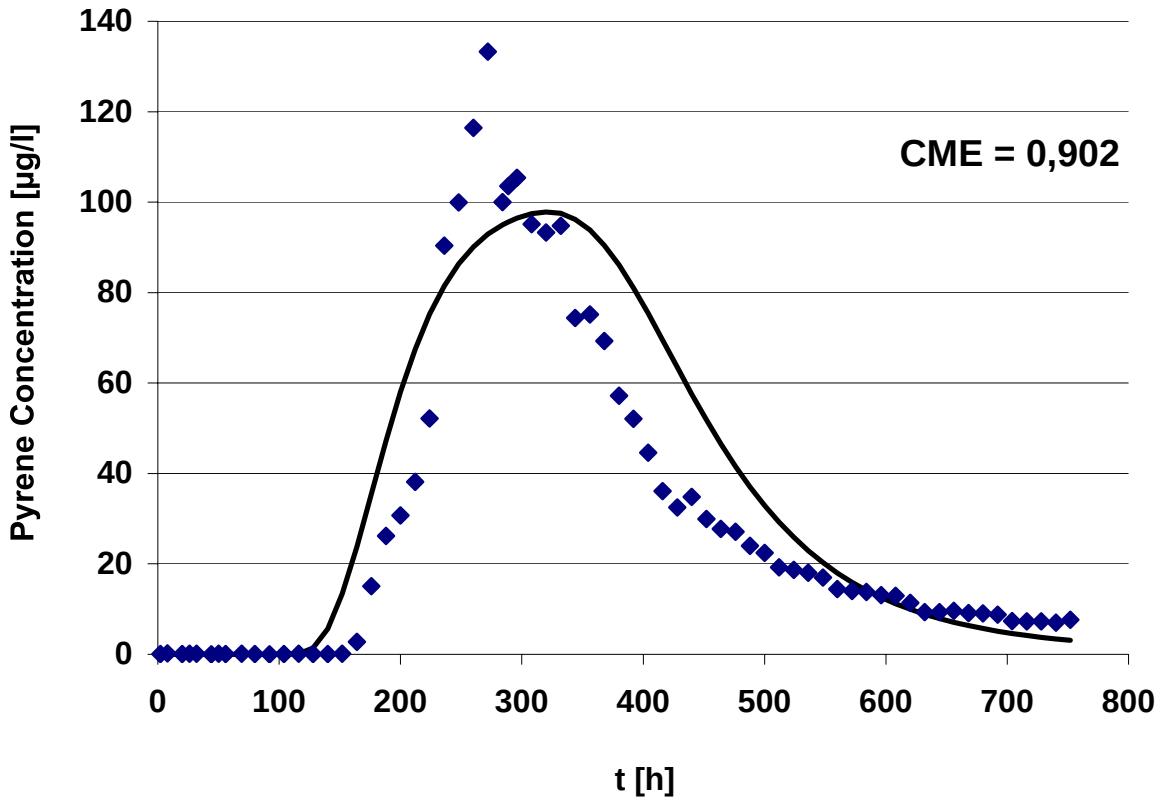

Fig. 51: Soil column experiment with the annealed forest soil Jülich. The graph shows the free pyrene concentration measured by LIF in the column outlet over time.

The table below shows the modelled K_d value and the optimised fitting parameter for the Hydrus 1D model (Fig. 46) The initial values for the model run are given in brackets. The number of iterations for the least squares analysis was six. For the forest soil Jülich, it was possible to model the data adequately with a Freundlich sorption isotherm. Calculating other values for β did not result in higher correspondence between model and experimental results.

Least squares analysis	Initial value
K_d = 41.5	(37.0)
f = 0.02	(0.10)
ϖ = 0.092	(0.066)
β = 0.0 (fixed)	

Comparing the pyrene breakthrough at the column outlet for both annealed soils (Fig. 46 and Fig. 51) some aspects are remarkable. The time before the increase of the free pyrene concentration in the annealed forest soil Jülich is almost twice as long as in the sandy soil Krauthausen. This corresponds well with the batch experiment data (Fig. 43). They also show a higher sorption capacity of the annealed forest soil. Anyway, the K_d values for both soils were significantly lower. To give a better overview, all K_d-values are listed again:

	Kaldenkirchen	Jülich
Batch experiment:	K_d = 4.5 L*kg^{-1}	K_d = 25.7 L*kg^{-1}
Soil column exp.:	K_d = 19.0 L*kg^{-1}	K_d = 41.5 L*kg^{-1}

Deviations between K_d values from batch and soil column experiments are well known in literature. Vereecken et al. (1999) reported deviations between batch and soil column experiments for uranin and aquifer sediments. Bilkert and Rao (1985) and Lion et al. (1990) found deviations between both systems up to 100 % for different organic compounds, and Piatt et al. (1996) reported deviations of an order of magnitude for PAH´s. The interpretation of the observed deviations has become even more difficult, since Maraqa et al. (1998) rejected in their work most of the explanations proposed before. The most plausible approaches are still deviations due to different soil to water ratios or effects of the batch mixing procedure.

As described before, the calculated data for K_d, f, ϖ and β were used for the forward calculation of the pyrene breakthrough (Fig. 52). In this context two further characteristics of the breakthrough curves should be mentioned. Although the increase of the pyrene concentration in the sandy soil is not as steep as in the forest soil, the shape of the measured values is still steeper than for the simulated data. Moreover, the measured data of the column outlet concentration show a more pronounced tailing than calculated by the Hydrus 1D model. In this context Connaughton et al. (1993) reported desorption times for naphthalene of up to eight days for soils with very low organic carbon contents (0.36 %). The shape of the desorption curve give cause for the assumption, that the tailing would have continued for several days, if the test would not have been finished.

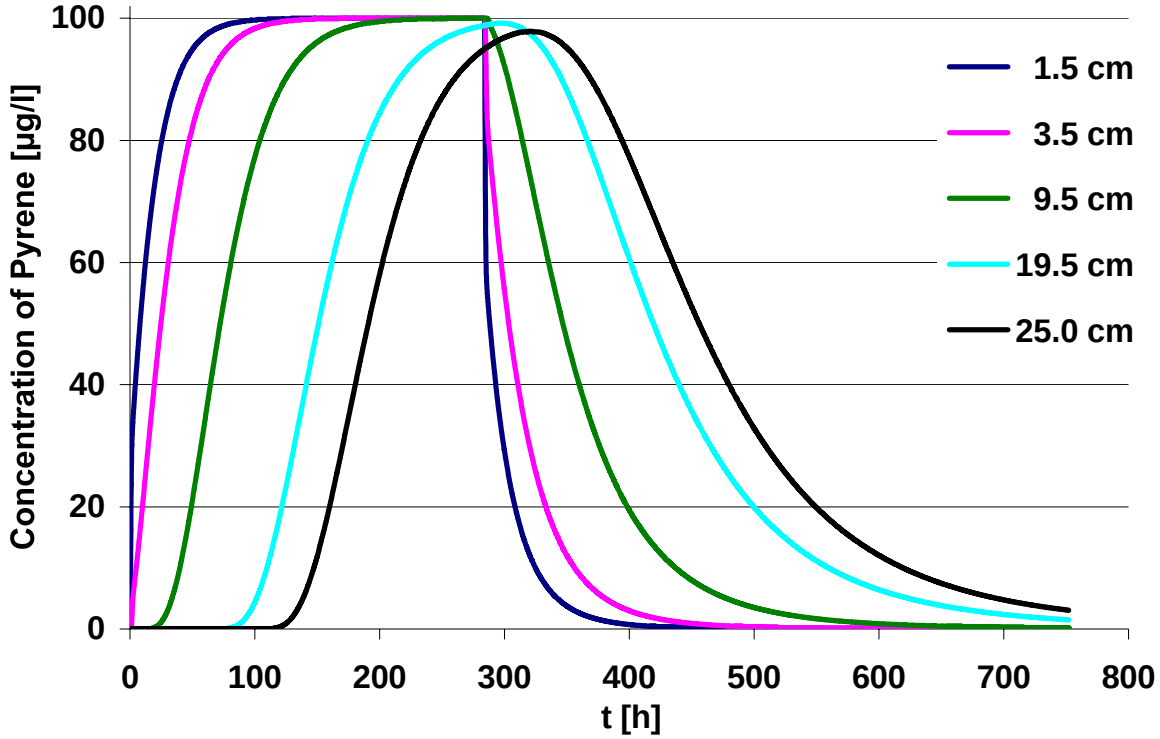

Fig. 52: Forward calculation of the pyrene concentration over time at different soil depths.

The model results illustrate very well a general effect of breakthrough curves of strong adsorbing substances like pyrene. The lower the soil depth, the longer the system remains under equilibrium conditions. The chart below shows a comparison of the model results and the measured data of probe head No. 6 on the 3.5 cm level.

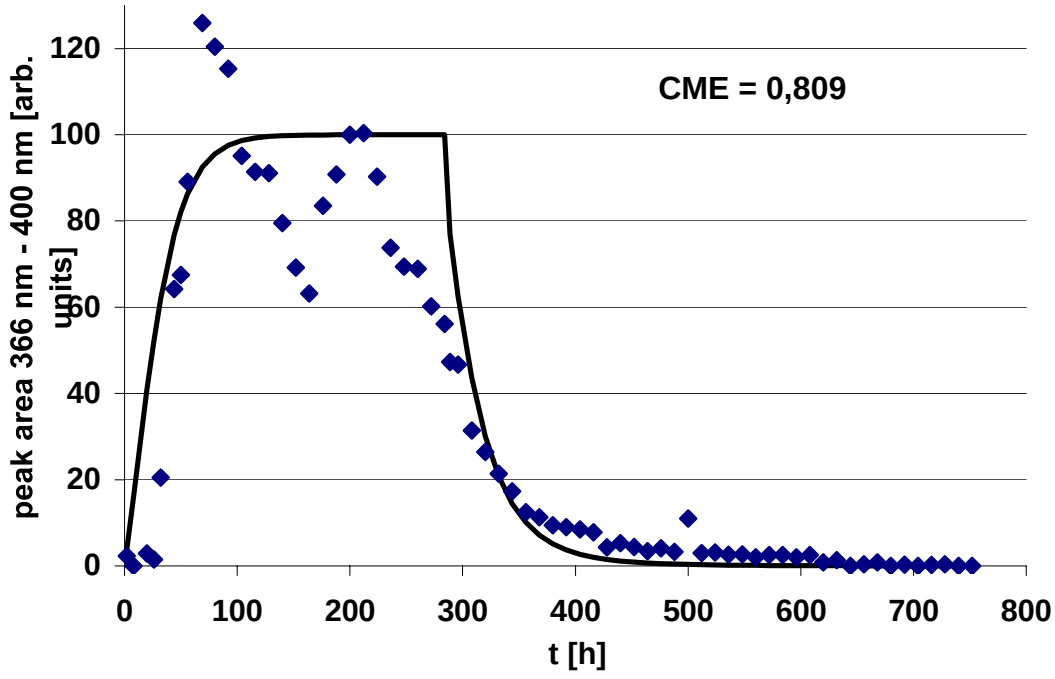

Fig. 53: Free pyrene concentration at LIF probe head No. 6 (3.5 cm) over time.

The forward calculation in Hydrus 1D corresponds well to the in-situ measured data. But as well as the sandy soil, the forest soil Jülich shows also the effect of very high pyrene concentrations directly after the substance breakthrough. The different aspects of this observation has been discussed above and further work will be necessary, to enlighten the effects that contribute to this phenomenon. Like the soil Kaldenkirchen, also the forest soil Jülich shows a drying effect for the probe head data. Fortunately, this effect is less pronounced, so that it is possible to analyse data from the 3.5 cm level. For the 1.5 cm level, the problems due to the drying effect are the same for both soils (Fig. 40, 41). In this context, the need of a stable hydrodynamic equilibrium at the begin of the test should be stressed once again.

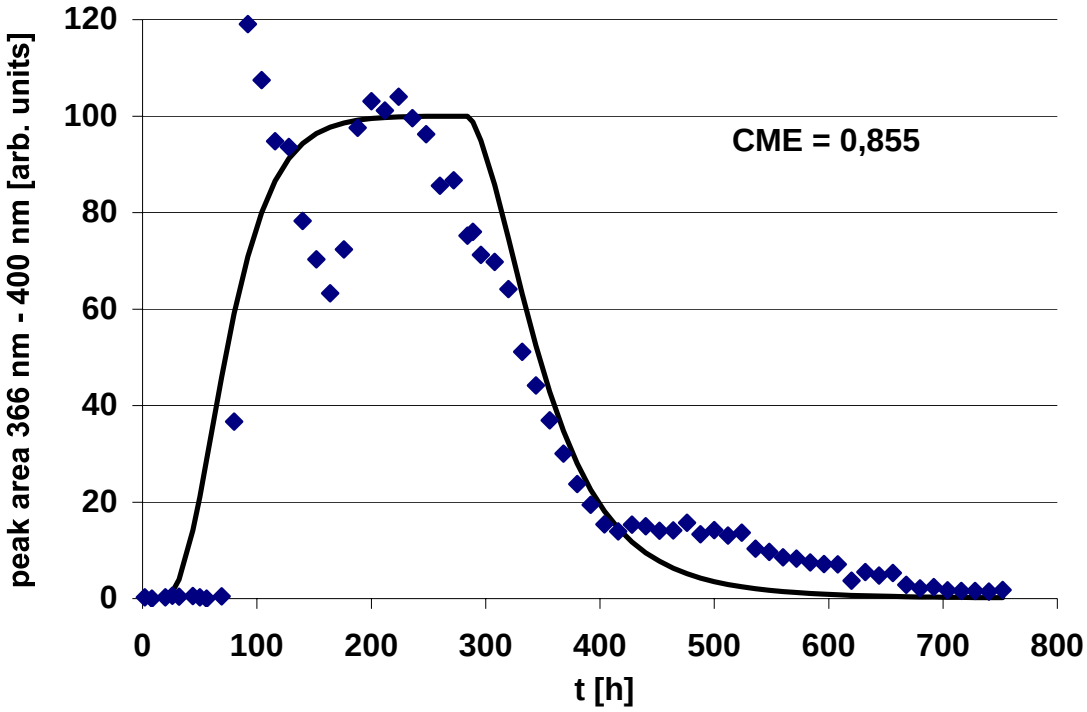

Fig. 54: Free pyrene concentration at LIF probe head No. 7 (9.5 cm) over time.

The data of probe head no. 7 give realistic values for the desorption phase. Without a significant drying effect, the laser probe head offers the opportunity to follow in-situ the desorption of pyrene. This could lead to new insights to adsorption/desorption hysteresis. For our data, the observed tailing is more pronounced than calculated by Hydrus 1D. Further experiments, were drying effects are excluded carefully, can give information about very slow desorption kinetics, which are reported by many authors. Karickhoff and Morris (1985) for example postulate, that for sensitive methods and accurate experimental conditions, the desorption of hydrophobic chemicals continues for weeks.

Until know, only 2D spectra have been discussed in this work, to give a better overview of specific experimental effects. Anyway, the LIF probe heads detect over the whole time period the complete spectral information of the sample. This offers the opportunity to generate real-time in-situ 3D spectra (Fig. 56). This unique opportunity of LIF probe heads, will lead to additional insights about the interaction of fluorescing substances like pyrene and the soil matrix. The spectra in Fig. 56 show the comparability of the in-situ spectra and classic fluorescence measurements in quartz cuvettes. The scattering effect, discussed in chapter 5.5 is also remarkable in the 3D spectra, but it does not influence significantly the quantification of pyrene.

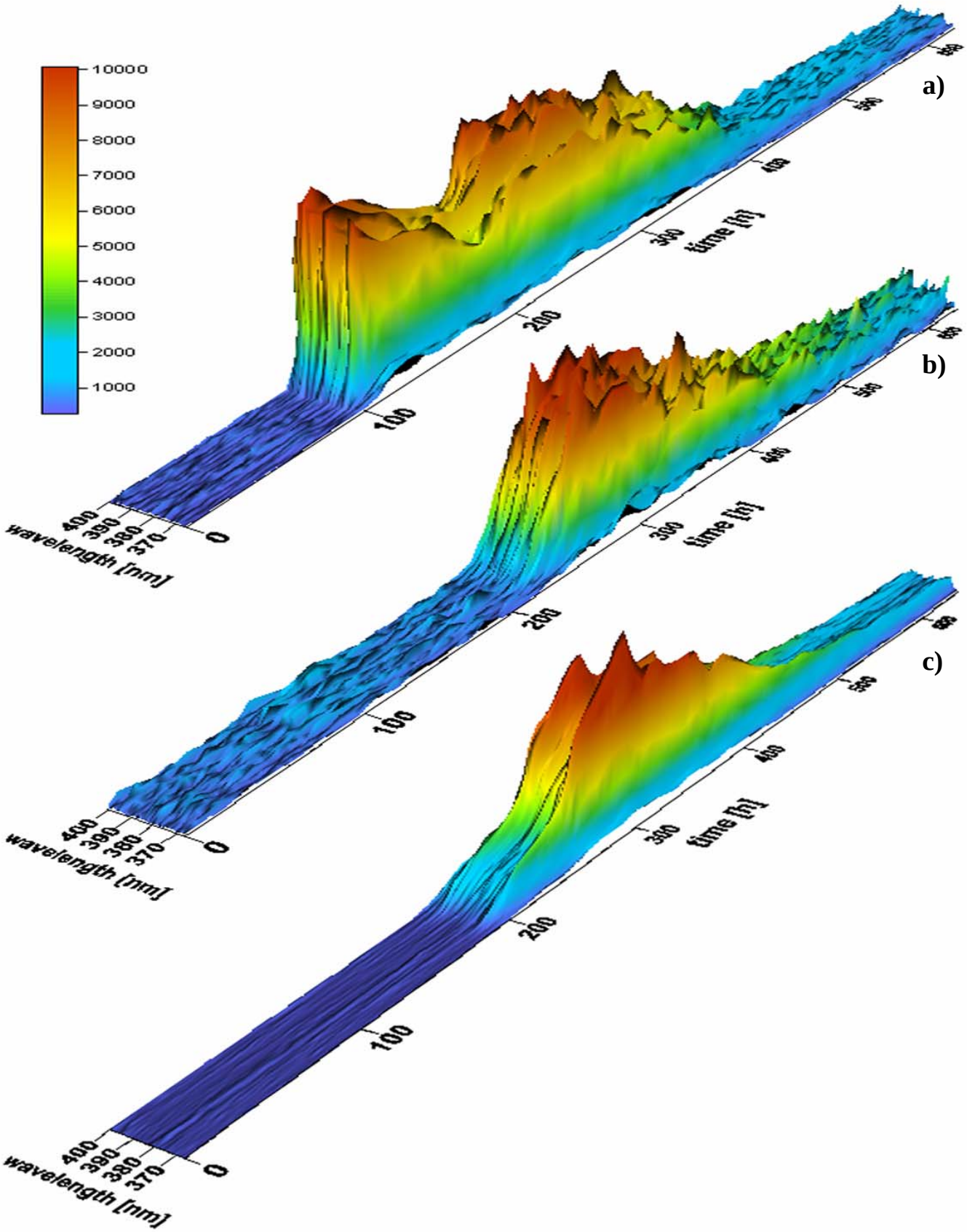

Fig. 56: Pyrene breakthrough at different soil depth in annealed forest soil. Spectrum a) was detected by a laser probe head at 9.5 cm, spectrum b) at 19.5 cm and spectrum c) at the column outlet (25.0 cm).

5.10 Conclusions

The most important aspects, that can be derived from this work are:

- The developed laser probe head allows real-time in-situ fluorescence measurements in soils.
- The final geometry and production process of the suprasil probe, complies with the postulated technical requirements
- The small dimensions of the probe head enables measurements with only minor disturbance of the soil structure (micro-invasive)
- The high temporal and spatial resolution of the system makes it possible, to generate in-situ 3D fluorescence spectra
- The probe head can be used to differentiate between dissolved pyrene and pyrene, adsorbed to soil organic matter
- The optical probe head offers the opportunity to follow in-situ pyrene adsorption kinetics
- The laser probe head can be integrated into soil column systems, to detect breakthrough curves at different soil depths
- The in-situ fluorescence data of the laser probe head are directly comparable with fluorescence data of the soil column outlet
- The breakthrough curves of pyrene in the soil column outlet can be simulated well by the Hydrus 1D model.
- The forward calculated probe head data fit well to the results of the in-situ fluorescence measurements
- For water saturated systems, the probe head measures reliable results, even at very low concentrations (in the 10 µg/kg range)
- In unsaturated systems the water content should be kept constant, to guarantee constant transition rates for the detection of the fluorescence light
- To avoid artefacts in the adsorption equilibrium, aqueous solutions of pyrene should be preferred for adsorption studies
- To avoid the photobleaching of pyrene as far as possible, laser pulses should be limited to 20 s per measurement
- The laser probe head offers the opportunity, to conduct batch experiments at natural water to soil ratios

5.11 Outlook

The results of this work open some new perspectives, that should be used to generate new insights about in-situ adsorption kinetics of fluorescing compounds.

To evaluate the potential of the LIF for soil science, it should be applied to other fluorescing compounds than pyrene. In principle, all fluorescing compounds can be analysed, regardless of their further chemical properties. For transport studies for example, uranin could be used in combination with pyrene or other PAH´s. Furthermore the research should be extended to more soils and also to sediment systems. It is our aim, to establish the laser-induced fluorescence spectroscopy for adsorption studies in saturated sediments and soils. The laser probe head opens the unique possibility to measure in real-time and in-situ 3D fluorescence spectra. Because artefacts due to sample preparation can be reduced to a minimum by in-situ methods, the resulting data will help to understand sorption mechanisms under more natural conditions.

For applying the LIF to unsaturated sediments and soils it is important to ensure, that the whole system is at hydrodynamic equilibrium at the start of the experiment. As discussed in this work, the sensitivity of the laser probe head against fluctuations of the water content are intrinsic, to a certain degree. Pronounced changes in the water content will influence the back-transition of the fluorescence light into the probe head, and therefore the measured fluorescence intensity. The consequence for our future work will be to limit our research with the LIF probe head to systems, were the water content can be kept constant, or to find correction terms for the mathematical correction of the fluorescence data. For the second approach it will be necessary to use TDR, or comparable systems, to monitor constantly the soil water content.

The integration of the laser probe head into soil columns can lead to important insights of transport phenomena above the column outlet level. Effects like fingering or preferential flow can be analysed with minimum disturbance of the soil column structure. We hope, that our method will contribute to a better temporal and spatial resolution in soil column experiments. Like TDR, the in-situ LIF analysis can be characterised as a micro-invasive method. These methods will become of great importance for future soil science.

6. Literature

Aiken G., Leenheer J. (1993)
Isolation and chemical characterization of dissolved and colloidal organic matter.
Chemistry and Ecology 8, 135-151

Akkanen J., Penttinen S., Haitzer M., Kukkonen J. (2001)
Bioavailability of atrazine, pyrene and benzo[a]pyrene in European river waters.
Chemosphere 45, 453-462

Altfelder S., Streck T., Maraqa M.A., Voice T.C. (2001)
Nonequilibrium sorption of dimethylphthalate – compatibility of batch and column techniques.
Soil Sci. Soc. Am. J. 65, 102-111

Amellal N., Portal J.-M., Berthelin J. (2001)
Effect of soil structure on the bioavailability of polycyclic aromatic hydrocarbons within aggregates of a contaminated soil
Applied Geochemistry 16, 1611-1619

Apitz S.E., Theriault G.A., Liebermann S.H. (1992)
Optimization of the optical characteristics of a fiber-optic guided laser fluorescence technique for the in situ evaluation of fuels in soils.
SPIE 1637, 241-254

Backhus D.A., Gschwend P.M. (1990)
Fluorescent polycyclic aromatic hydrocarbons as probes for studying the impact of colloids on pollutant transport in groundwater.
Environ. Sci. Technol. 24, 1214-1223

Baltussen E., Sandra P., David F., Cramers C. (1999)
Stir bar sorptive extraction (SBSE), a novel extraction technique for aqueous samples: theory and principles.
J. Microcolumn Separations 11(10), 737-747

Baumann T., Haaszio S., Niessner R. (2000)
Applications of a laser-induced fluorescence spectroscopy sensor in aquatic systems.
Water Research 34, 1318-1326

Belardi R.G., Pawliszyn J. (1989)
The application of chemically modified fused silica fibers in the extraction of organics from water matrix samples and their rapid transfer to capillary columns.
Water Pollut. Res. J. Can. 24, 179

Bilkert J.N., Rao P.S. (1985)
Sorption and leaching of three non-fumigant nematicides in soils.
J. Environ. Sci. Health B 20; 1-26

Billington J.W., Huang G.L., F. Szeto, W.Y. Shiu, Mackay D. (1988)
Preparation of aqueous solutions of sparingly soluble organic substances: I. Single component systems
Environmental Tox. and Chem. 7, 117-124

Brusseau M.L., Rao P.S. (1989)
Sorption nonideality during organic contaminant transport in porous media
Critical reviews in environmental control 19, Issue 1, 33-95

Canell D.S., Rondelez F. (1980)
Diffusion of polystyrenes through microporous membranes.
Macromolecules 13, 1599-1602

Caron G., Suffet I.H., Belton T. (1985)
Effect of dissolved organic carbon on the environmental distribution of nonpolar organic compounds.
Chemosphere 14, 993-1000

Chefetz B., Deshmukh A.P., Hatcher P.G., Guthrie E.A. (2000)
Pyrene sorption by natural organic matter.
Environ. Sci. Technol. 34, 2925-2930

Chen J.W., Kong L.R., Zhu C.M., Huang Q.G., Wang L.S. (1996)
Correlation between Photolysis rate constants of polycyclic aromatic hydrocarbons and frontier molecular orbital energy.
Chemosphere 33, 1143-1150

Chen R.F., Bada J.L. (1990)
A laser-based fluorometry system for investigations of seawater and porewater fluorescence.
Marine Chemistry 31, 219-230

Chen J., Quan X., Peijnenburg W.J. (2001)
Quantitative structure-property relationship studies on direct photolysis of selected polycyclic aromatic hydrocarbons in atmospheric aerosol.
Chemosphere 42, 263-270

Chien Y.Y., Bleam W.F. (1998)
Two-dimensional NOESY nuclear magnetic resonance study of pH-dependent changes in humic acid conformation in aqueous solution.
Environ. Sci. Technol. 32, 3653-3658

Chiou C.T., Malcolm R.L., Kile D.E. (1986)
Water solubility enhancement of some pollutants and pesticides by dissolved humic and fulvic acids.
Environ. Sci. Technol. 20, 502-508

Chiou C.T., Kile D.E. (1994)
Effects of polar and nonpolar groups on the solubility of organic compounds in soil organic matter.
Environ. Sci. Technol. 28, 1139-1144

Chiou C.T., McGroddy S.E., Kile D.E. (1998)
Partition characteristics of polycyclic aromatic hydrocarbons on soils and sediments.
Environ. Sci. Technol. 32, 264-269

Connaughton D.F., Stedinger J.R., Lion L.W., Shuler M.L. (1993)
Description of time-varying desorption kinetics: Release of naphthalene from contaminated soils.
Environ. Sci. Technol. 27, 2397-2403

Curtis G.P., Reinhard M., Roberts P.V. (1986)
Sorption of hydrophobic organic compounds by sediments.
American Chemical Society 191-216

Dabestani R., Ivanov I.N. (1999)
Invited Review: A compilation of physical, spectroscopic and photophysical properties of polycyclic aromatic hydrocarbons.
Photochemistry and Photobiology 70(1), 10-34

Danielsen K.M., Chin Y.P., Buterbaugh J.S., Gustafson T.L., Traina S.J. (1995)
Solubility enhancement and fluorescence quenching of pyrene by humic substances: the effect of dissolved oxygen on quenching processes.
Environ. Sci. Technol. 29, 2162-2165

de Maagd P.G., Dorien Th. E., Sijm Th. M. (1998)
Physicochemical properties of polycyclic aromatic hydrocarbons: aqueous solubilities, n-octanol/water partition coefficients, and Henry´s law constants.
Environmental Tox. and Chem. 17, 251-257

de Paolis F., Kukkonen J. (1997)
Binding of organic pollutants to humic and fulvic acids: influence of pH and the structure of humic material.
Chemosphere 34, 1693-1704

Döring U.M., Marschner B. (1998)
Water solubility enhancement of benzo(a)pyrene and 2,2‘,5,5‘-tetrachlorobiphenyl by dissolved organic matter (DOM).
Phys. Chem. Earth 23, 193-197

Donard O.F.X., Lamotte M., Belin C., Ewald M. (1989)
High-sensitivity fluorescence spectroscopy of mediterranean waters using a conventional or a pulsed laser excitation source.
Marine Chemistry 27, 117-136

Dunnivant F.M., Jardine P.M., McCarthy J.F. (1992)
Transport of naturally occurring dissolved organic carbon in laboratory columns containing aquifer material.
Soil Sci. Sco. Am. J. 56, 437-444

Frimmel F.H. (2000)
Development in aquatic humic chemistry
Agronomie 20, 451-463

Gauthier T.D., Shane E.C., Guerin W.F., Seitz W.R., Grant C.L. (1986)
Fluorescence quenching method for determining equilibrium constants for polycyclic aromatic hydrocarbons binding to dissolved humic materials.
Environ. Sci. Technol. 20, 1162-1166

Gauthier T.D., Seitz W.R., Grant C.L. (1987)
Effects of structural and compositional variations of dissolved humic materials on pyrene K_{OC} values.
Environ. Sci. Technol. 21, 243-248

Georgi A. (1997)
Sorption von hydrophoben organischen Verbindungen an gelösten Huminstoffen. Dissertation, Institut für analytische Chemie, Universität Leipzig

Guggenberger G., Kaiser K., Zech W. (1998)
Mobilization and immobilization of dissolved organic matter in forest soils.
Pflanzenernährung Bodenkunde 161, 401-408

Guillot G., Léger L., Rondelez F. (1985)
Diffusion of large flexible polymer chains through porous membranes.
Macromolecules 18, 2531-2537

Haitzer M., Höss S., Traunspurger W. Steinberg C. (1998)
Effects of dissolved organic matter (DOM) on the bioconcentration of organic chemicals in aquatic organisms – a review –
Chemosphere 37 (7), 1335-1362

Haitzer M., Löhmannsröben H.G., Steinberg Ch., Zimmermann U. (2000)
In vivo laser-induced fluorescence detection of pyrene in nematodes and determination of pyrene binding constants for humic substances by fluorescence quenching and bioconcentration experiments.
Journal Environ. Monitoring 2, 145-149

Hayes M.H., Swift R.S. (1990)
Genesis, isolation, composition and structures of soil humic substances. In soil colloids and their associations in aggregates.
DeBoodt M.F., Hayes M.H., Herbillon A. (eds.) Plenum, New York, 245-305

Herbert B.E., Bertsch P.M., Novak J.M. (1993)
Pyrene sorption by water-soluble organic carbon.
Environ. Sci. Technol. 27, 398-403

Höllrigl-Rosta A., Vinken R., Lenz M., Schäffer A. (2003)
Sorption and dialysis experiments to assess the binding of phenolic xenobiotics to dissolved organic matter in soil.
Environ. Toxicology and Chemistry 22/4, 746-752

Hopkins D.W., Chudek J.A., Shiel R.S. (1993)
Chemical characterisation and decomposition of organic matter from two contrasting grassland soil profiles.
Journal of Soil Science 44, 147-157

Hwang S., Cutright T.J. (2002)
The impact of contact time on pyrene sorptive behaviour by a sandy-loam soil.
Environmental Pollution 117, 371-378

Hwang S., Raminez N., Cutright T.J., Ju L.K. (2003)
The role of soil properties in pyrene sorption and desorption.
Water, air and soil pollution 143, 65-80

Institute of Organic Chemistry, University of Hamburg (2002)
Physikalisches Verhalten angeregter Zustände.
http://www.chemie.uni-hamburg.de/oc/marga/photochemie/de/kap8.htm (31.10.2002)

Jardine P.M., Weber N.L., McCarthy J.F. (1989)
Mechanisms of dissolved organic carbon adsorption on soil.
Soil Sci. Sco. Am. J. 53, 1378-1385

Johnson W.P. Amy G. L. (1995)
Facilitated transport and enhanced desorption of polycyclic aromatic hydrocarbons by natural organic matter in aquifer sediments.
Environ. Sci. Technol. 29, 807-817

Johnson W.P. (2000)
Sediment control of facilitated transport and enhanced desorption.
J. of environ. Engineering 126, 47-57

Jury W.A., Gardner W.R., Gardner W.H. (1991)
Soil Physics.
5th edition, John Wiley, New York

Kaiser K., Guggenberger G., Zech W., (1996)
Sorption of DOM and DOM fractions to forest soils.
Geoderma 74, 281-303

Karickhoff S.W. (1980)
Sorption kinetics of hydrophobic pollutants in natural sediments.
In R.A. Baker, ed., Contaminants and Sediments, Vol. II, Ann Arbor Science Publishers, Ann Arbor, MI, pp. 193-205

Karickhoff S.W., Morris K.R. (1985)
Sorption dynamics of hydrophobic pollutants in sediment suspensions.
Environ. Toxikology and Chemistry 4, 469-479

Kögel-Knabner I., Totsche K.U., Raber B. (2000a)
Desorption of polycyclic aromatic hydrocarbons from soil in the presence of dissolved organic matter: effect of solution composition and aging.
J. Environmental Quality 29, 906-916

Kubista M., Sjöback R., Eriksson S., Albinsson B. (1994)
Experimental correction for the inner-filter effect in fluorescence spectra.
Analyst 119, 417-419

Kumke M.U., Löhmannsröben H.G., Roch Th. (1994)
Fluorescence quenching of polycyclic aromatic compounds by humic acid.
Analyst 119, 997-1001

Lakowicz J.R. (1983)
Principles of Fluorescence Spectroscopy.
Plenum Press, New York

Laor Y., Rebhun M. (1997)
Complexation-flockulation: A new method to determine binding coefficients of organic contaminants to dissolved humic substances.
Environ. Sci. Technol. 31, 3558-3564

Laor Y., Farmer W.J., Aochi Y., Strom P.F. (1998)
Phenanthrene binding and sorption to dissolved and to mineral-associated humic acid.
Wat. Res. 32, No. 6, pp 1923-1932

Larson R.A., Weber E.J. (1994)
Reaction mechanisms in environmental organic chemistry.
CRC Press, Boca Raton

Lee C.L., Huang H.T., Kuo L.J. (2000)
Experimental validation of an OMS model for the sorption behaviours of PAH´s onto aluminum oxide coated with humic acids.
J. Environ. Sci. Health A35(4), 515-536

Leenher J.A. (1991)
Organic substances structures that facilitate organic contaminant transport and transformations in aquatic sediment, organic substances and sediments in water, 1.
Lewis Publishers, Chelsea, 1991

Lehto K.M., Vuorimaa E., Lemmetyinen H. (2000)
Photolysis of polycyclic aromatic hydrocarbons (PAHs) in dilute aqueous solutions detected by fluorescence.
J. of Photochem. and Photobiol. A 136, 53-60

Linnemann V., Noel J., Vereecken H. (2002)
Abschlussbericht des ECHO Projektes: Emission und chemische Umwandlung biogener flüchtiger organischer Verbindungen.
Agrospäre, Forschungszentrum Jülich GmbH

Lion L.W., Stauffer T.B., MacIntyre W.C. (1990)
Sorption of hydrophobic compounds on aquifer materials: Analysis methods and the effect of organic carbon.
Contam. Hydrol. 5, 215-234

Lobartini J.C., Orioli G.A., Tan K.H. (1997)
Characteristics of soil humic acid fractions separated by ultrafiltration.
Commun. Soil Sci. Plant Anal. 28, 787-796

Lochmüller C.H., Wenzel T.J. (1990)
Spectroscopic studies of pyrene at silica interfaces
J. Phys. Chem. 94, 4230-4235

Löhmannsröben H.G., Roch Th. (1997)
Laserfluoreszenzspektroskopie als extraktionsfreies Nachweisverfahren für PAK und Mineralöle in Bodenproben.
Analytiker Taschenbuch, H. Günzler et al. (eds.) Vol. 15, Springer, Berlin, pp. 217-253

Löhmannsröben H.G., Roch Th., Schaefer R.G., Schultze R.H., Vereecken H. (1997)
Laser-induced fluorescence (LIF) spectroscopy for in-situ analysis of fluorescence tracers in water and soil.
SPIE 3107, 207-216

Lüers F., ten Hulscher Th. (1996)
Temperature effect on the partitioning of polycyclic aromatic hydrocarbons between natural organic carbon and water.
Chemosphere 33, 643-657

MacDonald B.C., Lvin S.J., Patterson H. (1997)
Correction of fluorescence inner filter effects and the partitioning of pyrene to dissolved organic carbon.
Analytica Chimica Acta 338, 155-162

Mackenzie K., Georgi A., Kumke M., Kopinke F.D. (2002)
Sorption of pyrene to dissolved humic substances and related model polymers.
Environ. Sci. Technol. 36, 4403-4409

Mader B.T., Goss K.U., Eisenreich S.J. (1997)
Sorption of nonionic, hydrophobic organic chemicals to mineral surfaces.
Environ. Sci. Technol. 31, 1079-1086

Magee B.R., Lion L.W., Lemley A.T. (1991)
Transport of dissolved organic macromolecules and their effect on the transport of phenanthrene in porous media.
Environ. Sci. Technol. 25, 323-331

Maraqa M.A., Zhao X., Wallace R.B., Voice T.C. (1998)
Retardation coefficients of nonionic organic compounds determined by batch and column techniques.
Soil Sci. Soc. Am. J. 62, 142-152

Marhaba T.F., Member Ü.E., Lippincott R.L. (2000)
Application of fluorescence technique for rapid identification of DOM fractions in source waters.
Journal of environmental engineering 126, 1039-1044

Marschner B. (1999)
Sorption von polyzyklischen aromatischen Kohlenwasserstoffen (PAK) und poly-chlorierten Biphenylen (PCB) im Boden.
J. Plant Nutr. Soil Sci. 162, 1-14

Martin D., Srivastava P.C., Zech W. (1998)
Characteristics of humic substances in cultivated and natural forest soils of Sikkim.
Geoderma 84, 345-362

Maxin C.R., Kögel-Knabner I. (1995)
Partitioning of polycyclic aromatic hydrocarbons (PAH) to water-soluble soil organic matter .
European J. of Soil Science 46, 193-204

Mennicken (2000)
Untersuchung repräsentativ belasteter Böden mit Hilfe des Wasserlinsentests und nachfolgender bildanalytischer Auswertung zur Entwicklung einer ökotoxikologischen Testbatterie im Rahmen des Bodenschutzgesetzes.
Diplomarbeit, Lehrstuhl für Ökologie, Ökotoxikologie und Ökochemie, RWTH Aachen

McCarthy J.F., Jimenez B.D. (1985)
Interactions between polycyclic aromatic hydrocarbons and dissolved humic material: binding and dissociation.
Environ. Sci. Technol. 19, 1072-1076

Nash J.E and Sutcliffe J.V. (1970)
River flow forecasting through conceptual models: Part I – A discussion of principles. Journal of Hydrology 10, 282-290.

Niessner R., Panne U., Schröder H. (1991)
Fibre-optic sensor for the determination of polynuclear aromatic hydrocarbons with time-resolved, laser-induced fluorescence.
Analytica Chimica Acta 255, 231-243

Ohlenbusch G., Kumke M.U., Frimmel F.H. (2000)
Sorption of phenols to dissolved organic matter investigated by solid phase microextraction.
The Sci. of the Total Environm. 253, 63-74

O`Loughlin E.J., Traina S.J., Chin Y.P. (2000)
Association of organotin compounds with aquatic and terrestrial humic substances.
Environ. Toxicology and Chemistry 19, No. 8 pp., 2015-2021

Panne U. (1994)
Time-resolved, fibre-optical guided multidimensional fluorescence as a sensor principle for the detection of dissolved fluorophores.
Ph.D. thesis, University of Dortmund

Parker C.A. (1968)
Photoluminescence of solutions.
Elsevier, Amsterdam

Perminova I.V. (1999)
Size exclusion chromatography of humic substances: complexities of data interpretation attributable to non-size exclusion effects.
Soil Science 164, 834-840

Perminova I.V., Grechishcheva N.Y., Petrosyan V. S. (1999)
Relationship between structure and binding affinity of humic substances for polycyclic aromatic hydrocarbons: relevance of molecular descriptors.
Environ. Sci. Technol. 33, 3781-3787

Piatt JJ, Backhus D., Capel P.D., Eisenreich S.J. (1996)
Temperature-dependent sorption of naphthalene, phenanthrene and pyrene to low organic carbon aquifer sediments.
Environ. Sci. Technol. 30, 751-760

Piccolo A., Nardi S., Cocheri G. (1996a)
Micelle-like conformation of humic substances as revealed by size exclusion chromatography.
Chemosphere 33, 595-602

Piccolo A., Nardi S., Concheri G. (1996b)
Macromolecular changes of humic substances induced by interaction with organic acids.
European J. of Soil Science 47, 319-328

Piccolo A., Conte P., Cozzolino A. (1999)
Effects of mineral and monocarboxylic acids on the molecular association of dissolved humic substances.
European J. of Soil Science 50, 687-694

Piccolo A., Conte P., Buurmann P. (2002)
Reduced heterogeneity of a lignite humic acid by preparative HPSEC following interaction with an organic acid. Characterization of size-separates by Pyr-GC-MS and H-NMR
Environ. Sci. Technol. 36, 76-84

Popp P., Bauer C., Wennrich L. (2001)
Application of stir bar sorptive extraction in combination with column liquid chromatography for the determination of polycyclic aromatic hydrocarbons in water samples.
Analytica Chimica Acta 436, 1-9

Raber B., Kögel-Knabner I., Klem D. (1998)
Partitioning of polycyclic aromatic hydrocarbons to dissolved organic matter from different soils.
Chemosphere 36, 79-97

Rav-Acha Ch., Rebhun M. (1992)
Binding of organic solutes to dissolved humic substances and its effects on adsorption and transport in the aquatic environment.
Water Research 12, 1645-1654

Renkin E.M. (1954)
Filtration, Diffusion, and Molecular Sieving through porous cellulose membranes
Journal of general Physiology 38, 225-243

Reyes C.A., Medina M., Crespo-Hernandez C., Cedeno M.Z., Arce R., Rosario O., Steffenson D.M., Ivanov I.N., Sigman M.E., Dabestani R. (2000)
Photochemistry of pyrene on unactivated and activated silica surfaces.
Environ. Sci. Technol. 34, 415-421

Reza J., Trejo A., Vera-Avila L.E. (2002)
Determination of the temperature dependence of water solubilities of polycyclic aromatic hydrocarbons by generator column-on-line solid-phase extraction-liquid chromatographic method.
Chemosphere 47, 933-945

Rice J.A., Lin J.S. (1993)
Fractal nature of humic materials.
Environ. Sci. Technol. 27, 413-414

Richardson J.A., Ando M.E. (1977)
Sub-part-per-trillion detection of polycyclic aromatic hydrocarbons by laser induced molecular fluorescence.
Analytical Chemistry 49, 955-959

Rudnick S.M., Chen R.F. (1998)
Laser-induced fluorescence of pyrene and other polycyclic aromatic hydrocarbons (PAH) in seawater.
Talanta 47, 907-919

Schade W., Bublitz J. (1996)
On-site laser probe for the detection of petroleum products in water and soil.
Environ. Sci. Technol. 30, 1451-1458

Schlautmann M.A., Morgan J.J. (1993)
Effects of aqueous chemistry on the binding of polycyclic aromatic hydrocarbons by dissolved humic materials.
Environ. Sci. Technol. 27, 961-969

Schulten H.R., Schnitzer M. (1993)
A state of the art structural concept for humic substances.
Naturwissenschaften 80, 29-30

Schulze M. (1998)
Bedeutung des gelösten organischen Kohlenstoffs für das Schicksal hydrophober organischer Verbindungen in ungesättigten Bodenzonen.
Dissertation: Institut für Chemie und Dynamik der Geosphäre 4, Forschungszentrum Jülich

Selim H.M., Schulin R., Flühler H. (1987)
Transport and ion exchange of calcium and magnesium in an aggregated soil.
Soil Sci. Soc. Am. J. 51(4), 876-884

Shelton D.R., Doherty M.A. (1997)
A model describing pesticide bioavailability and biodegradation in soil.
Soil Sci. Soc. Am. J. 61, 1078-1084

Shor L.M., Rockne K.J., Tachon G.L., Young L.Y., Kosson D.S. (2003)
Desorption kinetics for field-aged polycyclic aromatic hydrocarbons from sediments.
Environ. Sci. Technol. 37, 1535-1544

Sigman M.E., Schuler P.F., Ghosh M.M., Dabestani R.T. (1998)
Mechanism of pyrene photochemical oxidation in aqueous and surfactant solutions.
Environ. Sci. Technol. 32, 3980-3985

Simpson A.J., Kingery W.L., Hofman M. (2002)
Molecular structures and associations of humic substances in the terrestrial environment.
Naturwissenschaften 89, 84-88

Šimůnek J., Šejna M., Van Genuchten M.T. (1995)
Numerical model for simulating multiple solute transport in variably-saturated soils. in Proc. "Water Pollution III: Modelling, Measurement and Prediction" Ed. Wrobel L.C., Southampton, U.K. pp. 21-30

Six J., Guggenberger G., Paustian K., Haumaier L., Elliott E.T., Zech W. (2001)
Sources and composition of soil organic matter fractions between and within soil aggregates.
European J. of Soil Science 52, 607-618

Steinfeld J.I., Francisco J.S., Hase W.L. (1989)
Chemical kinetics and dynamics.
Englewood Cliffs, N.J., Prentice Hall

Stevenson C.L., Vo-Dinh T. (1995)
Analysis of polynuclear aromatic compounds using laser-excited synchronous fluorescence.
Analytica Chimica Acta 303, 247-253

Stohrer W.D. (1991)
Die konzeptionellen Grundlagen der Photochemie.
Photochemie, PdN-Ch. 4/40, 15-22

Tausch M., Paterkiewicz D. (1988)
Phosphoreszenz und Fluoreszenz.
Photochemie, PdN-Ch. 1/37, 14-21

Todd A.T., Jarvis G.B., Xu H., Bevilacqua A.C., Kenny J.E. (1993)
Laser-based fluorescence EEM instrument for in-situ groundwater monitoring.
Analytical Instrumentation 21, 141-162

Tombacz E. (1999)
Colloidal properties of humic acids and spontaneous changes of their colloidal state under variable solution conditions.
Soil Science 164, 814-824

Toride N., Leij F.J., Van Genuchten M.T. (1993)
A comprehensive set of analytical solutions for nonequilibrium solute transport with first-order decay and zero-order production.
Water Resources Research 29 (7), 2167-2182

Totsche K.U., Danzer J., Kögel-Knabner I. (1997)
Dissolved organic matter-enhanced retention of polycyclic aromatic hydrocarbons in soil miscible displacement experiments.
J. Environ. Qual. 26, 1090-1100

Van Genuchten M.T., Wagenet R.J. (1989)
Two-site/two-region models for pesticide transport and degradation: Theoretical development and analytical solutions.
Soil Sci. Soc. Am. J. 53, 1303-1310

Varga B., Kiss G., Galambos I., Gelencsér A., Hlavay J., Krivácsy Z. (2000)
Secondary structure of humic acids. Can micelle-like conformation be proved by aqueous size exclusion chromatography?
Environ. Sci. Technol. 34, 3303-3306

Vereecken H., Jaeckel U., Esser O., Nitzsche O. (1999)
Solute transport analysis of bromide, uranin and LiCl using breakthrough curves from aquifer sediment.
J. of Contaminant Hydrology 39, 7-34

Vereecken H., Nitsche O., Schulze M. (2001)
Analysis of the transport of hydrophobic organic xenobiotics in the presence of dissolved organic carbon using soil column experiments
Soil Science Society of America, Chapter 22, 449-470

Wershaw R.L. (1986)
A new model for humic materials and their interaction with hydrophobic organic chemicals in soil-water or sediment-water systems.
J. of contaminant Hydrology 1, 29-45

Whitcomb J.L., Bystol A.J., Campiglia A.D. (2002)
Time-resolved laser-induced fluorimetry for screening polycyclic aromatic hydrocarbons on solid-phase extraction membranes.
Analytica Chimica Acta 22069, 1-12

Wolters A., Kromer T., Linnemann V., Ophoff H., Stork A., Vereecken H. (2002)
Votalization of [^{14}C]fluoranthene and [^{14}C]diflufenican after soil surface application under field-like conditions: measurement and comparison with different model approaches.
Agronomie 22, 337-350

Wu S.C., Gschwend P.M. (1986)
Sorption kinetics of hydrophobic organic compounds to natural sediments and soils.
Environ. Sci. Technol. 20, No. 7, 717-725

Xing B. (2001)
Sorption of naphthalene and phenanthrene by soil humic acids.
Environmental Pollution 111, 303-309

Zepp R.G., Schlotzhauer P.F. (1979)
Photoreactivity of selected aromatic hydrocarbons in water.
Polynuclear Aromatic Hydrocarbons edited by P.W. Jones and P. Leber
Ann Arbor Science Publishers, Inc. Ann Arbor, pp 141-158

Zimmermann U., Skrivanek Th., Löhmannsröben H.G. (1999)
Fluorescence quenching of polycyclic aromatic compounds by humic substances (Part 1, Methology for the determination of sorption coefficients).
Journal Environ. Monitoring 1, 525-532

7. Appendix

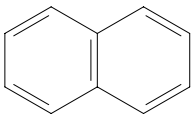
Naphthalene

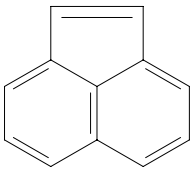
Acenaphthylene

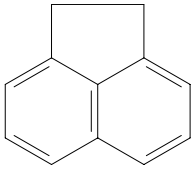
Acenaphthene

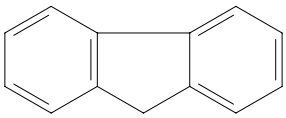
Fluorene

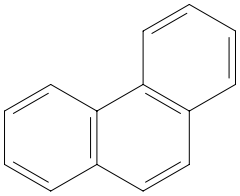
Phenanthrene

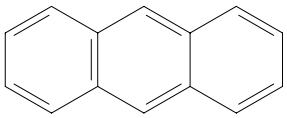
Anthracene

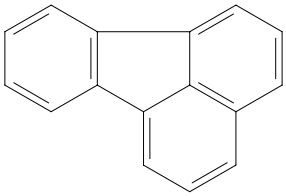
Fluoranthene

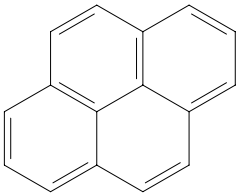
Pyrene

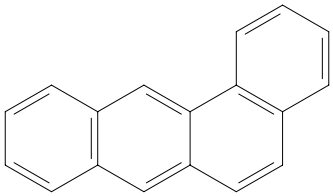
Benzo[a]anthracene

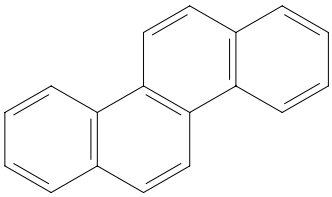
Chrysene

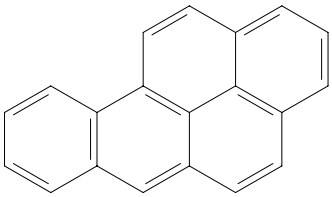
Benzo[a]pyrene

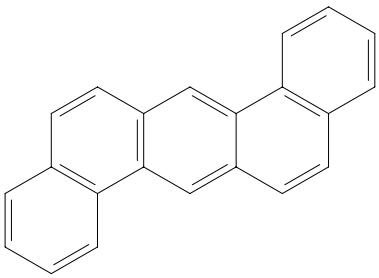
Dibenz[a,h]anthracene

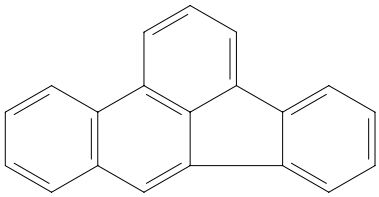
Benzo[b]fluoranthene

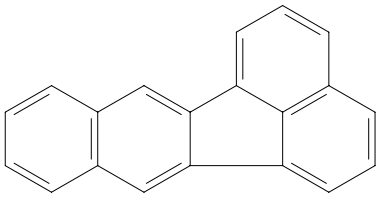
Benzo[k]fluoranthene

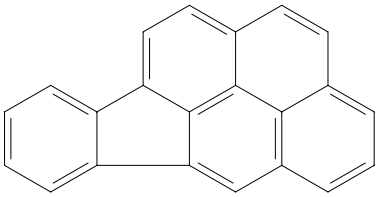
Indeno[1,2,3-cd]pyrene

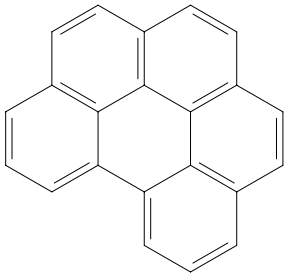
Benzo[g,h,i]perylene

Appendix 1: Formula of the EPA “Priority Pollutants“ PAK.

Analysis report

Atom emission spectroscopy with inductive coupled argon plasma.

Sample: Sand

Sample preparation:

The sample was ground. 100 mg of the sample was mixed with 500 mg lithiumborate and solubilised for 20 min. at 1000 °C. The cast was dissolved in 30 ml HCl (3%) and filled up to 100 ml.

The sample was analysed qualitative for 37 elements. Due to the disintegration mode, Li and B could not have been analysed.

Results:

Sample	Sample 1	Sample 2
% weight Al	1.0	1.0
% weight Ba	0.026	0.027
% weight Ca	0.024	0.025
% weight Fe	0.15	0.15
% weight K	1.0	0.89
% weight Mg	0.018	0.019
% weight Mn	b.d.l.	b.d.l.
% weight Na	0.11	0.11
% weight Si	41.1	43.2
% weight Sr	b.d.l.	b.d.l.
% weight Ti	0.027	0.027

* b.d.l. = below detection limit of 0.005 % weight

The specific surface of the sand was determined by multipoint BET measurements:

Specific surface:	0.57 m^2g^{-1}
Slope:	7.44
y-axis intercept:	0.18
C-value :	41.77
Vm :	0.13
Correlation coefficient:	0.9974

Appendix 2: Analysis of the elemental composition and the specific surface area of “Sand 1”

Analysis report

Sample name: Sandy soil „Kaldenkirchen“

Soil type: „Schwach pseudovergleyte saure Braunerde“

Analysis of the CHNS content [% mass]:		Particle size analysis by
C_{total}	1.10	Wolters et al. 2002 :
H	0.13	clay: 3.6 %
N	0.12	silt: 23.1 %
S	0.03	sand: 73.3 %

Carbon content [% mass]

C_{total}	1.019
C_{org}	0.961

The specific surface of the soil was determined by multipoint BET measurements:

Specific surface:	1.32 m^2g^{-1}
Slope:	3.22
y-axis intercept:	0.06
C-value :	49.98
Vm :	0.30
Correlation coefficient:	0.9999

Sample name: Sandy soil „Kaldenkirchen“, annealed at 600 °C for 48 hours

Carbon content [% mass]

C_{total}	0.001
C_{org}	0.001

The specific surface of the soil was determined by multipoint BET measurements:

Specific surface:	2.63 m^2g^{-1}
Slope:	1.62
y-axis intercept:	0.022
C-value :	73.64
Vm :	0.60
Correlation coefficient:	0.9999

Appendix 3: Analysis of the elemental composition and the specific surface area of “Kaldenkirchen”

Analysis report

Sample name: Forest soil „Jülich"

Soil type: „Parabraunerde Haftnässepseudogley " (Luvisol)

Vegetation: Beech grove (approx. 80 years old) with a constantly high groundwater level

Particle size analysis

by Linnemann et al. 2002:

clay: 14 %

silt: 73 %

sand: 13 %

Carbon content [% mass]

C_{total}	6.74
C_{org}	6.40

The specific surface of the soil was determined by multipoint BET measurements:

Specific surface:	2.27 m^2g^{-1}
Slope:	1.84
y-axis intercept:	0.069
C-value :	27.84
Vm :	0.52
Correlation coefficient:	0.9992

Sample name: Forest soil „Jülich", annealed at 600 °C for 48 hours

Carbon content [% mass]

C_{total}	0.011
C_{org}	0.010

The specific surface of the soil was determined by multipoint BET measurements:

Specific surface:	7.41 m^2g^{-1}
Slope:	0.581
y-axis intercept:	0.0070
C-value :	83.39
Vm :	1.70
Correlation coefficient:	0.9999

Appendix 4: Analysis of the carbon content and the specific surface area of the forest soil "Jülich"

Analysis report

Sample name: Field soil „Krauthausen"

Soil type: „Parabraunerde (Pseudogley)"

Vegetation: Test site with grassland for more than ten years

Carbon content [% mass]

C_{org}	2.3

The specific surface of the soil was determined by multipoint BET measurements:

Specific surface:	6.14 m^2g^{-1}
Slope:	0.696
y-axis intercept:	0.0125
C-value :	56.79
Vm :	1.41
Correlation coefficient:	0.9999

Sample name: Field soil „Krauthausen", annealed at 600 °C for 48 hours

Carbon content [% mass]

C_{total}	0.002
C_{org}	0.002

The specific surface of the soil was determined by multipoint BET measurements:

Specific surface:	8.81 m^2g^{-1}
Slope:	0.488
y-axis intercept:	0.0061
C-value :	81.09
Vm :	2.02
Correlation coefficient:	1.0000

Appendix 5: Analysis of the carbon content and the specific surface area of "Krauthausen"

Danksagung

Ich möchte an dieser Stelle der Deutschen Forschungsgemeinschaft danken, die durch ihre finanzielle Unterstützung diese Arbeit erst ermöglicht hat.

Darüber hinaus möchte ich mich bei allen Mitarbeitern der Agrosphäre für eine sehr angenehme Arbeitsatmosphäre bedanken. Auch die Kollegen, die nicht direkt mit meiner Fragestellung befasst waren, hatten jederzeit ein offenes Ohr für Probleme und Fragen.
Vielen Dank hierfür!

Professor Dr. A. Schäffer danke ich für die Übernahme des Referates. Auch aus der Ferne war er stets sehr konkret am Fortgang meiner Arbeit interessiert und bei Fragen stets erreichbar.

Professor Dr. H. Vereecken danke ich für die gute Betreuung vor Ort. Trotz turbulenter Zeiten (2 Umzüge, Neugründung des Institutes) hat er sich stets Zeit genommen und mir mit präzisen Ratschlägen stets auf den Erkenntnispfad zurückgeholfen.

Mein besonderer Dank gilt meinem Betreuer Jean-Marie Séquaris, der meiner spontanen, manchmal zu forschen Art stets mit Ruhe und Gelassenheit begegnet ist. Diese Mischung hat zu einem angenehmen, dynamischen und zielorientierten Arbeitsklima geführt.

Bei meinen Eltern möchte ich mich für alle Unterstützung bedanken, die sie mir für meine lange Ausbildung gegeben haben. Nach jetziger Planung wird mein MBA Studium dann auch das letzte Studium sein. Wir werden sehen...

Ich danke Dir, Kathrin für Motivation und Verständnis in einer stressigen Zeit.
Du hast sie zu einer guten Zeit gemacht. Tausend Dank!

Ich freue mich auf eine schöne Zeit mit Dir - ganz ohne Doktorarbeit! Wir sehen uns am Fels!

Forschungszentrum Jülich
in der Helmholtz-Gemeinschaft

Jül-4178
Juli 2005
ISSN 0944-2952